8-9-2019 10:00 AM

Studies on the Liquefaction Behaviour of Tailings and Natural Sand

Guillermo Riveros, *The University of Western Ontario*

Supervisor: Sadrekarimi, Abouzar, *The University of Western Ontario*

A thesis submitted in partial fulfillment of the requirements for the Master of Engineering Science degree in Civil and Environmental Engineering

Studies on the Liquefaction Behaviour of Tailings and Natural Sand

Abstract

This series of studies explores the liquefaction behaviour of cohesionless mine tailings and a natural sand and examines the effectiveness of a bio-mediated treatment for the mitigation of liquefaction. The first study investigates the flow liquefaction failure of the Fundão tailings dam (2015) by analytically assessing the stability of the breached abutment, accounting for the specific triggering mechanism and subsequent strength loss that led to its collapse. The second study evaluates the static liquefaction behaviour of gold mine tailings and its correlations with shear-wave velocity through an experimental program comprised of direct simple-shear and bender element tests. The last study investigates the static and cyclic liquefaction behaviour of Fraser River sand and assesses the efficiency of a Microbially Induced Calcite Precipitation treatment in improving the sand's resistance to liquefaction. Overall, liquefaction is shown to produce substantial strength loss, and bio-mediation is proven to successfully mitigate it in the natural sand.

Keywords

Static liquefaction, tailings, Fundão dam, instability, flow failure, Fraser River sand, Cyclic liquefaction, MICP, cone penetration test, critical state

Summary for Lay Audience

Soil liquefaction is a phenomenon in which soils exhibit great loss of strength and subsequently seem to behave and flow like liquids. Wet granular soils such as saturated sands and silts are particularly susceptible to liquefaction and exhibit such a strength loss when loaded without allowing their volume to change. In this series of studies, the liquefied behaviours of granular mine waste materials, known as tailings, and a natural sand are explored. Additionally, the effectiveness of a soil strengthening treatment that relies on a particular metabolic process of certain types of bacteria is evaluated for the reduction of strength-loss caused by liquefaction.

The first study in the series investigates the flow failure of the Fundão tailings dam (2015), reported to have failed as consequence of liquefied tailings. The stability of the failing section of the dam is assessed by accounting for typical site conditions and the specific mechanism believed to have generated liquefaction of the tailings that ultimately led to the dam's collapse.

The second study evaluates the liquefied behaviour of gold mine tailings when subjected to consistently increasing loading without allowing any changes in volume to occur, in an experimental program comprised of direct simple-shear and bender-element tests. The results obtained are associated with the velocity at which small-displacement shear waves travel through the samples (known as shear-wave velocity), in order to establish trends to estimate strength and determine liquefaction susceptibility from these velocity values.

The third and last study investigates the liquefied behaviour of a natural sand from the Fraser River delta when subjected to consistent and cyclic loads without allowing changes in volume to occur. This study subsequently explores the efficiency of a strengthening treatment involving the by-products of a particular metabolic process of certain types of bacteria in improving the sand's resistance to strength loss by means of carbonate bonding of the soil particles.

Succinctly, this series provides insights into the nature of soil liquefaction, explores the various loading mechanisms that generate it, applies an innovative analysis method in evaluating dam stability against liquefaction flow failure, and proposes a soil improvement technique for liquefiable natural sands.

Co-Authorship Statement

This thesis has been prepared in accordance for an Integrated-Article format thesis stipulated by the School of Graduate and Postdoctoral Studies at the University of Western Ontario and has been co-authored as:

Chapter 3: Static Liquefaction Analysis of the Fundão Dam Failure

All experimental work was completed by Guillermo Riveros under supervision of Dr. Abouzar Sadrekarimi. A paper co-authored by Guillermo Riveros and Abouzar Sadrekarimi has been submitted to the Canadian Geotechnical Journal.

Chapter 4: Static Liquefaction and Liquefaction Triggering of a Gold Tailings

All experimental laboratory work was completed by Guillermo Riveros under supervision of Dr. Abouzar Sadrekarimi. A paper co-authored by Guillermo Riveros and Abouzar Sadrekarimi has been submitted to the Canadian Geotechnical Journal.

Chapter 5: Study on the Effects of MICP Treatment on the Monotonic and Cyclic shear behaviour of Fraser River sand

All experimental work was completed by Guillermo Riveros under supervision of Dr. Abouzar Sadrekarimi. A paper co-authored by Stephen Jones and Abouzar Sadrekarimi will be submitted to the Canadian Geotechnical Journal.

Acknowledgments

First and foremost, the author would like to express his appreciation for the constant advice and guidance provided by Dr. Abouzar Sadrekarimi from the Department of Civil and Environmental Engineering at the University of Western Ontario during the development of this series of studies. Likewise, the assistance of fellow graduate researchers Mr. Keyvan Mirbaha and Mr. Stephen Jones, as well as Laboratory Technicians Melodie Richards and Caitlin Concoran is greatly acknowledged and appreciated. The sincerest thanks are also expressed to Dr. Paul Simms from Carleton University for his assistance in obtaining the samples of gold mine tailings used in the development of part of this study. Finally, an extended thanks to Dr. Shirin Bahrami from the Department of Civil and Environmental Engineering and Mr. Hemanta Mainali from the Department of Biology at the University of Western Ontario for all their support in the research program of Microbially Induced Calcite Precipitation (MICP) methods and bacteria culturing.

Table of Contents

List of Tables

List of Figures

List of Symbols

CDSS	Cyclic direct simple shear test
CPT	Cone penetration test
CRR	Cyclic resistance ratio
CSL	Critical state line (Critical state locus)
CSR	Cyclic stress ratio
$\mathbf{D_r}$	Relative density (%)
$\mathbf{D_{rc}}$	Consolidation relative density (%)
DSS	Direct simple shear test
$\mathbf{D_{50}}$	Median particle size (mm)
e	Void ratio
$\mathbf{e_c}$	Consolidation void ratio
$\mathbf{e_0}$	Initial void ratio
ESA	Effective Stress Analysis
$\mathbf{e_{max}}$	Maximum void ratio
$\mathbf{e_{min}}$	Minimum void ratio
$\mathbf{\phi'_{yield}}$	Yield effective friction angle (^{O})
$\mathbf{\phi'_{liq}}$	Post-liquefied effective friction angle (^{O})
FC	Fines content (%)
FS	Factor of Safety
$\mathbf{G_{max}}$	Maximum shear modulus (MPa)
$\mathbf{G_s}$	Specific gravity
$\mathbf{I_b}$	Brittleness index
IL	Instability Line
$\mathbf{K_O}$	At-rest earth pressure coefficient
LVDT	Linear variable differential transformer
β	Stress normalization exponent

MT	Moist tamped sample preparation technique
N_L	Number of loading cycles to achieve liquefaction
P_a	Atmospheric pressure (kPa)
p'_c	Effective mean stress (kPa)
q_c	Cone tip resistance (MPa)
q_{c1}	Normalized cone tip resistance value for overburden stress (MPa)
R^2	Coefficient of determination (%)
r_u	Pore water pressure coefficient
SEM	Scanning electron microscopic images
SPT	Standard penetration test
S_u(yield)	Yield undrained shear strength (kPa)
S_u(liq)	Post-liquified undrained shear strength (kPa)
u	Pore water pressure (kPa)
USA	Undrained Strength Analysis
USR	Undrained strength ratio
V_S	Shear wave velocity (m/s)
V_{S1}	Normalized shear wave velocity measurement for overburden stress (m/s)
XRD	X-ray diffraction analysis
σ'_v	Effective vertical stress (kPa)
σ'_{vc}	Effective vertical consolidation stress (kPa)
ρ	Mass density of soil (kg/m^3)
τ	Shear stress (kPa)
τ_{max}	Maximum shear stress (kPa)
ψ	Critical state parameter
γ	Shear strain (%)

Chapter 1

1. Introduction

Over the last few decades, soil liquefaction has been recognized to be the cause of many geotechnical infrastructure failures and their related fatalities. As early as in 1964, it was the weakening behaviour of the soil witnessed during the magnitude 7.3 (Richter scale) earthquake in Niigata, Japan, that helped raise awareness in the geotechnical engineering community of cyclic-induced liquefaction and its catastrophic consequences. Similarly, the breach of the Merriespruit tailings dam in Virginia, South Africa (1994) reminded the mine-waste management industry to the reality of static liquefaction and the very sudden and severe strength loss it involves. However, and despite the many early lessons learned, recent catastrophic events like the magnitude 6.3 earthquake in New Zealand (2011) and the collapse of the Fundão tailings dam in Brazil (2015) have shown there is much more to be learned regarding the nature and triggering of soil liquefaction.

With the objective to explore the weakened behaviour of liquefiable materials and the possible strengthening benefits of bio-mediation, the series of studies presented herein were undertaken. In the chapters that follow, the case history of the Fundão dam failure is examined in a static liquefaction triggering analysis that helps to comprehend the magnitude of the decrease in instability caused by the liquefied mine tailings. Furthermore, the liquefaction behaviours of cohesionless mine tailings and a natural sand are assessed in a series of laboratory tests, and empirical correlations are established in order to estimate the materials' shear strength, as well as to determine their susceptibility to liquefaction. Lastly, the effectiveness of a bio-mediated treatment involving the production of calcium carbonate through enzymatic processes is evaluated for the mitigation of liquefaction. Altogether, this series of studies presents the use of an innovative static liquefaction analysis method that incorporates variations in mode of shear, anisotropic consolidation along the failure surface, and the constant-shear stress triggering of static liquefaction; provides an analytical tool to determine the susceptibility to static liquefaction exclusively for gold mine tailings, as well as empirical correlations of their undrained strength with shear wave velocity; and investigates the strengthening benefits of a bio-mediated soil

improvement method employing a little-known bacterial strain on a real natural sand. The individual abstracts of each of the chapters are presented below.

1.1. Static Liquefaction Analysis of the Fundão Dam Failure

On November 5, 2015, roughly 32 million m^3 of iron mine tailings were accidentally released in the collapse of Fundão dam in Minas Gerais, Brazil. Totaling about 61% of the impoundment's contents, the spilled tailings buried the town of Bento Rodrigues, claiming the lives of 19 villagers, and causing a major environmental concern. This study presents a comprehensive static liquefaction triggering analysis performed on the failing section of the dam prior to its collapse, with the goal to determine its susceptibility to liquefaction under its ultimate loading condition. The method of analysis implemented accounts for variations in mode of shear and anisotropic consolidation along the failure surface normally encountered in the field. The instability line concept in flow liquefaction is used in conjunction with in-situ test data to estimate liquefaction triggering and post-liquefaction undrained shear strengths for loose and saturated tailings in the dam's section. These are subsequently applied in iterative limit equilibrium analyses (LEA) to obtain the factors of safety for liquefaction triggering and flow failure. After convergence in this process, the failing dam's section was found to be susceptible to static liquefaction flow failure with a factor of safety of 0.56.

1.2. Static Liquefaction and Liquefaction Triggering of Gold Tailings

Since the undrained strength and the shear wave velocity of cohesionless materials are primarily controlled by effective confining stresses and void ratio, this study presents a practical static liquefaction triggering analysis method specifically developed for gold mine tailings based on correlations between the undrained yield and post-liquefied strength of gold mine tailings with their shear-wave velocity. The shearing response of sand tailings to monotonic loading under plane-strain boundary conditions is examined through a series of constant-volume and drained direct simple-shear tests on slurry-deposited and moist-tamped samples. Laboratory shear-wave

velocity measurements made by means of bender element tests are subsequently used to connect these small-strain measurements to the tailings' behaviour at undrained yield and critical state. In general, the critical state behaviour of gold tailings is found to be similar to those reported by other researchers. Soil fabric differences produced by distinct depositional methods do not translate into significant differences in undrained yield strength and the critical state of the tailings tested. Sand tailings, as opposed to whole tailings, are found to be highly brittle, with increasing values of peak undrained strength as void ratio decreases. Additionally, and regardless of the difference in fines content between the sand and whole tailings, a common trend in post-liquefaction strength with respect to void ratio, and similar values of the critical state friction angle are observed. Thus, and notwithstanding the strong dependency on void ratio exhibited by the tailings' shear-wave velocity, an empirical method to evaluate static liquefaction triggering and failure of gold mine tailings using shear-wave velocity is proposed to assist in the prevention of mine-waste storage facility failures due to static liquefaction.

1.3. Study on the Effects of MICP Treatment on the Monotonic and Cyclic shear behaviour of Fraser River sand

The effectiveness of a microbially induced calcite precipitation (MICP) treatment in improving the undrained monotonic shear behaviour and cyclic shear resistance of Fraser River sand was examined in this study within a critical state framework. After employing *Sporosarcina ureae* as the ureolytic organism in a single application of the treatment, improvements in the sand's stiffness, undrained shear strength, and resistance to cyclic shear loading caused by the precipitation of $CaCO_3$ were investigated in a series of bender element and direct simple shear tests. Through SEM imaging, particle-to-particle cementation and increased particle angularity were observed in treated specimens. Shear-wave velocity in these samples was observed to be as much as 60 – 75 m/s higher than the original sand depending on the confining stress applied. Although similarly improved by the treatment, the increase of post-liquefied strength in treated samples was generally higher than that of yield strength, which ensued a reduction of brittleness in undrained shear relative to that of the original sand. The treatment also produced an increase in the cyclic resistance of the sand, with treated samples exhibiting CRR_{15} values higher than the

untreated sand for the range of densities tested. This strengthening effect of MICP treatment was seen to partially remain by also reducing the liquefaction potential of the treated sand in secondary seismic events.

Chapter 2

2. Literature Review

The following sections present a series of summaries of the various studies researched in the development of the investigation conducted herein. The main topics studied are static liquefaction through a critical state approach, particularly its effects on gold mine tailings as related to Chapter 4; and cyclic liquefaction and the biomineralization of calcium carbonate through Microbially Induced Calcite Precipitation (MICP), both pertinent to the material discussed in Chapter 5 in the mitigation of liquefaction by means of calcite cementation.

2.1. Static Liquefaction (Literature Review for Chapter 4)

Static liquefaction is likely the most common mode of failure in tailings impoundments, but there is limited mention of it in regulatory literature as it is often not explained, or it is used as a term to explain a non-seismically triggered flow failure. Hydraulically deposited tailings may be sufficiently loose after deposition, which in combination with a high state of saturation may leave the material susceptible to static liquefaction (Blight 2010).

To show the typical strain-softening behaviour of a soil element susceptible to static liquefaction, let's consider the undrained (i.e. constant-volume, CV) loading stress path shown in Figure 3-1(a) from a direct simple-shear (DSS) test carried out in this study on gold sand tailings specimens consolidated to a vertical stress (σ'_{vc}) of 400 kPa and a relative density (D_{rc}) of 52%. As shown, the tailings' effective stress is consistently reduced as the imposed shear stress is increased; this is due to the development of pore-water pressure as plastic strains are generated under undrained conditions. Strain softening and strength loss ensue when the applied shear stress surpasses the undrained yield strength, S_u(yield). The softening behaviour produced after triggering this undrained strength loss continues with further shear displacement until an undrained post-liquefaction strength, S_u(liq), is reached along what is known as the critical state line (CSL). Flow liquefaction flow failure occurs when the S_u(liq) falls below the applied shear stress.

Critical state is defined here as the state at which a soil deforms at a constant shear stress, constant pore water pressure, and at a constant void ratio (Casagrande 1936; Roscoe et al. 1958; Schofield and Wroth 1968), irrespective of the drainage condition (Been et al. 1991; Been and Jefferies 1985; Alarcon-Guzman 1988; Sadrekarimi and Olson 2012). The loci of critical states of a particular soil in the void ratio - effective stress space is often described by a semi-logarithmic relationship called the "critical state line" (CSL), and it is described by the equation below:

(Eq. 2-1) $$e_{CS=\Gamma-\lambda_{10}\log\sigma'_{cs}}$$

where e_{cs} and σ'_{cs} are respectively the void ratio and effective stress at critical state; and Γ and λ_{10} are the line's intercept at σ'_{cs} = 1 kPa and slope, respectively. The shear stress required for the constant deformation in critical state can be expressed in terms of a critical state friction angle, ϕ'_{cs} (alternatively, the critical stress ratio, M_{cs}) (Jeffries and Been 2016), or a critical undrained shear strength, S_u(crit) (Terzaghi et al. 1996). This critical strength has also been referred to as the undrained residual strength, S_r (Seed1987), or as the post-liquefied shear strength, S_u(liq) (Stark et al. 1998). Based on the National Science Foundation international workshop reported by Stark et al. (1998), the term S_u(liq) is adopted in this study.

Because soils exist in a variety of states (i.e. in both their density and stress conditions), which ultimately affect their shear behaviour, it is important to be able to measure or have a relative sense of the state of a soil element in order to express its susceptibility to liquefaction. This can be described by the critical state parameter (ψ), defined as the difference between the consolidation void ratio (e_c) at a given consolidation effective stress (σ'_c) and that at critical state (e_{cs}) as shown below (Jeffries and Been 1987):

(Eq. 2-2) $$\psi = e_C - e_{CS}$$

According to this relationship, negative values of state parameter indicate a dilative or strain-hardening behaviour, while positive values suggest a contractive loose soil that may be susceptible to undrained strain softening and liquefaction.

2.1.1. Observed Liquefaction Behaviour of Gold Tailings in Laboratory Settings

Given the cohesionless non-plastic nature of gold tailings, as well as their relatively loose and saturated state upon deposition as a slurry, static liquefaction is a concern for the stability of continuously raised tailings impoundments. For this reason, various studies have been conducted with the goals to examine the behaviour of liquefied gold tailings, and to establish a framework for determining the liquefaction potential of these materials.

Studies by Fourie and Papageorgiou (2001), Fourie et al. (2001), Papageorgiou (2004), and Fourie and Tshabalala (2005) have focused on determining the CSL for the gold mine tailings from the Merriespruit tailings dam by conducting isotopically- and anisotropically-consolidated undrained triaxial compression tests (ICU- and ACU-TxC). Given the variable fines content found in the samples they obtained (from 20-60% for in-situ samples), a single CSL could not be established for these tailings. Instead, individual CSLs for each of the gradations tested were observed, with that for samples containing the greatest amount of fines plotting below all others – a finding consistent with those made by other researchers such as Dobry et al. (1985), who obtained different CSLs for the same sand when tested with and without fines; Pitman et al. (1994), who concluded that 20% fines content was the limit for sand-governed shear behaviour in silty sands; and Sadrekarimi (2013), who observed a reduction in Γ_{cs} with increasing fines content, and an essentially unchanged λ when the fines are comprised of the particle shape as that of the base sand. With respect to friction angles observed, the authors of these studies report $\phi'_{cs} = 33^{o}$ with $c'=0$. Lastly, these researchers noted that water- and air-pluviated tailings samples dilated upon shearing, which together with a concern of strain-localization and the development of heterogeneous void ratio profiles inside the specimens (Sladen 1985), prompted them to adopt moist-tamping as the sample preparation technique for these studies.

In a separate investigation, Qiu and Sego (2001) assessed the engineering properties of gold and other common mine tailings. Upon conducting a series of isotropically-consolidation undrained TxC tests on slurry-deposited gold tailings samples (FC = 81%) to evaluate their shear strength, they reported observing cohesionless shear behaviour with a ϕ'_{cs} of 33^{o}. Also, perhaps due to the use of hydraulic deposition in sample preparation, they report noticing a slight strain-softening behaviour in the tailings followed by a strong dilative response, as similarly to that observed by Fourie and Papageorgiou (2001).

With an interest in evaluating the shear strength of thickened gold tailings (i.e. dewatered tailings with non-Newtonian fluid behaviour), Al-Tarhouni et al. (2011) conducted a series of monotonic and cyclic direct simple-shear (DSS) tests on reconstituted tailings samples with about 70% fines content. The monotonic shear test results on these samples exhibited slight strain-softening behaviour in some specimens before reaching critical state, and significant continuous dilation in others. As consequence of the resulting large scatter in their data, these researchers were unable to accurately determine a consistent CSL for these tailings. Additionally, by using undrained shear strengths at the critical (for loose samples) or the phase transformation (for dilative samples) states, Al-Tarhouni et al. (2011) established a clear trend of undrained strength ratio (USR) with void ratio.

Concerning the effect of fabric on the shear behaviour of gold tailings, Chang et al. (2011) conducted an experimental program on undisturbed and reconstituted samples of tailings obtained from a South African mine. The program included image analysis by scanning electron microscopy (SEM) and a series of ICU-TxC tests to determine the influence of fabric on the behaviour of otherwise identical specimens. The reconstituted samples were prepared by slurry-deposition as well as moist-tamping and were tested at the same state (void ratio and effective stress) as the undisturbed samples. Furthermore, three different gradations corresponding to those tailings at various locations inside the impoundment (namely the upper beach (30% FC), middle beach (50% FC), and pond (90% FC)) were used to account for the particle segregation that typically occurs upon deposition. The image analysis results obtained indicate a clear difference in fabric among specimen preparation types for the beach gradations, and a negligible difference for those of the pond. The shear behaviour, in contrast, was found to be relatively unaffected by gradation and fabric, with values of ϕ'_{cs} ranging from 31.1^{o}—34.3^{o}. However, at large strains, critical state was

attained at different stress states for the various fabrics and gradations, thus exhibiting the dependence of the CSL on these soil characteristics.

Lastly, in a study conducted by Schnaid et al. (2013), the behaviour of gold tailings was evaluated within a critical state framework, and an effort was made to couple it with the ratio of elastic stiffness (obtained from shear-wave velocity measurements) to shear strength, in order to estimate the state parameter. A laboratory experimental program, consisting of compression and extension triaxial tests on moist-tamped tailings samples with FC = 43% from a mine in northeastern Brazil, resulted in a highly curved CSL. Bender elements (BE) were used to measure shear-wave velocity (V_s) for each of the sheared samples as the axial strain was applied, and a general decrease in V_s with increasing strain was observed until minimum values were reached at the critical state.

2.2. Cyclic Liquefaction (Literature Review for Chapter 5)

In cyclic liquefaction, stresses and strains are applied cyclically to a soil element. This is similar to the loading imposed on soil deposits by ground shaking during earthquakes. Just as in static liquefaction, the principal condition that causes cyclic liquefaction failure is the development of pore-water pressure in the saturated cohesionless soil, as plastic strains are applied quickly and accumulate, thus preventing the pore-water from draining freely as shown in Figures 5-14 and 5-15. However, unlike in static liquefaction, which requires a given soil to be loose in order to develop pore pressures, in cyclic liquefaction, increases in pore-pressures arise from the densification produced by the changes in cyclic stress, which causes the close packing of soil particles (Jeffries and Been 2016). Hence, in this regard, cyclic liquefaction can also affect dense cohesionless soils, as cyclic-induced deification affects any soil.

To show the behaviour of a soil element imposed to cyclic loading, let's consider the stress path shown in Figure 5-14(a) from a constant-volume cyclic direct simple-shear (DSS) test carried out in this study on a cemented Fraser River sand specimen consolidated to a vertical stress (σ'_{vc}) of 100 kPa and a relative density (D_{rc}) of 62%. As shown, the sand's stress path moves relatively quickly to the left, as the buildup of excess pore water pressure produced with each cycle reduces the effective stress of the specimen (see Figure 5-15). Eventually, when zero (or near-zero)

effective stress is reached, the weakened sand begins to oscillate from positive to negative shear along the drained failure envelope, exhibiting large deformations in the process.

Cyclic liquefaction is strain-limited in dense cohesionless soils. At small strains, the slight densification of these soils produces the gradual development of pore pressure during cyclic loading. However, at larger strains, the characteristic dilation of the dense packing in these soils takes effect and begins to offset the excess pore pressure previously generated (Jeffries and Been 2016), thus not ultimately reaching a zero- effective stress condition. Consequently, cyclic liquefaction produces a softening effect in dense soils instead of the complete loss of strength observed in loose soils.

To understand how a soil behaves in response to cyclic loading, a mathematical approach involving the physical phenomenon of fatigue can be employed (Jeffries and Been 2016). Accordingly, cyclic behaviour, characterized as cyclic stress ratio ($CSR = \tau/\sigma'_{vc}$), can be linearly related to the logarithm of the number of cycles to produce liquefaction failure (N_L) in what is known as laboratory cyclic strength curves (Kramer 1996). These curves can be used to concisely present the relationship between a soil's density, the applied cyclic stress amplitude, and the number of cycles to reach liquefaction. The liquefaction failure criterion implemented in this study for direct-simple-shear testing is defined as the number of cycles required to cause a double-amplitude shear strain (γ_{DA}) of 3.75% or a single-amplitude shear strain (γ_{SA}) of 7.5% (Vaid and Sivathayalan 1996; Wijewickreme et al. 2005). As shown in Figure 5-23, the number of loading cycles required to produce liquefaction decreases with increasing CSR.

2.3. Biomineralization of Calcium Carbonate (Literature Review for Chapter 5)

Despite being the least abundant element in the Earth's crust (Weast and Astle 1982), carbon is commonly found on the planet's surface as large reservoirs of organic matter or as inorganic carbon in carbonate rocks such as limestone (Bosaket al. 2015). Many organisms mediate in what is known as the carbon cycle, by fixing inorganic carbon to form organic carbon and re-mineralizing it back to inorganic carbon. Particularly, bacteria facilitate the deposition of carbonate

minerals on the Earth's surface by precipitating calcium carbonate ($CaCO_3$) extracellularly as a result of their metabolic processes (Bavendamm 1932; Chafetz and Buczynski 1992; Krumbein 1974; Monty 1972). In environments with enough concentration of calcium ions (Ca^{2+}), $CaCO_3$ precipitation is stimulated by microbial metabolisms that increase the pH and the concentration of carbonate ions (CO_3^{2-}) on the cells' surface, which in turn serve as nucleation sites for the precipitated mineral. This process is generally referred to as microbially induced calcite precipitation (MICP) and can occur via different metabolic processes. Several of such processes have been studied extensively (Bosak and Newman 2003, 2005; Ferrer et al. 1988; Thompson and Ferris 1990; Ferris et al. 1995; Stocks-Fischer et al. 1999), of which the enzymatic hydrolysis of urea (or urea hydrolysis) has become of particular interest in the improvement of strength and stiffness of soils (Mitchell and Santamarina 2005; DeJong et al. 2006, 2010; Martinez 2012; Montoya 2012; Cheng et al. 2014; Murtala et al. 2016; Feng and Montoya 2016; and Chou et al. 2011).

MICP via urea hydrolysis involves the use of the microbial enzyme urease (urea amidohydrolase; EC 3.5.1.5) to hydrolyze or break down the organic compound urea. Urease positive bacteria use urea as a source of nitrogen and energy (Stocks-Fischer et al. 1999) and produce the enzyme at very different levels depending on the strain (Anbu et al. 2016). The bio-chemical reaction in Equation (2-3) describes the hydrolysis of one mole of urea [$CO(NH_2)_2$] to one mole of ammonia [NH_3] and one mole of carbamic acid [NH_2COOH] as catalyzed by microbial urease. Subsequently, the one mole of carbamic acid is spontaneously hydrolyzed to an additional mole of ammonia and one mole of carbonic acid [H_2CO_3] as shown in Equation (2-4).

(Eq. 2-3) $$CO(NH_2)_2 + H_2O \rightarrow^{urease} NH_2COOH + NH_3$$

(Eq. 2-4) $$NH_2COOH + H_2O \rightarrow NH_3 + H_2CO_3$$

Carbonic acid is equilibrated in water to form bicarbonate ions as shown in Equation (2-5), and the two moles of ammonia are equilibrated to form two moles of ammonium [NH^+_4] and two moles of hydroxide [OH^-] ions as described in Equation (2-6).

(Eq. 2-5) $$H_2CO_3 \leftrightarrow HCO_3^- + H^+$$

(Eq. 2-6) $$2NH_3 + 2H_2O \leftrightarrow 2NH_4^+ + 2OH^-$$

The production of hydroxide ions raises the pH of the solution and shifts the bicarbonate equilibrium to carbonate ions [CO^-_3] as in Equation (2-7) (Fujita et al. 2008). Since the surface of most bacterial cells is negatively charged (Mitchell and Santamarina, 2005), calcium ions in a supersaturated environment are attracted to the cellular surface and react with the carbonate ions produced to precipitate $CaCO_3$ as in Equation (2-8).

(Eq. 2-7) $$HCO_3^- + H^+ + 2OH^- \leftrightarrow CO_3^- + 2H_2O$$

(Eq. 2-8) $$Cell\ Ca^{+2} + CO_3^- \rightarrow Cell\ CaCO_3$$

Precipitation of $CaCO_3$ in solution typically begins with the formation of an amorphous form of $CaCO_3$ with low stability and high solubility, followed by a transformation into a metastable and transitional phase known as vaterite, and ending in the subsequent transformation into the more thermodynamically stable calcite (Spanos and Koutsoukos 1998). Several calcium sources have been shown to produce different phases of $CaCO_3$, and calcium chloride is reported to produce calcite most frequently (Gorospe et al. 2013).

pH is an important factor in the efficiency of the biomineralization process. Urease is only active in environments with pH values suitable for urea hydrolysis. For instance, Stocks-Fisher et al. (1999) report maximum urease activity in *Bacillus pasteurii* (now *Sporosarcina pasteurii*) at a maximum pH = 8.0, after which a steep decline in activity is observed. Furthermore, if pH levels become acidic, any precipitated $CaCO_3$ will begin to dissolve as opposed to fostering further precipitation in the above chain of reactions. Consequently, it has been observed that $CaCO_3$ precipitation is optimum at pH = 8.7 – 9.5 (Ferris et al. 2003).

The biological nature of MICP has made it an appealing and environmentally friendly process to be used as a ground improvement method. Microorganisms already play a natural role in the formation of many soils and can alter soil behaviour (Mitchell and Santamarina 2005). By harnessing the bio-chemical reactions involved in MICP, strength and stiffness of soils can be purposefully improved to meet specific geotechnical requirements.

Most notably, DeJong et al. (2010) present an overview of the bio-mediated calcite precipitation process and its application in the improvement of soil engineering properties. Based on observations made by Mitchell and Santamarina (2005), who established that microbial transport through a soil matrix is partly controlled by the size of a single bacterium relative to size of a soil's pore-throat (estimated using D_{10}, i.e. the particle diameter at which 10% of the soil mass is finer), as well as other studies, DeJong et al. (2010) present approximate guidelines on the geometric limitations of applying microbiological treatments in soils. The region defined by the ratios 1:2 and 1:200 in Figure 2-1 indicates the range of particle sizes suitable for MICP treatment. Additionally, following an experimental program by flushing an MICP treatment reagent through samples of Ottawa 50 -70 sand using *Bacillus pasteurii* (now known as *Sporosarcina pasteurii*) as the ureolytic bacteria, DeJong et al. (2006) analyzed the effect of MICP treatment on the soil matrix. Scanning electron microscopy (SEM) images revealed that a greater concentration of $CaCO_3$ precipitated at the particle-to-particle contacts, which led to a reduction of pore-space and an increase in solids content. Because cementation increases the shear stiffness of soils, bender element (BE) tests were used to measure shear-wave velocity (V_s) and monitor the bio-mediated method as several flushes were applied. V_s was seen to increase with each application of the treatment, reaching a maximum limit where no further increase was observed with respect to time. The first application caused a strong increase in V_s of about 60 m/s, which the researchers attributed to the initial binding of the microbes to the soil matrix. The response to undrained monotonic loading was also studied in a series of isotropically consolidated triaxial compression tests (TxC) performed at the end of the sequence of treatment flushes, and revealed the modified behaviour of the sand, from originally contractive in its untreated state to dilative after 11 applications of MICP treatment. The results showed a remarkable increase in strength and a slight increase in the critical stress ratio (M) of the sand, which the researchers attributed to the combined effects of bio-densification, increased particle angularity, and particle cementation.

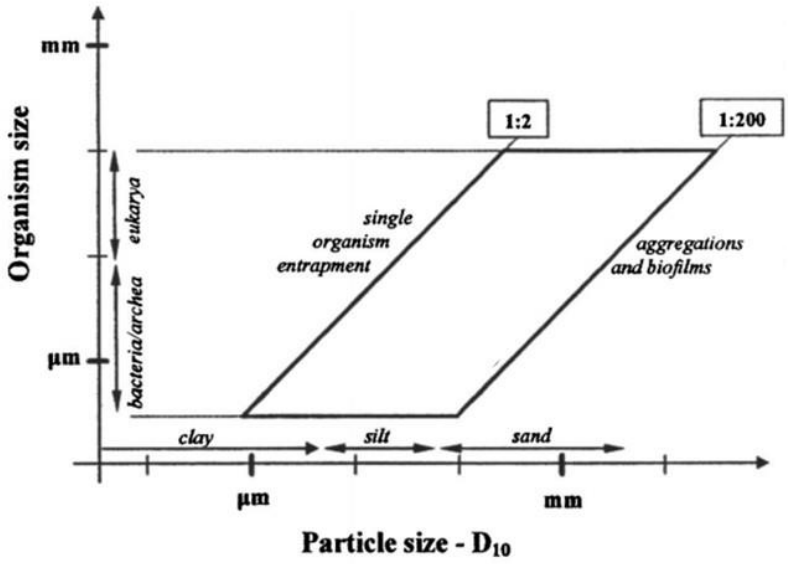

Figure 2-1: Bacterial size limits for use in the treatment of soils showing the organism to particle size ratio boundaries for single organism entrapment and biofilm generation. Adapted from Mitchell and Santamarina (2005).

Regarding the shearing behaviour of an MICP-treated sand, Feng and Montoya (2016) established that cementation level and confining pressure were the two influential factors. Their experimental program consisted of drained isotropically consolidated TxC tests on Ottawa 50 – 70 sand, flushed with an MICP treatment solution of *S. pasteurii*. The samples were treated to various degrees of cementation and consolidated to mean pressures (p'_c) of 100, 200, and 400 kPa. Greater cementation levels in the sand resulted in higher stiffness and strength gains, while higher confining stresses seemed to restrict the dilative tendency produced by higher cementation levels. While the residual friction angle increased at higher cementation levels, it was shown to decrease with increasing confining stress. Although not specifically highlighted by these researchers, the treatment was shown to cause an upshift in the location of the critical state line (CSL) in the void ratio versus effective stress space.

In a separate study, Feng and Montoya (2017) contend that the effectiveness of MICP in improving a sand's shear strength was better evaluated by measuring its shear-wave velocity (V_s) than by estimating the mass of precipitated calcite. Their experimental program consisted of two similar

triaxial specimens of Ottawa 50 – 70 sand, flushed several times with an MICP treatment using *S. pasteurii* to produce the same mass of precipitated calcite but with different V_S. The samples were subsequently subjected to cyclic loading to compare the difference in cyclic resistance after reaching a maximum V_S. Their results indicated that the specimen with a higher V_S indeed possessed a much higher liquefaction resistance, sustaining a total of ~968 cycles before liquefying. In contrast, the specimen with a lower V_S only required ~105 cycles to fail. The difference in cyclic resistance was ultimately attributed to differences in the uniformity of cementation as well as the cementation fabric between the two specimens.

The influence of bacterial growth stage on the effectiveness of MICP treatment in sand was studied by Chou et al. (2011). Samples of ground silica sand (99.7 % quartz) were flushed with an MICP treatment using *S. pasteurii* prepared at three different cell concentrations, namely 10^3 and 10^7 CFU/mL, and dead cells. The relative increase in shear strength was evaluated in a series of direct shear tests. Bacterial growth was found to continue during treatment inside the samples inoculated with live bacteria, as exhibited by changes in pH and concentrations of urea and calcium. With regards to their shear strength, these samples were shown to experience an increase in friction angle, with those treated at higher cell densities exhibiting a friction angle of 38^o (compared to 27^o for the untreated sand). In contrast, dead cells produced a negligible increase in strength.

Indigenous bacteria in natural soil have also been stimulated to induce the precipitation of $CaCO_3$. Burbank et al. (2013) treated natural alluvial sand samples with an enrichment solution containing molasses and urea to promote the growth of native bacteria that can use urea as a nitrogen source. Their laboratory cone-penetration tests showed an increase in tip resistance after treatment relative to the untreated sand. Similarly, cyclic triaxial testing showed a remarkable increase in cyclic resistance, with the cyclic resistance increasing by 2.5 to 4.5 times that of untreated samples. This significant improvement in behaviour was attributed to the highly uniform distribution of $CaCO_3$ precipitation. Cyclic liquefaction mitigation through MICP has also been studied by Zamani et al. (2018). In cyclic triaxial tests on three types of silica sand, each with distinct particle properties, the improvement in cyclic resistance due to MICP treatement was shown to be influenced by grain size and shape. Sands with more angular particle shapes or with smaller particle sizes exhibited greater levels of improvement.

In contrast to the typical application of MICP in sand specimens through flushing or injection, Cheng and Shahin (2016) investigated the effects of combining the precipiated $CaCO_3$ at its early unstable stages (which they called bio-slurry) with pure silica sand. The bio-slurry was prepared by mixing Bacillus *sphaericus* bacterial culture with specific amounts of urea and calcium chloride, and separating the precipitated crystal "slurry". After mixing the sand with bio-slurry and depositing the mixture into sand columns, the distribution of urease activity was observed to be highly uniform throughout, with rhombohedral $CaCO_3$ crystals forming predominatly in the pore-space as consequence of the high (95%) and uniform retention of the bioslurry. The strength of the treated sand and the effects of subsequent multiple cementation solution flushes in the sand's mechanical behaviour, as measured in unconfined compression strength (UCS) tests, showed that compressive strength seemed to asymptotically increase and reach a maximum value with each additional flush, exhibiting a decrease in treatment efficiency from flush to flush. This was explained as being caused by the encapsulation of the bacterial cells, which resulted in a consistent decrease in urease activity.

The effects of the many possible conditions, such as freeze-and-thaw and acid rain exposure, that may impact the applicability of MICP at large scales were studied in a very comprehensive assessment by Cheng et al. (2012). In their study, these researchers investigated the effects of bio-cementation with a Bacillus *sphaericus* bacterial culture at different levels of saturation (30, 65, and 100%) and cementation (measured in $CaCO_3$ content), as well as its effects on strength and durability. Pure silica sand (both coarse and fine) columns were prepared and flushed in a controlled manner with cementation reagents to achieve the prescribed saturation and cementation levels. Triaxial compression tests on the treated specimens show that higher effective shear strength parameters (i.e. cohesion and effective friction angle) were achieved at 30% saturation, with higher exponential gains in strength with increasing $CaCO_3$ content. Fine sand samples were observed to derive their higher strength mainly from increases in cohesion rather than in friction angle. Unconfined compression strength (UCS) tests conducted in samples exposed to 10 cycles of freezing and thawing (FT) in order to assess the treatment's durability show that a less than 10% reduction in strength was produced as consequence of the FT cycles. Thorugh SEM imaging, the crystals formed at particle-particle contacts were seen to maintain the connection without restricting porewater mobility during the FT cycles. Lastly, due to the carbonate nature of MICP cementation, acid rain may be detrimental to its strengthening effects in cohesionless soils.

Therefore, additional UCS tests were conducted on MICP treated samples exposed to artificial acid rain (pH = 3.5) flush cycles. As a result, MICP cementation was seen to continuously erode; and after flushing 12 L of acid rain, UCS results show an insignificant reduction of strength in the bottom section of the sand column and a 40% strength reduction in the top section.

2.4. References

Alarcon-Guzman, A., Leonards, G., and Chameau, J. L. (1988). Undrained monotonic and cyclic strength of sands. *Journal of Geotechnical Engineering*, 114(10), 1089-1109.

Anbu, P., Kang, C. H., Shin, Y. J., and So, J. S. (2016). Formations of calcium carbonate minerals by bacteria and its multiple applications. *SpringerPlus*. doi:DOI 10.1186/s40064-016-1869-2.

Al-Tarhouni, M. (2008). *Liquefaction and Post-liquefaction Behaviour of Gold Mine Tailings under Simple Shear Loading.* Ottawa: Carleton University.

Al-Tarhouni, M., Simms, P., and Sivathayalan, S. (2011). Cyclic behaviour of reconstituted and desiccated-rewet thickened gold tailings in simple shear. Canadian Geotechnical Journal, 48(7),1044.

Bavendamm, W. (1932). Die mikrobiologische Kalkfällung in der tropischen. *Arch Microbiol*, 3:205–276.

Been, K., and Jeffries, M. G. (1985). A state parameter for sands. *Geotechnique*, 35(2), 99-112.

Been, K., Jeffries, M. G., and Hachey, J. E. (1991). The critical state of sands. *Geotechnique*, 41(3), 365-381.

Bosak, T., and Newman, D. K. (2003). Microbial nucleation of calcium carbonate in the Precambrian. *Geology*, 31:577–580.

Bosak, T., and Newman, D. K. (2005). Microbial kinetic controls on calcite morphology in supersaturated solutions. *J Sed Res*, 75:190–199.

Bosak, T., Stolarski, J., and Meiborn, A. (2015). Microbial Formation and Degradation of Carbonates. In H. L. Ehrlich, D. K. Newman, and A. Kappler, *Ehrlich's Geomicrobiology* (6th ed., pp. 209-236). Chapman and Hall/CRC.

Burbank, M., Weaver, T., Lewis, R., Williams, T., Williams, B., and Crawford, R. (2013). Geotechnical Tests of Sands Following Bioinduced Calcite Precipitation Catalyzed by

Indigenous Bacteria. *J. Geotech. Geoenviron. Eng.*, 139(6): 928-936. doi:10.1061/(ASCE)GT.1943-5606.0000781

Casagrande, A. (1936). Characteristics of cohesionless soils affecting the stabilityof earth fills. *Journal of Boston Society of Civil Engineers*, 23, 257-276.

Chafetz, H. S., and Buczynski, C. (1992). Bacterially induced lithification of microbial mats. *Palaios*, 7:277–293.

Chang, N. (2009). *The Effect of Fabric on the Behaviour of Gold Tailings.* Hatfield: University of Pretoria.

Chang, N., Heymann, G., and Clayton, C. (2011). *The effect of fabric on the behaviour of gold tailings.* Géotechnique 2011 61:3, 187-197.

Cheng, L., Cord-Ruwisch, R., and Shahin, M. A. (2013). Cementation of sand soil by microbially induced calcite precipitation at various degrees of saturation. *Canadian Geotechnical Journal*, 50(1), 81-90. doi:10.1139/cgj-2012-0023

Cheng, L., Shahin, M. A., and Cord-Ruwisch, R. (2014). Bio-cementation of sandy soil using microbially induced carbonate precipitation for marine environments. *Geotechnique*, 64, No. 12, 1010–1013. Retrieved from http://dx.doi.org/10.1680/geot.14.T.025.

Cheng, L., and Shahin, M. A. (2016). Urease active bioslurry: A novel soil improvement approach based on microbially induced carbonate precipitation. *Canadian Geotechnical Journal*, 53(9), 1376-1385. doi:10.1139/cgj-2015-0635

Chou, C. W., Seagren, E. A., Aydilek, A. H., and Lai, M. (2011). Biocalcification of Sand through Ureolysis. *Journal of Geotechnical and Geoenvironmental Engineering*, 1179–1189. doi:10.1061/(ASCE)GT.1943-5606.0000532.

DeJong, J. T., Fritzges, M. B., and Nüsslein, K. (2006). Microbially Induced Cementation to Control Sand Response to Undrained Shear. *Journal of Geotechnical and Geoenvironmental Engineering*, 1381–1392.

DeJong, J. T., Mortensen, B. M., Martinez, B. C., and Nelson, D. C. (2010). Bio-mediated soil improvement. *Ecological Engineering*, 36: 197–210.

Dobry, R., Vasquez-Herrera, A., and Ramly, M. (1985). Liquefaction flow failure of silty sand by torsional cyclic tests. *Advances in the art of testing soils under cyclic conditions* (pp. 29-50). Detroit, MI: ASCE.

Feng, K., and Montoya, B. M. (2016). Influence of Confinement and Cementation Level on the Behavior of Microbial-Induced Calcite Precipitated Sands under Monotonic Drained Loading. *J. Geotech. Geoenviron. Eng.,* 142(1): 04015057. doi:10.1061/(ASCE)GT.1943-5606.0001379.

Feng, K., and Montoya, B. M. (2017). Quantifying Level of Microbial-Induced Cementation for Cyclically Loaded Sand. *Journal of Geotechnical and Geoenvironmental Engineering*, 143(6):. doi:10.1061/(ASCE)GT.1943-5606.0001682

Ferrer, M. R., Quevedo-Sarmiento, J., Bejar, V., Delgado, R., Ramos-Cormenzana, A., and Rivadeneyra, M. A. (1988). Calcium carbonate formation by Deleya halophila: Effect of salt concentration and incubation temperature. *Geomicrobiol J*, 6:49–57.

Ferris, F. G., Fratton, C. M., Gerits, J. P., Schultze-Lam, S., and Lollar, B. S. (1995). Microbial precipitation of a strontium calcite phase at a groundwater discharge zone near Rock Creek, British Columbia, Canada. *Geomicrobiol J* , 13:57–67.

Ferris, F. G., Phoenix, V., Fujita, Y., and Smith, R. W. (2003). Kinetics of calcite precipitation induced by ureolytic bacteria at 10 to 20 °C in artificial groundwater. *Geochim Cosmochim Acta*, 67:1701–1710.

Fourie, A. B., Blight, G. E., and Papageorgiou, G. (2001). Static liquefaction as a possible explanation for the Merriespruit tailings dam failure. *Canadian Geotechnical Journal*, 8(4), 707–719.

Fourie, A., and Papageorgiou, G. (2001). Defining an appropriate steady state line for Merriespruit gold tailings . *Canadian Geotechnical Journal*, 38, 4: pp.695-706.

Fourie, A. B., and Tshabalala, L. (2005). Initiation of static liquefaction and the role of K^sub 0^ consolidation. *Canadian Geotechnical Journal*, 42(3), 892-906. Retrieved from https://www-lib-uwo-ca.proxy1.lib.uwo.ca/cgi-

bin/ezpauthn.cgi?url=http://search.proquest.com.proxy1.lib.uwo.ca/docview/213356536?accountid=15115

Fujita, Y., Taylor, J. L., Gresham, T., Delwiche, M., Colwell, F., McLing, T., . . . Smith, R. (2008). Stimulation of microbial urea hydrolysis in groundwater to enhance calcite precipitation. *Environ Sci Technol*, 42:3025–3032.

Gorospe, C., Han, S., Kim, S., Park, J., Kang, C., Jeong, J., and So, J. (2013). Effects of different calcium salts on calcium carbonate crystal formation by Sporosarcina pasteurii KCTC 3558. *Biotechnology and Bioprocess Engineering*, 903-908. doi:10.1007/s12257-013-0030-0

Jeffries, M., and Been, K. (2016). *Soil Liquefaction -- A Critical State Approach, 2nd Ed.* Boca Raton: Taylor and Francis Group.

Kramer, S. L. (1996). *Geotechnical earthquake engineering*. Upper Saddle River, N.J: Prentice Hall

Krumbein, W. E. (1974). On the precipitation of aragonite on the surface of marine bacteria. *Naturwissenschaften*, 61:167.

Martinez, B. C. (2012). *Up-Scaling of Microbial Induced Calcite Precipitation in Sands for Geotechnical Ground Improvement.* UC Davis, Civil and Environmental Engineering. Ann Arbor, MI: UMI.

Martinez, B. C. (2013). *Up-scaling of microbial induced calcite precipitation in sands for geotechnical ground improvement.* Ann Arbor, MI: ProQuest LLC.

Mitchell, J. K., and Santamarina, J. C. (2005). Biological Considerations in Geotechnical Engineering. *J. Geotech. Geoenviron. Eng.*, 131(10): 1222-1233.

Montoya, B. M. (2012). *Bio-mediated soil improvement and the effect of cementation on the behavior, improvement, and performance of sand.* Ann Arbor, MI: ProQuest LLC.

Montoya, B. M., and DeJong, J. T. (2015). Precipitation, Stress-Strain Behavior of Sands Cemented by Microbially Induced Calcite. *J. Geotech. Geoenviron. Eng.*, 141(6): 04015019. doi:10.1061/(ASCE)GT.1943-5606.0001302.

Montoya, B. M., Dejong, J. T., and Boulanger, R. W. (2013). Dynamic response of liquefiable sand improved by microbial-induced calcite precipitation. *Geotechnique 63*, No. 4, 302–312. Retrieved from http://dx.doi.org/10.1680/geot.SIP13.P.019

Monty, C. L. (1972). Recent algal stromatolitic deposits, Andros Island, Bahamas. Preliminary report. *Geol Rundschau*, 61:742–783.

Murtala, U., Khairul, A. K., and Kenny, T. P. (2016). Biological process of soil improvement in civil engineering: A review. *Journal of Rock Mechanics and Geotechnical Engineering*, 767-774. Retrieved from http://dx.doi.org/10.1016/j.jrmge.2016.02.004

Papageorgiou, G. (2004). *Liquefaction Assessment and Flume Modelling of the Merriespruit Gold and Bafokeng Platinum Tailings.* Johannesburg: University of the Witwatersrand.

Pitman, T. D., Robertson, P. K., and Sego, D. C. (1994). Influence of fines on the collapse of loose sands. *Canadian Geotechnical Journal*, 31(5): 728-739. Retrieved from https://doi-org.proxy1.lib.uwo.ca/10.1139/t94-084

Qiu, Y., and Sego, D. (2001). Laboratory Properties of Mine Tailings. *Canadian Geotechnical Journal*, 38:pp. 183-190.

Roscoe, K., Schofield, A. N., and Wroth, C. P. (1958). On the yielding of soils. *Geotechnique*, 8(1), 22-53.

Sadrekarimi, A. (2013). Influence of fines content on liquefied strength of silty sands. *Soil Dynamics and Earthquake Engineering* 55 (2013) 108–119. DOI: http://dx.doi.org/10.1016/j.soildyn.2013.09.008

Sadrekarimi, A., and Olson, S. M. (2012). Effect of Sample-Preparation Method on Critical-State Behaviour of Sands. *Geotechnical Testing Journal*,, ol. 35, No. 4, 2012, pp. 548-562. Retrieved from https://doi-org.proxy1.lib.uwo.ca/10.1520/GTJ104317

Schnaid, F., Bedin, J., Viana da Fonseca, A., and de Moura Costa Filho, L. (2013). Stiffness and Strength Governing the Static Liquefaction of Tailings. *Journal of Geotechnical and Geoenvironmental Engineering*, Vol. 139, No. 12, pp. 2136-2144.

Schofield, A., and Wroth, C. P. (1968). *Critical state soil mechanics.* London, UK: McGraw Hill.

Seed, H.B. 1987. Design problems in soil liquefaction. *Journal of Geotechnical Engineering Division*, ASCE, 113(8): 827-845.

Spanos, N., and Koutsoukos, P. G. (1998). The transformation of vaterite to calcite: effect of the conditions of the solution in contact with the mineral phase. *Crystal Growth*, 191:783–790.

Stocks-Fischer, S., Galinat, J. K., and Bang, S. S. (1999). Microbiological precipitation of CaCO3. *Soil Biology and Biochemistry*, 31: 1563-1571.

Sladen, J. A., D'hollander, R. D., Krahn, J. (1986). Liquefaction of sands, a collapse surface approach, *can geotech J* V22, N4, nov 1985, P564–P578. *International Journal of Rock Mechanics and Mining Sciences and Geomechanics Abstracts*, 23(4), 138-138. doi:10.1016/0148-9062(86)90748-5

Terzaghi, K., Peck, R., and Mesri, G. (1996). *Soil Mechanics in Engineering Practice, 3rd Ed.* John Wiley and Sons.

Thompson, J. B., and Ferris, F. G. (1990). Cyanobacterial precipitation of gypsum, calcite and magnesite from natural alkaline lake waters. *Geology*, 18:995–998.

Vaid, Y. P., and Sivathalayan, S. (1996). Static and cyclic liquefaction potential of FRaser Delta sand in simple shear and triaxial tests. *Canadian Geotechnical Journal*, 33(2), 281-289.

Weast, R. C., and Astle, M. J. (Eds.). (1982). *CRC Handbook of Chemistry* (63rd ed.). Boca Raton, FL: CRC Press.

Wijewickreme, D., Sriskandakumar, S., and Byrne, P. (2005). Cyclic loading response of loose air-pluviated fraser river sand for validation of numerical models simulating centrifuge tests. *Canadian Geotechnical Journal*, 42(2), 550-561. doi:10.1139/t04-119

Zamani, A., and Montoya, B. M. (2018). Undrained Monotonic Shear Response of MICP-Treated Silty Sands. *J. Geotech. Geoenviron. Eng.*, 144(6): 04018029. doi:10.1061/(ASCE)GT.1943-5606.0001861

Zamani, A., Feng, K., and Montoya, B. M. (2018). Improved Liquefaction Resistance from Microbial Induced Carbonate Cementation. *Geotechnical Earthquake Engineering and Soil Dynamics*, 296-303.

Chapter 3

3. Static Liquefaction Analysis of the Fundão Dam Failure

3.1. Introduction

Continued failure of tailings dams around the world in the last few decades has brought about many interrelated implications to the global mining community. Statistics taken from 1970 to 2001 indicate that 1 in every 700 tailings dams failed every year during that time period (LePoudre 2015). The fatal and costly consequences of many of these disasters have undoubtedly increased a negative publicity, undermining the credibility of the mining industry and jeopardizing its social license to operate (Blight 2010). By focusing on the failure of Fundão dam, one of the costliest tailings dam disasters in recent years, the objectives of this study are to investigate the static liquefaction phenomenon hypothesized to have caused the dam's collapse, and to demonstrate the need to implement a static liquefaction analysis method that accounts for real field conditions. The stability of the Fundão dam's failing slope is evaluated by modifying the static liquefaction triggering and flow failure analyses method developed by Sadrekarimi (2016) for constant-shear stress paths and employing the dam's geotechnical characterization and advanced testing data obtained and reported by Morgenstern et al. (2016).

3.1.1. History of Fundão dam

The Fundão dam was an iron tailings impoundment built in the state of Minas Gerais, Brazil. Due to the use of separation by gravity and subsequent flotation concentration methods in iron mining (Vick 1990), two types of tailings were produced and delivered separately in slurry form to the dam: sand tailings, which consisted of a mixture of sand-sized and finer silt particles that were free-draining but susceptible to liquefaction when loose and saturated; and slimes, which in contrast were much finer and clay-like in nature with low permeability (Morgenstern et al. 2016). Initial design of the embankment made use of a compacted earth fill starter dam that was to be raised using the upstream method. The sands deposited behind the dike would in turn retain slimes deposited farther upstream, and with a sand beach-distance of not less than 200 m, they would

prevent these water-borne slimes from being deposited near the crest (Morgenstern et al. 2016). Based on this initial design, saturation of the sands was to be prevented by a high-capacity drainage system built at the base of the starter dam that would allow free-drainage of water from the deposited sands.

A series of incidents beginning shortly after construction in 2009 required certain modifications to the initial plans and promoted the eventual triggering of static liquefaction in the sands (Morgenstern et al. 2016). The first of these was the discovery of construction defects in the base drain that forced the closure of the entire drainage system. The revised design made use of a blanket drain that had to be built at a higher elevation due to the existing height of contained tailings in the impoundment, thus allowing more widespread saturation of the sands. The second incident involved the mismanagement of the sand-slime beach required to prevent slime deposits and water encroachment near the embankment's crest, which allowed slimes to settle out in areas closer to the crest than originally designed. The third and last incident was the structural deficiency of the concrete conduit beneath the dam's left abutment, which was found incapable of sustaining any further loading generated by raising of the dam. Consequently, the alignment of the embankment's crest was set back towards the tailings pool in order to reduce loading on the concrete conduit but placed the embankment directly over previously deposited slimes at the left abutment. Lastly, although not believed to have directly triggered the flow failure, a series of three small seismic shocks that occurred three hours before the breach may have slightly accelerated the hypothesized failure mechanism.

On November 5th, 2015 the Fundão tailings storage dam failed in a liquefaction flow slide that began at the embankment's left abutment where the alignment setback had been built. The slide released a significant volume of saturated tailings that swept away the nearby town of Bento Rodrigues, killed 19 villagers, and caused a major environmental disaster (da Fonseca and da Fonseca 2016).

Liquefaction flow sliding was found to have been triggered in the left abutment, because it presented all the necessary conditions for static liquefaction to occur in contrast to those in the right abutment. The more compressible slimes that had encroached the sand beach area inhibited the free-drainage required to control the phreatic surface, enhancing saturation and inducing undrained shearing of the tailings (Morgenstern et al. 2016), and were ultimately located beneath

the slope during upstream-raising of the dam as consequence of the crest setback. Conversely, drained conditions continued to govern in the right abutment, where more favorable lower piezometric conditions existed, and no lateral spreading was induced due to the nearly complete absence of slimes.

3.2. Problem statement and objective

Following the failure, a Review Panel (Panel) was formed to investigate the cause of the failure which is described in a technical report Static liquefaction of the tailings in the left abutment was identified as the cause of the Fundão dam's failure by the Panel. The "Report on The Immediate Causes of the Failure of Fundão Dam" by Morgenstern et al. (2016) describes two different loading conditions that can induce static liquefaction, and later identifies one of them as the mechanism that led to the dam's collapse.

Figure 3-1(a) presents different stress paths from two direct simple-shear (DSS) tests carried out in this study on gold sand tailings specimens consolidated to a vertical stress (σ'_{vc}) of 400 kPa and relative densities (D_{rc}) of 52 and 55%. In the undrained (i.e. constant-volume, CV) loading stress path, strain softening, and strength loss occur when the applied shear stress exceeds the undrained yield strength, S_u(yield). The instability line (IL) refers to the locus of yield points that projects as a straight line down to the origin of the stress path (Lade 1992; Chu et al. 2003). The strain softening produced after triggering undrained strength loss continues with further shear displacement until an undrained post-liquefaction strength, S_u(liq) is reached along the critical state line (CSL). A liquefaction flow failure would ensue if S_u(liq) falls below the applied shear stress. Conversely, the *drained constant-shear stress* (DCSS) unloading stress path describes a condition in which the sample is slowly unloaded with a constant applied shear stress in drained conditions. In this case, S_u(yield) is never exceeded, but as shown in Figures 3-1(b) and 3-1(c), a rapid increase in shear strain and decrease in void ratio occur approximately when the stress path crosses IL. This corresponds to a mobilized friction angle (ϕ'_{mob}), equal to the IL slope, termed the yield friction angle, ϕ'_{yield}. Morgenstern et al. (2016) identified this second mechanism, induced by the lateral spreading (deformation) of the slimes layer under the left abutment, as the behaviour that contributed to the Fundão dam's collapse. The observed explosion of a jet of dirty water out

of the drainage feature in the left abutment prior to dam failure indicated the existence of high pore water pressure beneath the dam probably caused by the rapid rate of rise. This further suggested that effective stress reduction and unloading were the probable liquefaction triggering mechanism. Similar cases, such as the static liquefaction failure of the Nerlerk berm in 1983, have also been attributed to foundation spreading due to deformations in the underlying softer layers (Hicks and Boughrarou 1998).

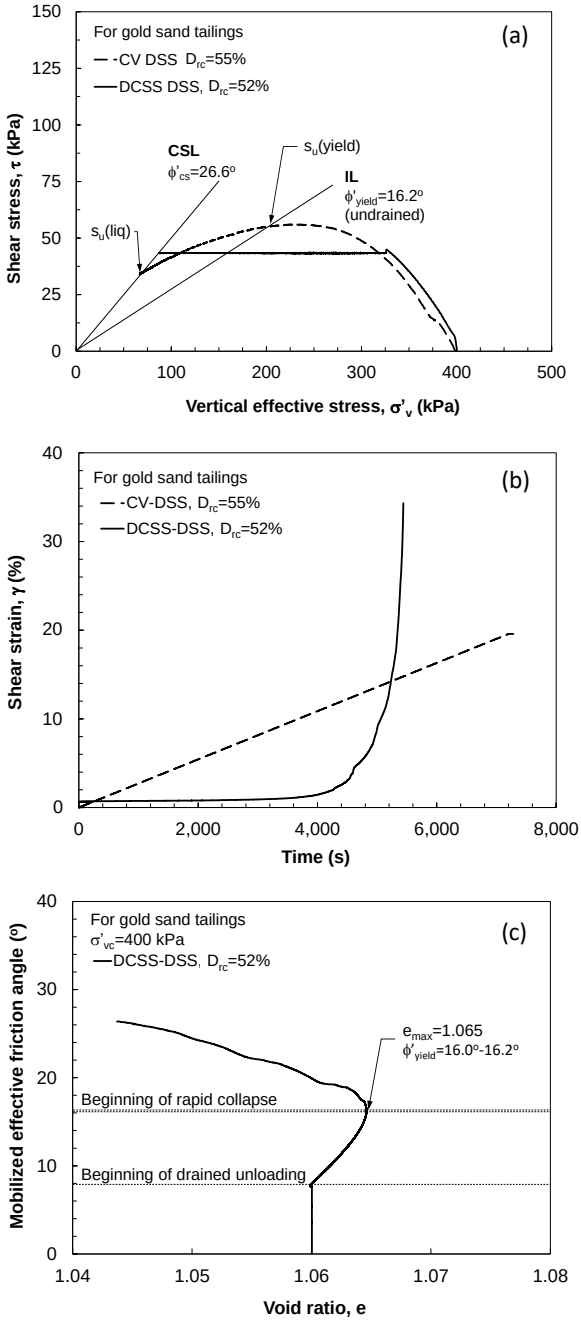

Figure 3-1: (a) Stress paths for undrained loading and for drained constant shear stress unloading of gold sand tailings; (b) Changes in shear strain with respect to time for both stress paths; (c) Changes in void ratio with mobilized friction angle for the drained constant shear stress test on gold sand tailings.

In addition to the triggering mechanism, Morgenstern et al. (2016) conducted a typical static liquefaction triggering analysis, whereby S_u(yield) of cohesionless tailings were determined by empirical correlations based on in-situ penetration tests. However, as noted by Sadrekarimi (2016), these correlations do not account for the effects of anisotropic consolidation, intermediate principal stress, and modes of shear in the degree of strain-softening and brittleness of cohesionless soils. Hence, in order to accurately characterize the shearing behaviour of loose saturated sand tailings in embankments such as the Fundão dam, a more thorough analysis must be undertaken using a procedure that incorporates variations in mode of shear and initial stress anisotropy for estimating ϕ'_{yield} from in-situ penetration tests. The goal in this study is to demonstrate the method's suitability for the evaluation of static liquefaction in hard-rock mine tailings impoundments.

3.3. Static liquefaction analysis

Liquefaction triggering analysis of the left abutment of the Fundão dam was carried out in this study by means of a series of Limit Equilibrium Analyses (LEA). This section describes the characteristics and strength parameters of Fundão's tailings required for computer modelling of the failing slope and the static liquefaction analysis conducted. No attempt was made to determine strains or displacements, since this type of analysis fell outside the scope of this study and would require a more sophisticated finite element analysis with an advanced constitutive model.

3.4. Fundão tailings material properties and deposition cycle

As mentioned earlier, the tailings found in the Fundão dam consisted of two different types, namely sand and slime tailings. The sand was classified as a cohesionless silty sand (SM) with a bulk unit weight of 19 kN/m^3, which depending on its density and saturation level was susceptible to liquefaction. In contrast, the iron slimes consisted of a low-plastic silt and clay (CL-ML) with liquid and plastic limits of 26% and 19%, respectively, and possessed low permeability that impeded the free flow of water. Figure 3-2 shows the average particle size distributions of both materials. Because of their contrasting features, the main design basis for the Fundão dam was to

maintain a separation of the two materials. Characterization and strength properties for both materials were obtained from laboratory and in-situ test results conducted by Morgenstern et al. (2016).

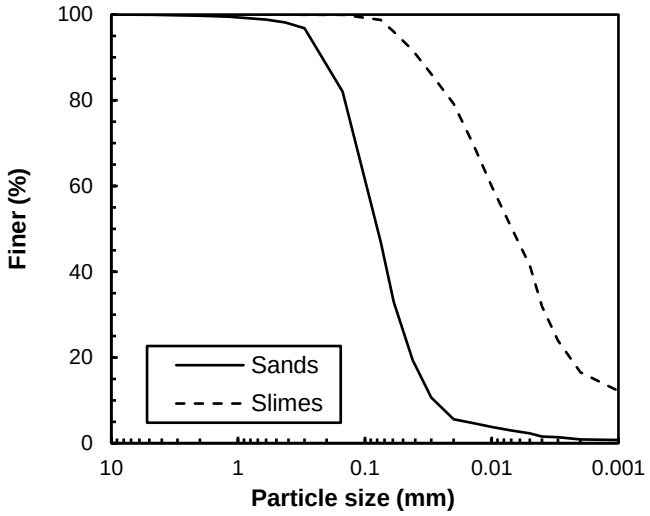

Figure 3-2: Average particle size distributions of sand and slime tailings at Fundão dam.

3.4.1. Dam geometry

A key element in the reconstruction of the dam's geometry and its materials for LEA was the determination of the deposition cycles and layers of slimes and sands. In order to estimate the extent of slimes deposited, a combination of data collected by Morgenstern et al. (2016) was used. The slimes boundaries identified ultimately represent areas where slime layers could have been present due to the ingress of pond water over the sloping sand deposit. A mass balance analysis conducted by Morgenstern et al. (2016) better defines the stratigraphy of the slimes, with a gradual transition from predominantly slimes to isolated slimes moving upslope towards the crest.

The slope geometry, the geotechnical and hydrogeological parameters, and the dam-raise and deposition time histories were obtained from Morgenstern et al. (2016). This information was used for the development of the computer model for Fundão dam's left abutment profile prior to failure as shown in Figure 3-3, as well as for the initial model parameters listed in Table 1-1 for the initial effective stress analysis. GeoSlope's SLOPE/W® software was used to define the dam section and

carry out the series of analyses. Figure 3-4 shows the cone penetration testing (CPT) profiles carried out about 9 months before the failure from the investigation report. These CPT results were used in this study to determine the in-situ strength of tailings in conjunction with the analytical method described in later sections.

Table 3-1: Parameters for the initial LEA model of Fundão dam's left abutment

Material	γ (kN/m^3)	ϕ'_{cs} [º]	c' [kPa]
Compacted sands	22	35	5
Loose sands	22	33	0
Slimes	22	28	0

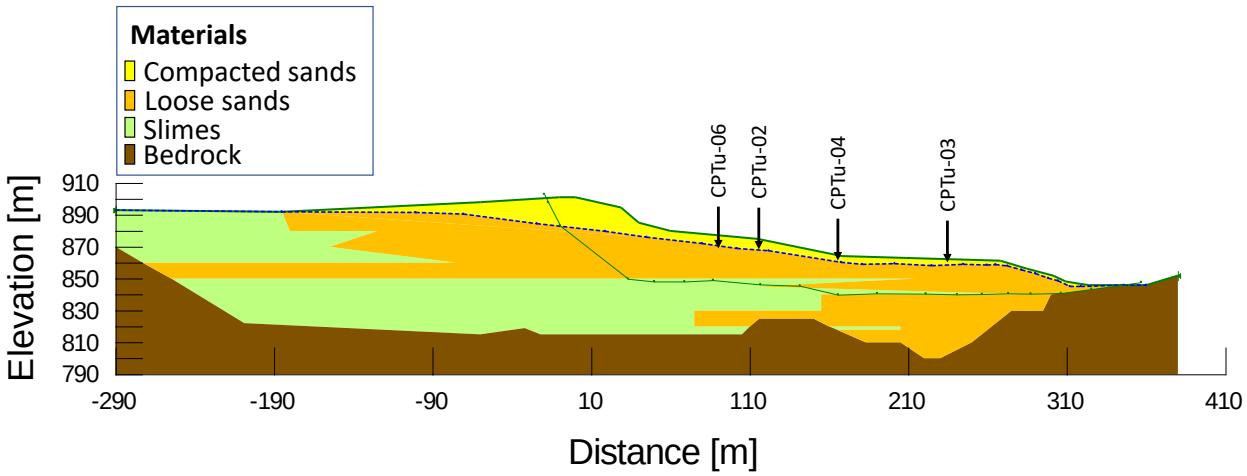

Figure 3-3: LEA model of Fundão dam's left abutment.

Another important element in modelling the dam for a liquefaction triggering analysis was the identification of the phreatic surface at the left setback where failure was described to have initiated. For this purpose, piezometric readings from nine piezometers were used by Morgenstern et al. (2016). As noted in the investigation report (Morgenstern et al. 2016), despite a steeply sloped stripped ground surface moving away from the left abutment, the piezometric records show a

relatively flat phreatic surface, implying the existence of an obstruction of drainage towards the blanket drain, supporting the believed presence of slimes below the dam fill.

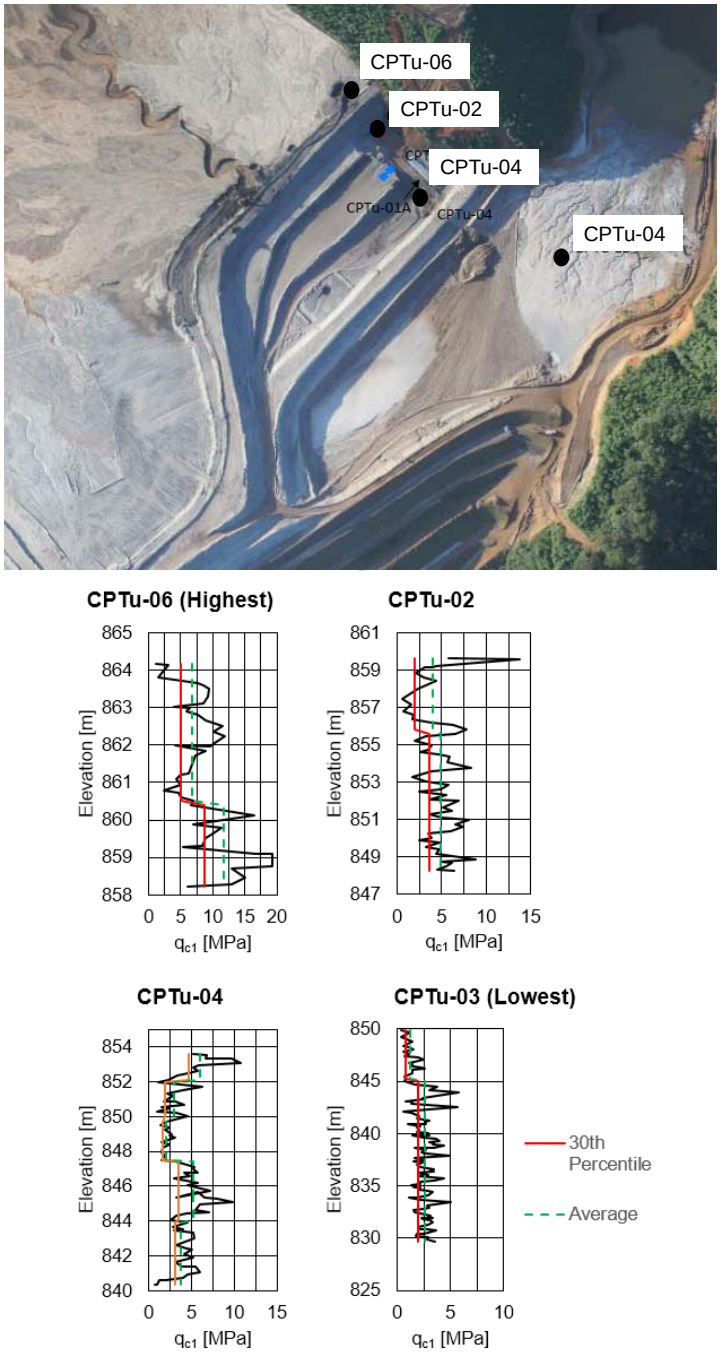

Figure 3-4: Profiles of CPT tip resistances through the iron mine tailings in Fundão dam (Morgenstern et al. 2016).

3.4.2. Description of Static Liquefaction Analysis

Static liquefaction analysis of the Fundão dam was carried out by first determining if rapid strength loss could have occurred in the loose cohesionless tailings under the given loading conditions. This is called the "liquefaction triggering analysis", which was accomplished here by comparing field loading conditions with the yield shear strength under which strain-softening and strength loss occur. The stability of the dam against flow liquefaction failure was subsequently examined once the dam zones undergoing static liquefaction were identified. These procedures are discussed in the following paragraphs.

The undrained strength of a loose cohesionless soil is typically characterized by undrained strength ratios: the undrained yield strength ratio, $S_u(yield)/\sigma'_{vo}$, and the undrained post-liquefaction strength ratio, $S_u(liq)/\sigma'_{vo}$. These ratios, which consist of the respective undrained strength normalized by the in-situ effective vertical stress prior to failure (σ'_{vo}), have found great use in the characterization of shear strength in laboratory testing and back-calculation of shear strength in liquefaction case studies (Been and Jefferies 1985; Olson and Stark 2003; Stark and Mesri 1992; Robertson 2010; Sadrekarimi and Olson 2011). There are presently several methods for determining the undrained strength of saturated cohesionless soils. These include expensive series of laboratory shear tests, numerical analysis of constitutive models, and using empirical correlations with in-situ penetration tests. As the most common approach in practice, empirical correlations with Standard Penetration Test (SPT) and Cone Penetration Test (CPT) have been developed from previous liquefaction flow failures by Mesri (2007), Olson and Stark (2003), and Stark and Mesri (1992). These are often used for estimating the in-situ triggering strength due to their simplicity, convenience, low cost, and nearly continuous measurements. However, these methods estimate the same value of undrained shear strength for a given penetration resistance, irrespective of the mode of shear, stress-induced anisotropy, and boundary conditions. A comprehensive liquefaction analysis must therefore consider the combined effects of all these, as these mechanisms produce microstructural strains and can have a profound effect on undrained triggering, $S_u(yield)$, and post-liquefaction, $S_u(liq)$, strengths (Sadrekarimi 2016). By combining soil behaviour from a large database of laboratory tests and from back-analyses of undrained strength in case histories of static liquefaction failures, Sadrekarimi (2016) introduced a procedure

for incorporating the effects of mode of shearing, stress anisotropy, and boundary conditions in predicting $S_u(yield)/\sigma'_{vo}$ and $S_u(liq)/\sigma'_{vo}$ from in-situ penetration tests.

As discussed earlier, $S_u(yield)/\sigma'_{vo}$ is not applicable for liquefaction triggered by a drained constant-shear stress path as hypothesized to have occurred during the Fundão dam failure. Irrespective of stress path, the instability line is an ideal representation of the liquefaction triggering condition. However, a major difficulty with ϕ'_{yield} is that an empirical relationship with in-situ penetration resistance does not exist. A different approach is pursued below to predict ϕ'_{yield} from $S_u(yield)/\sigma'_{vo}$ and an approximate change in effective vertical stress from σ'_{vo} to that at the triggering of static liquefaction, $\sigma'_v(yield)$.

(Eq. 3-1) $$\phi'_{yield} = tan^{-1}\left[\frac{s_u(yield)}{\sigma'_{v0}} \times \frac{\sigma'_{v0}}{\sigma'_v(yield)}\right]$$

According to Equation (1), ϕ'_{yield} could be determined if the vertical stress ratio, $\sigma'_{vo}/\sigma'_v(yield)$, representing the amount of effective stress reduction at the triggering of static liquefaction, is known. A very conservative estimate could be found with $\sigma'_{vo}/\sigma'_v(yield) = 1$. For a more accurate analysis, a series of constant-volume monotonic direct simple shear tests were carried out in this study to determine the probable range of $\sigma'_{vo}/\sigma'_v(yield)$. Since samples from the Fundão dam were not available for testing, these tests were carried out on gold sand tailings from a mining site in northern Ontario. These tailings were composed of angular to sub-angular particles with 10% fines content. Loose specimens were prepared by tamping moist tailings inside the specimen mold in order to resemble the moisture content and the minimal compaction of a sandy tailings embankment. Index characteristics of these tailings were $G_S = 3.10$, $e_{max} = 1.35$, and $e_{min} = 0.79$, all measured following ASTM standard procedures. Typical stress paths from these tests are shown in Figure 3-5, demonstrating static liquefaction behaviour.

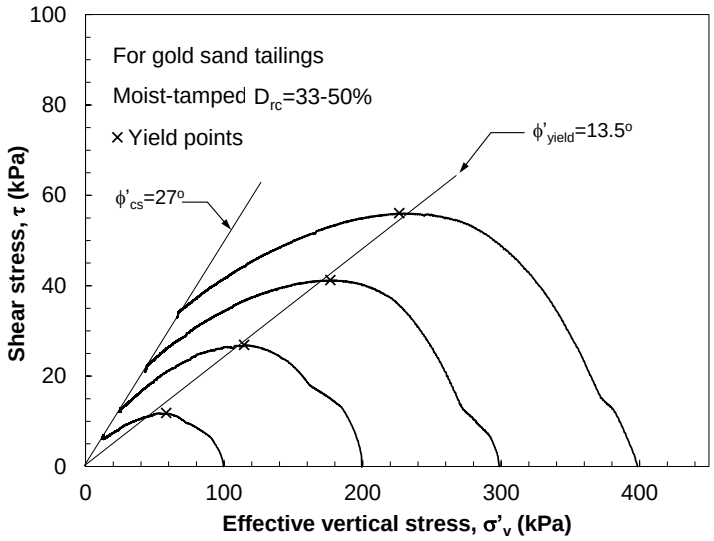

Figure 3-5: Typical stress paths of constant-volume DSS tests on gold sand tailings carried out in this study.

The ratios of σ'_{vo}/σ'_v(yield) obtained from all the tests are shown in Figure 3-6, where σ'_{vo} is the vertical stress after consolidation and prior to shearing. According to this figure, σ'_{vo}/σ'_v(yield) narrowly varies within a range of 1.68 to 1.96 with an average of 1.81. Data from several constant-volume DSS and undrained triaxial compression (TxC) tests by Morgenstern et al. (2016) on iron mine sand tailings are also added for comparison. The effective major principal stress was used to determine the vertical stress ratio, σ'_{1o}/σ'_1(yield) from the TxC tests.

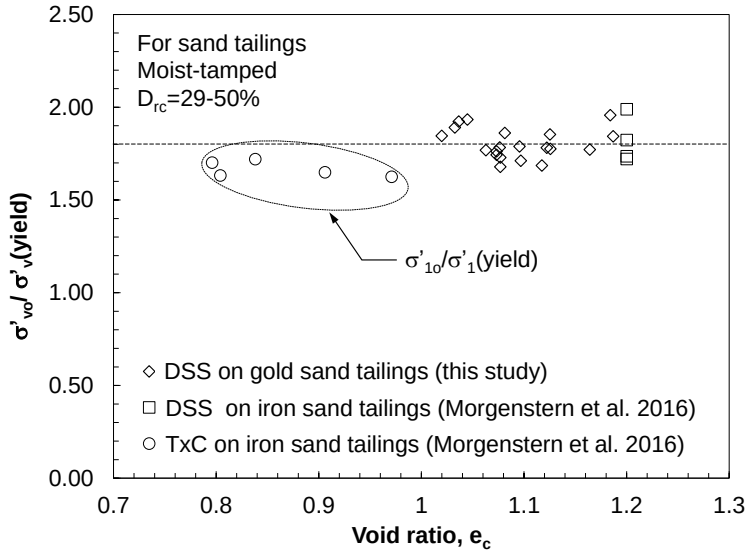

Figure 3-6: Ratios of σ'_{vo}/σ'_{v}(yield) from constant-volume DSS on gold sand tailings and undrained triaxial compression tests on iron sand tailings (Morgenstern et al. 2016).

By choosing the average σ'_{vo}/σ'_{v}(yield) = 1.81, ϕ'_{yield} can be calculated from S_u(yield)/σ'_{vo} and Equation (1). Using the Sadrekarimi (2016) analytical procedure for predicting S_u(yield)/σ'_{vo} from in-situ penetration resistance, Figure 3-7 shows trends of ϕ'_{yield} with q_{c1} for different modes of shear and consolidation stress ratio (K_C). The ranges of ϕ'_{yield} from our DSS tests, as well as those from a number of DSS and TxC tests carried out by the Panel on sandy tailings are shown for comparison. As presented, the derived values of ϕ'_{yield} from q_{c1} in simple-shear for a K_C value of 0.5 fall within the limits of those obtained through laboratory DSS testing. Assuming an average K_C = 0.54 in the DSS tests (estimated from $K_C = 1-\sin\phi'_{cs}$ for simple shear), the analytical method seems to accurately account for the effects of anisotropic consolidation and mode of shear in predicting ϕ'_{yield}. Likewise, the derived values of ϕ'_{yield} from q_{c1} in compression for a K_C value of 1.0 fall within the limits of those obtained through laboratory TxC testing of isotropically consolidated iron sand samples by the Panel.

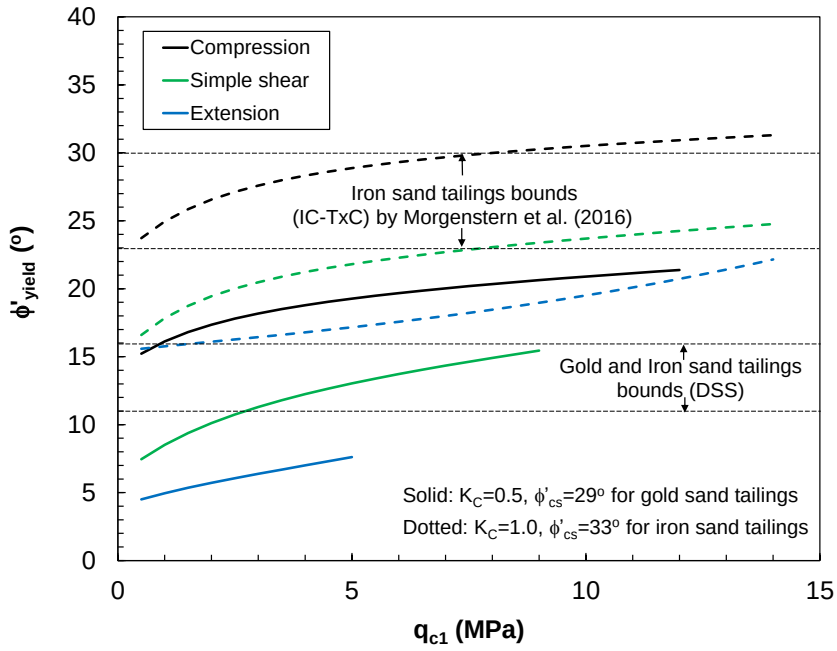

Figure 3-7: Comparison of ϕ'_{yield} estimated from q_{c1} with the range of those observed in DSS testing of gold sand tailings in this study and DSS and IC-TxC testing on iron sand tailings by Morgenstern et al. (2016).

Profiles of corrected cone penetration resistances (q_{c1}) from four digitized CPT readings (Morgenstern et al. 2016) adjacent to the section of the Fundão dam analyzed in this study were shown in Figure 3-4. Evaluation of these CPT readings led to a rough classification of tailings with respect to the USCS ranging from silty-sand to sand, as well as estimations of $S_u(yield)/\sigma'_{vo}$ and $S_u(liq)/\sigma'_{vo}$ in accordance with Sadrekarimi (2016). All else being equal, the layer with the lowest q_{c1} will have the least resistance to liquefaction. While the lowest value may be a testing error, higher values could be unconservative and may not sufficiently characterize the behaviour of loose tailings at critical locations (Rowe and Craig 1976; Jefferies and Been 2016). Consequently, average values were selected due to inherent uncertainties in selecting a representative q_{c1} value for a given liquefiable soil layer.

The method employed here consists of an iterative LEA procedure, in which ϕ'_{mob} at the base of each slice is compared against the ϕ'_{yield} for slices below the water level, accounting for the effects of mode of shear, plane-strain boundary conditions, and initial stress anisotropy (K_C). For the case

of sloping grounds (such as a tailings dam), the angle of a failure plane with respect to the horizontal (θ) varies along the failure surface. This variation produces further variations in principal stress directions, thus producing different modes of shear along the failure plane, ranging from compression near the crest, simple shear towards the seat, and extension near the toe. As illustrated in Figure 3-8, different modes of shear are approximately given based on the counter-clockwise angle of the failure plane to the horizontal (θ): for angles with $\theta > 15^o$, $15^o > \theta > -15^o$, and $\theta < -15^o$, compression, simple shear, and extension shear modes are respectively assigned. These ranges provide a simplified approach to relate the geometry of a failure surface to the loading conditions found in the field (Sadrekarimi 2016).

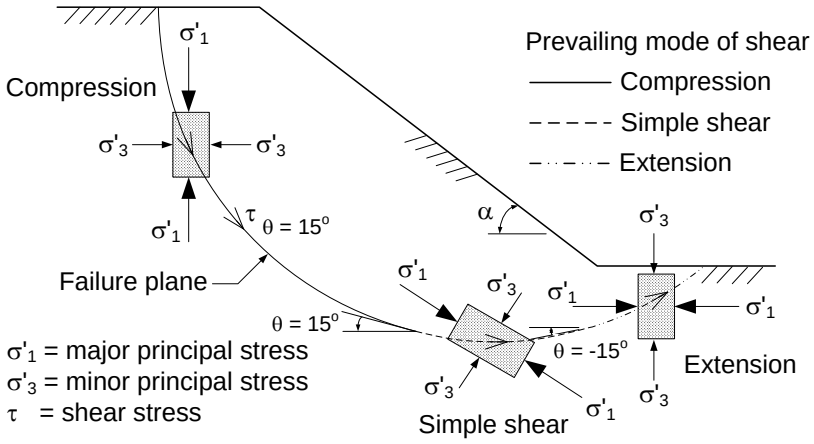

Figure 3-8: Variation of mode of shear along a failure surface (Sadrekarimi 2016).

The first LEA model was carried out to calculate K_C and ϕ'_{mob} at the base of each slice. Following the procedure described by Sadrekarimi (2016), values of $S_u(yield)/\sigma'_{vo}$ and $S_u(liq)/\sigma'_{vo}$ were calculated for different modes of shearing at the base of each slice below the water table based on the q_{c1} readings and K_C. Equation (1) was subsequently used to determine ϕ'_{yield} and model the drained unloading mechanism that ultimately caused the dam's failure. For slices where $\phi'_{mob} \leq \phi'_{yield}$, the estimated ϕ'_{yield} was assigned to the base of that slice. However, if $\phi'_{mob} > \phi'_{yield}$, static liquefaction and strength loss was deemed to have been triggered, and $s_u(liq)/\sigma'_{vo}$ estimated from the correlation with CPT tip resistance was assigned. Above the water table, drained strength using critical state friction angles (ϕ'_{cs}) of 29° and 33° determined from direct simple shear tests on

Fundão dam iron slimes and sand tailings (Morgenstern et al. 2016) were respectively assigned. Using the newly assigned strength values, the LEA was iteratively repeated to incorporate these estimated values along the failure surface. The use of lower strengths for liquefied slices resulted in a redistribution of stresses and spreading of liquefaction to other slices. The LEA was repeated, maintaining the liquefied slices as such, until stress redistribution became negligible and no additional slices liquefied. The factor of safety (FS) calculated in the final LEA was thus the FS for liquefaction flow failure. Sadrekarimi (2016) provides further details of the analysis method and different parameters used to estimate undrained strength ratios from q_{c1}.

3.5. Results

The results of the static liquefaction analysis of Fundão dam are summarized in this section. The FS and the slip surface for liquefaction flow failure based on the final LEA are presented along with the summarized changes of FS from iteration to iteration, and comparisons of mobilized shear strength along the slip surface.

As an initial reference analysis, a drained LEA of the selected cross section was conducted using the Morgenstern-Price method to compare its results with those by Morgenstern et al. (2016) and confirm the adequate reconstruction of the dam's cross section. With both models yielding the same FS of 2.5, the reconstructed computer model using the dam's slimes depositional information and crest raising records are confirmed to be similar to that used in the official investigation report. This step served as a reference point for the subsequent comparisons between the FS for liquefaction flow failure provided by Morgenstern et al. (2016) and that obtained in this study.

The first static liquefaction stability analysis (Iteration 0 in Fig. 1-9) was conducted using gravitational stresses in each slice in an LEA with a uniform $\phi'_{yield} = 9.7^o$ – corresponding to an equivalent $s_u(yield)/\sigma'_{vo}=0.17$. A subsequent LEA was carried out after finding specific values of K_C and ϕ'_{yield} and determining the triggering of static liquefaction at the base of each slice. This resulted in a FS = 1.52 – slightly higher, yet similar to the FS for static liquefaction triggering reported by Morgenstern et al. (2016) assuming a constant $S_u(yield)/\sigma'_{vo} = 0.31$. This corresponds to an approximate 40% reduction in FS from the initial drained LEA due to the lower ϕ'_{yield} of

tailings below the phreatic surface compared to the ϕ'_{cs} assigned previously. The higher-than-unity FS obtained in this iteration is not necessarily an indication of a stable slope as stress redistribution could spread liquefaction to other slices and lower FS.

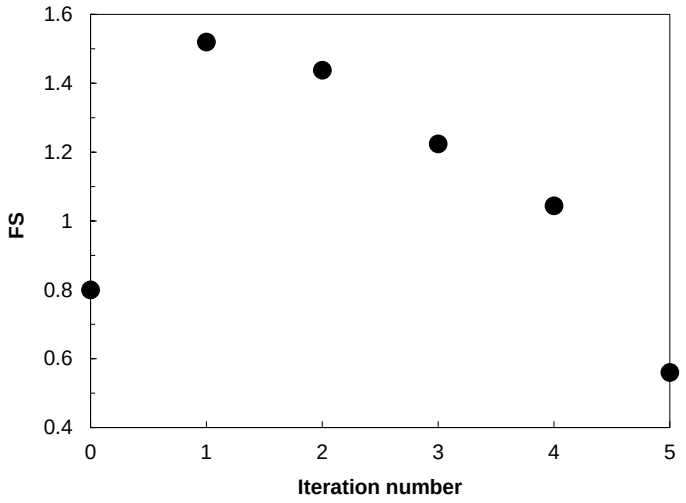

Figure 3-9: Variation in factor of safety for each iteration.

3.5.1. Analysis of liquefaction flow failure

As shown in Figure 3-9, FS continuously decreases for iterations 1 through 5, indicating strength reduction in liquefied slices and stress redistribution among liquefied and non-liquefied slices. Convergence was reached in the 5^{th} iteration when 85% of the slices below the water level liquefied as shown in black in Figure 3-10. No new slices liquefied beyond this iteration, reaching a FS = 0.56 for liquefaction flow failure. This low value of FS (< 1.0) demonstrates the imminent susceptibility of the Fundão dam's left abutment to flow liquefaction that ultimately led to its collapse.

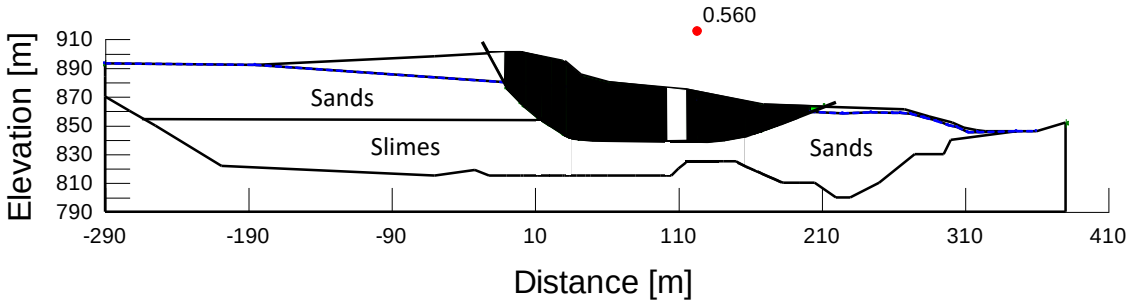

Figure 3-10*:* Zones of liquefied (*black*) and non-liquefied slices following the 5th LEA iteration for Fundão dam.

With regards to changes in stress anisotropy during stress redistribution, Figure 3-11 shows variations of K_C along the slip surface at the beginning of liquefaction (iteration 1) and flow failure (iteration 5) of Fundão dam. According to this figure, the break-out section of the failure surface displays the highest values of K_C, where extension shear exists. Likewise, it is in this section that static liquefaction was first manifested. These two observations are consistent with typical soil behaviour, because higher anisotropic consolidation promotes strain-softening of soils (Sadrekarimi 2016). Additionally, Figures 3-12 and 3-13 display respective changes in mobilized shear strength along the slip surface for the beginning of liquefaction and flow failure and compare the results with those obtained using the undrained strength ratios (USR= S_u/σ'_{vo}) adopted by the Panel.

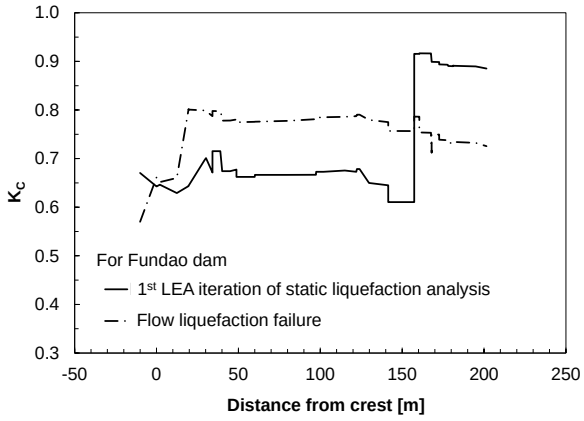

Figure 3-11*:* Variations of K_C along the slip surface in the first iteration of static liquefaction analysis and flow failure.

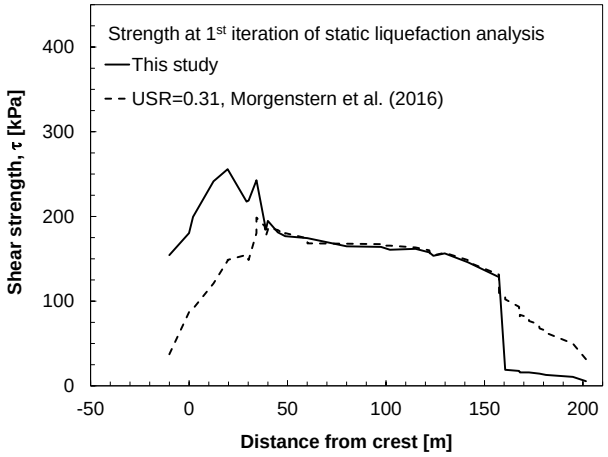

Figure 3-12*:* Variations of mobilized shear strength along the failure plane in the first iteration of static liquefaction analysis.

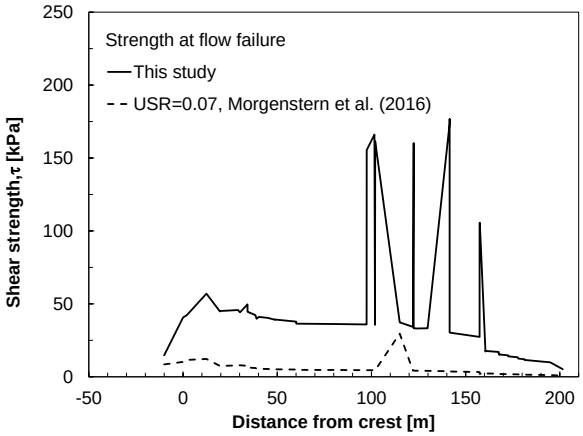

Figure 3-13: Variations of mobilized shear strength along the failure plane at flow failure (iteration 5).

3.6. Comparison with Morgenstern et al. (2016)

A summary of the investigation Panel's stability analyses based on field data from June 2015 on the same section of the Fundão dam (labelled Section 01) can be found in Appendix H of Morgenstern et al. (2016). In the first undrained strength analysis (USA) reported by Morgenstern et al. (2016) to determine FS for static liquefaction triggering, drained strength was assigned to tailings above the phreatic surface and a constant $S_u(yield)/\sigma'_{vo}$= 0.31 to those below the phreatic surface based on CPT empirical correlations (Olson and Stark 2003). This approach disregards the effects of the different modes of shear and stress anisotropy (K_C) found along a failure surface. Moreover, the use of an undrained strength ratio is not applicable for the constant-shear stress path hypothesized to have occurred in the failure of Fundão dam. As shown in Figure 3-12, the use of a constant $S_u(yield)/\sigma'_{vo}$ = 0.31 leads to an underestimation of shear strength in the backscarp section (-10 to 40 m from the crest), and a great overestimation in the break-out section (160 to 200 m from the crest) where the highest stress anisotropy and the initiation of static liquefaction were observed. Nonetheless, despite these differences, the estimated FS = 1.48 by the Panel is relatively similar to the FS = 1.52 obtained in this study.

In a second USA, Morgenstern et al. (2016) attempted to incorporate the effect of shearing mode by assigning different values of $s_u(yield)/\sigma'_{vo}$ to tailings below the phreatic surface based on field

data obtained in June 2015 and using empirical correlations by Sadrekarimi (2014). For the backscarp (compression zone), $S_u(yield)/\sigma'_{vo}$ = 0.30; for the horizontal segment (simple shearing zone), $S_u(yield)/\sigma'_{vo}$ = 0.22; and for the breakout section (extension zone), $S_u(yield)/\sigma'_{vo}$ = 0.14 were assigned. Despite this effort, the mobilized shear strength in the extension zone is overestimated, probably due to the important effects of stress anisotropy (K_C) and the DCSS stress path followed. Nevertheless, the overall FS of 1.14 obtained by the Panel is lower than that estimated here, perhaps also due to the use of average q_{c1} values in the analyses of this study.

In a third slope stability assessment, the Panel carried out a "collapse surface analysis" by running an effective stress analysis (ESA), assigning ϕ'=33^o for sand tailings above the water table and a low-strength variant for saturated loose tailings and slimes using a friction angle of 16^o based on IC-TxC tests. The resulting FS=1.28 obtained by the Panel differs from that obtained in this study, and it does not reflect true field conditions primarily because the analysis overlooks the following three aspects that affect the magnitude of the mobilized ϕ'_{yield}. First, as shown in Figure 3-11, different values of K_C exist along the slip surface, which indicate an inherent state of anisotropy in the dam's slope. Second, upon the development of a failure surface, different modes of shear are characteristically induced along the profile as shown in Figure 3-8. And third, different materials exhibit different ϕ'_{yield} depending on their respective ϕ'_{cs}, as illustrated in Figure 3-7 for gold and iron sand tailings. Consequently, adopting a uniform total stress friction angle of 16^o for sands and slimes based on IC-TxC tests underestimates the ϕ'_{yield} of the sand tailings in the backscarp section, for which K_C=0.6-0.7 (see Figure 3-11) and a compression mode of shear is induced; and conversely overestimates the mobilized ϕ'_{yield} in the seat and breakout sections of the failure surface, where K_C ranges from about 0.8 to 1.0 and simple-shear and extension modes of shear are respectively produced.

Finally, in a fourth undrained stability analysis reported by Morgenstern et al. (2016), a post-liquefaction stability analysis was conducted by assigning a uniform $S_u(liq)/\sigma'_{vo}$ = 0.07 based on in-situ test correlations (Olson and Stark 2002) to the tailings below the water surface. As with the first analysis, this approach did not include the effects of the different modes of shear and K_C along the failure surface. Consequently, an underestimated FS of 0.36 was calculated when compared to that obtained here (FS = 0.56). Similarly, the mobilized shear strength values along the slip surface calculated using $s_u(liq)/\sigma'_{vo}$ = 0.07 as adopted by the panel (in Fig. 13) are found to be consistently

lower than those estimated in this study, hence indicating a general underestimation of the tailings' post-liquefaction strength.

3.7. Conclusions

An analytical method is introduced in this study for simulating the triggering of static liquefaction for drained constant-shear-stress conditions as hypothesized to have occurred in the collapse of the Fundão dam. This method accounts for variations in mode of shear and anisotropic consolidation, as well as stress redistribution from loose zones to adjacent denser areas in the propagation of failure along a failure surface. Through the use of the instability line and its slope, ϕ'_{yield}, which are considered to mark the initiation of strain-softening and static liquefaction behaviour in liquefiable soils, this strength loss mechanism was simulated in a series of LEA models. In order to estimate ϕ'_{yield} for the Fundão iron sand tailings, a combination of in-situ CPT data and the results of a series of constant-volume direct simple-shear tests on gold sand tailings were employed. The laboratory test results helped to determine an average effective stress reduction at the triggering of static liquefaction, $\sigma'_{vo}/\sigma'_{v}(yield)$, which was then used to calculate ϕ'_{yield} from values of $S_u(yield)/\sigma'_{vo}$ estimated from field CPT data.

Results of this iterative analytical method on the failing section of the Fundão dam suggest that the slope was reasonably susceptible to liquefaction flow failure with a safety factor of 0.56. This further supports the hypothesis that failure may have been triggered by lateral spreading and foundation deformation, thus illustrating the adequacy of the method for tailings sand embankments. Comparison of these results with those reported by Morgenstern et al. (2016) indicate that the effects of stress anisotropy, mode of shear, and stress path play a crucial role in the estimation of shear strength from in-situ test data. Despite the similarity in the factor of safety first obtained, it was observed that by adopting a constant value of $S_u(yield)/\sigma'_{vo}$ as initially done by the Panel, liquefiable areas of high anisotropy in extension shear (the breakout section) were overlooked. Similarly, in spite of the lower factor of safety later obtained by the Panel, the use of heterogeneous $S_u(yield)/\sigma'_{vo}$ values along the slip surface to account for the various modes of shear still overestimated the shear strength in this same section. It was also observed that by adopting a

constant value of ϕ'_{yield} for the saturated tailings as done by the Panel in their attempt to conduct a collapse surface analysis, the mobilized strength was underestimated in the backscarp section and overestimated in the seat and breakout sections of the slip surface, thus resulting in a FS unrepresentative of true field conditions. Lastly, the assumption of a low homogeneous liquefied strength through the use of a constant $S_u(liq)/\sigma'_{vo}$ by the Panel resulted in the underestimation of strength, due to the excessively conservative perception that the mobilized strength is only dependent on vertical effective stress, irrespective of the mode of shear and anisotropic state.

One last point to note is that many other phenomena such as 3D effects, partial saturation, and void redistribution may have affected the actual failure of Fundão dam. The analysis shown in this paper demonstrates the application of ϕ'_{yield} in a liquefaction analysis method based on laboratory tests in sands and silty sands. It is solely presented as an example and may not represent the complete failure process in the field. Additionally, the possible effects of microstructure generation through geochemical reactions in the deposited tailings is not considered, as more material-specific laboratory tests may be required to characterize the tailings' behaviour.

3.8. References

Been, K. and Jefferies, M. 1985. A State Parameter for Sands. *Geotechnique* 35:291-303.

Blight, G., 2010. *Geotechnical Engineering for Mine Waste Storage Facilities,* CRC Press, London, UK.

Chu, J., Leroueil, S. and Leong, W. K. 2003. Unstable behaviour of sand and its implication for slope stability. *Canadian Geotechnical Journal*, 40(5): 873 - 885.

da Fonseca, P. and da Fonseca, I., 2016. Brazil's Greatest Environmental Catastrophe - Samarco's Fundão Tailings Dam. *Environmental Policy and Law: Amsterdam*, 46 (5): 334-337.

Hanazawa, H., Itoh, Y., and Suzuki,(1980). Shear Characteristics of a Quick Sand in the Arabian Gulf. *International Journal of Rock Mechanics and Mining Sciences and Geomechanics Abstracts, 17(5)*, 81-81. doi:10.1016/0148-9062(80)90840-2.

Hicks, M. A., and Boughrarou, R. (1988). Finite Element Analysis of The Nerlerk Underwater Berm Failures. *Géotechnique*, 48(2): 169-185.

Jeffries, M., and Been, K. (2016). *Soil Liquefaction -- A Critical State Approach, 2nd Ed.* Boca Raton: Taylor and Francis Group.

LePoudre, D., 2015. Examples, Statistics and Failure Modes of Tailings Dams and Consequence of Failure. *Environmental Services Association of Alberta*, 88.

Mesri, G., 2007. Yield Strength and Critical Strength of Liquefiable Sands in Sloping Ground. *Geotechnique 57*(3): 309–311.

Morgenstern, N., Vick, S. G., Viotti, C. B. and Watts, B. D., 2016. *Report on the Immediate Causes of the Failure of the Fundão Dam*, Gottlieb Steen and Hamilton LLP.

Olson, S. M. and Stark, T. D., 2002. Liquefied Strength Ratio from Liquefaction Flow Failure Case Histories. *Canadian Geotechnical Journal,* 39: 629-647.

Olson, S. and Stark, T., 2003. Use of Laboratory Data to Confirm Yield and Liquefied Strength Ratio Concepts. *Canadian Geotechnical Journal,* 40: 1164-1184.

Robertson, P., 2010. Evaluation of Flow Liquefaction and Liquefied Strength. *J. Geotech. Geoenviron. Eng.*, 136(6): 842-853.

Rowe, P., and Craig, W. (1976). Studies of Offshore Caissons Founded on Oostershelde Sand. In, *Design and Construction of Offshore Structures,* ed. J. Monroe (pp. 49-55). London, U.K.: Institution of Civil Engineers.

Sadrekarimi, A., 2014. Effect of The Mode of Shear on Static Liquefaction Analysis. *J. Geotech.* Geoenviron. Eng., ASCE, 04014069:1-12.

Sadrekarimi, A., 2016. Static Liquefaction Considering Principal Stress Directions and Anisotropy. *Geotech Geol Eng.*, 1135-1154.

Sadrekarimi, A. and Olson, S., 2011. Yield Strength Ratios, Critical Strength Ratios, and Brittleness of Sandy Soils from Laboratory Tests. *Canadian Geotechnical Journal*, 48: 493-510.

Sladen, J. A., D'hollander, R. D., and Krahn, J. (1985). The Liquefaction of Sands, A Collapse Surface Approach. *Canadian Geotechnical Journal No. 4*, 564-578.

Stark, T. D. and Mesri, G., 1992. Undrained Shear Strength of Liquefied Sands for Stability Analysis. *Journal of Geotechnical Engineering ASCE*, 118:1727-1747.

Stark, T. and Mesri, G., 1992. Undrained Shear Strength of Liquefied Sands. *J. Geotech. Eng.*, 118(11): 1727-1747.

Chapter 4

4. Static Liquefaction and Liquefaction Triggering of Gold Tailings

4.1. Introduction

4.1.1. Flow Failure of Tailings Dams

Static liquefaction failure of tailings impoundments has been a consistent issue for the mining and mine-waste management industries over many decades. From the failure of the platinum tailings dam in Bafokeng, South Africa in 1974 to the recent failure of the gold/silver tailings dam at the Cieneguita mine in Chihuhua, Mexico (2018), the resulting deaths and environmental disasters have negatively impacted the general public's perception towards mining, thus jeopardizing the industry's credibility, its reliability, and ultimately its social license to operate. As a counteracting measure, some research has been carried out over the years to better understand and prevent flow failure of tailings, and a few studies have been conducted as part of post-failure investigations. Such are the cases of the Merriespruit (1994) and the Fundão (2015) dam failures, from which valuable information regarding the behaviour of tailings and best mine-waste management practices were particularly obtained. These two cases are summarized below.

4.1.1.1. Merriespruit Dam Failure (1994)

The disaster in Merriespruit involved the collapse of a 31-m high tailings dike upstream of the Merriespruit township (suburb of Virginia), South Africa, built as part of a group of mine-waste storage impoundments for the Harmony Gold mine. The whole gold tailings (or slimes as they're locally called) were deposited using spigots and subsequently drained by means of built-in penstocks and pipe-drains in the dikes (Van Niekerk and Viljoen 2005).

Because the failing section of the dam had shown distress for many years in the form of seepage and minor sloughing, tailings deposition had been discontinued fifteen months before the failure. However, excess water with tailings continued to be illicitly transported to and stored in the dam by mine operators, resulting in the displacement of the pool away from the penstock and causing it to relocate near the failing dike.

On February 22, 1994, a few hours after a thunderstorm that brought 30 to 50 mm of rain, the dike breached and released about 600,000 m^3 of liquefied tailings that flowed through the town and caused the death of 17 people (Blight 2010). Following the disaster, a series of investigations were launched, and the findings were reported by Wegener et al. (1997). The primary cause of failure was identified to be the overtopping of pool water over the dike's crest, which caused large-scale removal of the dike's tailings on the downstream slope, thus exposing previously confined tailings. This newly steepened slope subsequently induced higher shear stresses under undrained conditions, generating a sequence of slumping failures as the slope's geometry continued to change. Furthermore, field evidence suggests that as retrogressive failure continued, the breach eventually exposed saturated tailings that were in a metastable state, causing these to flow like a liquid as far as 3 km away from the dam (Fourie et al. 2001).

4.1.1.2. Fundão Dam Failure (2015)

The Fundão dam was an iron tailings impoundment built in the state of Minas Gerais, Brazil. Two types of tailings were produced and delivered separately in slurry form into the dam: sand tailings, which consisted of a mixture of sand-sized and finer silt particles that were free-draining but susceptible to liquefaction when loose and saturated; and slimes, which in contrast were much finer and clay-like in nature with low permeability (Morgenstern et al. 2016).

The initial design of the embankment made use of a compacted earth-fill starter dam that was to be raised by the upstream method, and sand tailings were to be deposited behind it. The sands would in turn retain slimes deposited on the opposite side of the dam and maintain a beach distance of no less than 200 m to prevent the water-borne slimes from being deposited in the sands near the crest (Morgenstern et al. 2016). A very important feature of the design was a high-capacity drainage system at the base of the starter dam, which would allow water to drain from the sands and prevent unwanted saturation.

Shortly after construction in 2009, a few incidents required certain modifications to the initial plans and promoted the eventual triggering of static liquefaction in the sands (Morgenstern et al. 2016). First, construction defects in the base drain were discovered, which forced the closure of the entire drainage system. The revised design made use of a blanket drain built over deposited tailings that

would consequently allow more widespread saturation of the sands below it. The second incident was the mismanagement of the tailings beach required to prevent slime deposits and water encroachment near the crest of the embankment, which allowed slimes to settle out in areas where they were not intended to exist. The third and last incident involved the structural deficiency of a concrete conduit beneath the dam's left abutment, which could not sustain any further loading generated by raising of the dam. As a result, the embankment's crest was set back upstream in order to maintain operations during the remedial work, placing the embankment directly over previously deposited slimes. Lastly, a series of three small seismic shocks occurred three hours before the breach, which are believed to have slightly accelerated the hypothesized failure mechanism.

The Fundão dam failed in a liquefaction flow slide on November 5, 2015, which began at the embankment's left abutment where the alignment setback was built. Morgenstern et al. (2016) identified extrusion of the compressible encroached slimes as the liquefaction triggering mechanism that slowly decreased the sands strength until failure. The slide of saturated tailings swept away the nearby town of Bento Rodrigues, killing nineteen villagers, and causing a major environmental disaster after polluting the local water system (da Fonseca and da Fonseca 2016).

4.1.2. Problem Statement and Objective

Despite the many failures of tailings impoundments in recent history and active research on the shear behaviour of mine tailings, there is still very limited information and no consensus reached regarding the liquefaction triggering and flow failure of tailings, possibly due to their varying nature and engineering properties. Moreover, existing liquefaction triggering correlations are mostly based on CPT and SPT (Sadrekarimi 2016; Olson and Stark 2003; Stark and Mesri 1992; Robertson 2010) and are derived for sands and silty-sands, but not exclusively for mine tailings. Hence, the aim of this study is to present an experimental liquefaction triggering method specifically for gold sand tailings based on correlations with laboratory shear-wave velocity measurements. Additionally, the behaviour of the tailings in undrained monotonic shear is analyzed for two different sample preparation methods (i.e. slurry deposition and moist tamping), in order to identify within a critical state soil mechanics framework how the difference in fabric produced by compaction and hydraulic deposition may affect the tailings' response.

4.1.3. Scope

Due to the complex nature of tailings and their depositional mechanism, this study is limited to establishing a liquefaction triggering correlation for gold sand tailings and their shear-wave velocity. As will be discussed later, tailings' gradations may be extremely variable in a single tailings impoundment. Consequently, sieved sand tailings are considered to simulate tailings elements susceptible to liquefaction in the impoundments, typically produced by the use of spray-bars or cycloning. No attempt is made to determine correlations with shear-wave velocity for the whole tailings, and solely their critical state is explored. Although the shearing behaviour of saturated and consolidated tailings is analyzed, the effects of creep, swelling, and recompression on tailings behaviour are not considered to be within the scope of the current investigation.

4.1.4. Tailings and their Disposal/Storage

4.1.4.1. Mine Tailings

From the perspective of those in charge of mineral extraction at a mine, tailings are the "waste" material associated with an ore deposit that must be mined in order to reach the desired ore. The tailings material is often made of crushed rock particles deposited in slurry form, with very distinct and complex chemical and physical characteristics. The nature and characteristics of tailings are highly dependent on the extracted ore and the mineral extraction processes involved. Ore types dictate the tailings' mineralogy, as the mineral residue is related to the specific ore deposit being mined. Similarly, the different physical extraction processes (e.g. crushing, grinding, cycloning) and chemical separation methods (e.g. flotation and leaching) affect the mechanical and chemical properties of the tailings produced. Nevertheless, all types of tailings are almost universally transported and deposited in slurry form by means of spigots or rotating single-points of discharge into what are known as tailings impoundments at pulp densities (defined as the weight of solids per the total weight of slurry) of about 40-50% (Vick 1990).

Tailings impoundments are large structures such as dams and ponds built to retain the tailings. Initially constructed using local natural soil to temporarily store the first amount of tailings produced, these embankments are often raised using the same deposited tailings by compacting them in the raising outer slopes. Therefore, these structures are continuously constructed and raised alongside with the production of tailings during mining operations for convenience and financial benefits (Vick 1990; Blight 2010).

Deposition of the tailings into the impoundments begins after transportation from the processing plants through pipes. Single-discharge points or spigots are connected through a discharge pipe located at the crest of the dikes, and deposit the tailings upstream, generating a tailings beach near the crest and a decant pool/pond farther upstream. Many researchers (Blight and Steffen 1979; Volpe 1979; Soderberg and Busch 1977) have observed that this depositional process often produces a heterogeneous beach deposit caused by particle segregation along the beach, with coarser particles deposited near the crest and finer colloidal particles in the decant pool. This observation was also confirmed by the varying amounts of fine contents in the in-situ samples analyzed in the case of the Merriespruit tailings dam collapse in 1994 (Papageorgiou 2004). Consequently, the in-situ relative density of the coarser particles on the beach may reach values of 30-50% for those tailings that undergo high-degree of particle segregation upon deposition (Vick 1990). The settled pond water is subsequently decanted by means of pumps or siphons on floating barges, or by penstocks connected to pipe drainage systems built underneath the dam, where the water is allowed to drain and collected for reuse in the mineral extraction process when possible.

Embankment raising may take form in three different configurations: Upstream, downstream, and centre line. The main difference among these is the location where the new dike is built, accordingly moving the dam's crest either upstream, downstream, or maintaining the crest's original alignment. Because of its low-cost and simplicity, the upstream method is commonly used, whereby the tailings beach near the spigots become the foundation for the new perimeter dikes, and the process continues as the embankment is raised (Vick 1990). An advantage of this method is the lower volume of mechanically compacted tailings fill required for construction of the dikes. Nevertheless, tailings dams constructed by the upstream method often have higher susceptibility to liquefaction, as in the case of the Fundão dam collapse in 2015.

4.1.4.2. Typical Properties of Gold Mine Tailings

Common minerals found in gold mine tailings include quartz, chlorite, pyrite, as well as carbonates and phyllosilicates, among others (Bedin et al. 2012; Al-Tarhouni 1997; Chang 2009).

As with typical hard-rock tailings, gold tailings contain both sand and fine fractions, with a wide range of particle size distributions due to the fact that efficiency of mineral extraction by leaching is related to the fineness of the grind (Vick 1990). Figure 4-1 presents a few gradation curves for gold mine tailings and other hard-rock tailings reported by several researchers. The term *whole tailings* refers to the gradation of those tailings as produced by the mill, and *sand tailings* denotes those tailings separated for use in dam raising. From the figure, several details can be observed: first, gold tailings are typically poorly-graded regardless of gradation type; second, as-milled whole gold tailings have fines-contents ranging from about 60-90%; and third, cycloning of sands produces tailings with fines-contents of 10-15%.

Because common gold deposits contain very little clay, gold mine tailings show low to no plasticity (Hamel and Gunderson 1973). Furthermore, their specific gravity varies from about 2.6 to 3.5 (Soderberg and Busch 1977; Hamel and Gunderson 1973; Al-Tarhouni 1997; Schnaid et al. 2013; Bedin et al. 2012; Fourie and Papageorgiou 2001; Qiu and Sego 2001; Pettibone and Kealy 1971; East et al. 1988; and Vermeulen 2001), with the higher values possibly due to higher pyrite content in some tailings (Blight and Steffen 1979).

With respect to their chemical composition and effluent, gold tailings often contain arsenic, cyanide, and sulfides. Arsenic is universally found in hydrothermal gold, thus commonly found in gold ores (U.S. Geological Survey 1857). Conversely, cyanide is added to the tailings during the extraction and concentration processes as a leaching reagent in the form of sodium-cyanide (Vick 1990), thus the resulting effluents often contain varying concentrations of left-over cyanide. Lastly, pyrite (FeS_2) is a very common mineral found in gold ores, rejected from the concentrate in the separation process, and disposed of in the tailings.

4.2. Characteristics of Materials Used

The gold tailings used in the present study were obtained from a mine in northern Ontario, Canada. Although not explicitly described by the provider, the tailings are believed to have been collected from the mill due to the gradation obtained (see Figure 4-1), which is similar to that for whole gold tailings used by other researchers, indicating little to no separation or particle segregation. For the reasons previously described regarding the variability of gradations found in tailings impoundments, the coarser sand particles were separated by sieving to simulate separation by cycloning or the use of spray-bars and were subsequently used for comprehensive analyses of their mechanical behaviour. This was deemed appropriate in order to establish a reference gradation for the material and to imitate the gradation of tailings elements susceptible to liquefaction in the embankment. Because some fine particles remained attached to the larger sand particles after sieve separation, the resulting particle size distribution for the sand tailings included a 9% fines content, which is comparable with the gradation for sand tailings (gold and other hard rock minerals) reported by other researchers as shown in Figure 4-1.

Sieve analyses for both the whole and sand tailings were conducted in compliance with ASTM D-422. The average gradations obtained for each material are highlighted in red in Figure 4-1. As shown in the figure, the whole tailings consist of about 73% fine particles (<0.075 mm) and 27% fine sand, which along with their non-plastic characteristics in accordance to ASTM D-4318, classifies the tailings as a low-plastic silt (ML) with sand per the Unified Soil Classification System (USCS). In contrast, the separated sands consist of about 9% fines and 91% fine sands, with C_u=1.5, thus classifying as a poorly-graded sand with silt (SP-ML). Additionally, hydrometer analyses were carried out for the <#200 sieve portion as per ASTM D-422, for which the whole gold tailings indicate having less than 5% clay-size particles (< 2 μm), and the sands having a very negligible amount of clay.

Specific gravity (G_S) measurements were conducted in accordance to ASTM D-854 for both materials. The whole and the sand tailings exhibited average G_s values of 3.28 and 3.10, respectively. The relatively high G_S values are indicative of the pyrite content in their mineralogy (Blight 2010). The minimum and maximum void ratios (e_{min} and e_{max}) of both materials were determined using ASTM standards D1557-12 and D4254-16, respectively. For the whole tailings,

values of e_{min}=0.59 and e_{max}=1.28 were measured. The sands, in contrast, exhibited values of e_{min}=0.79 and e_{max}=1.35. The overall characterization results are summarized in Table 2-1.

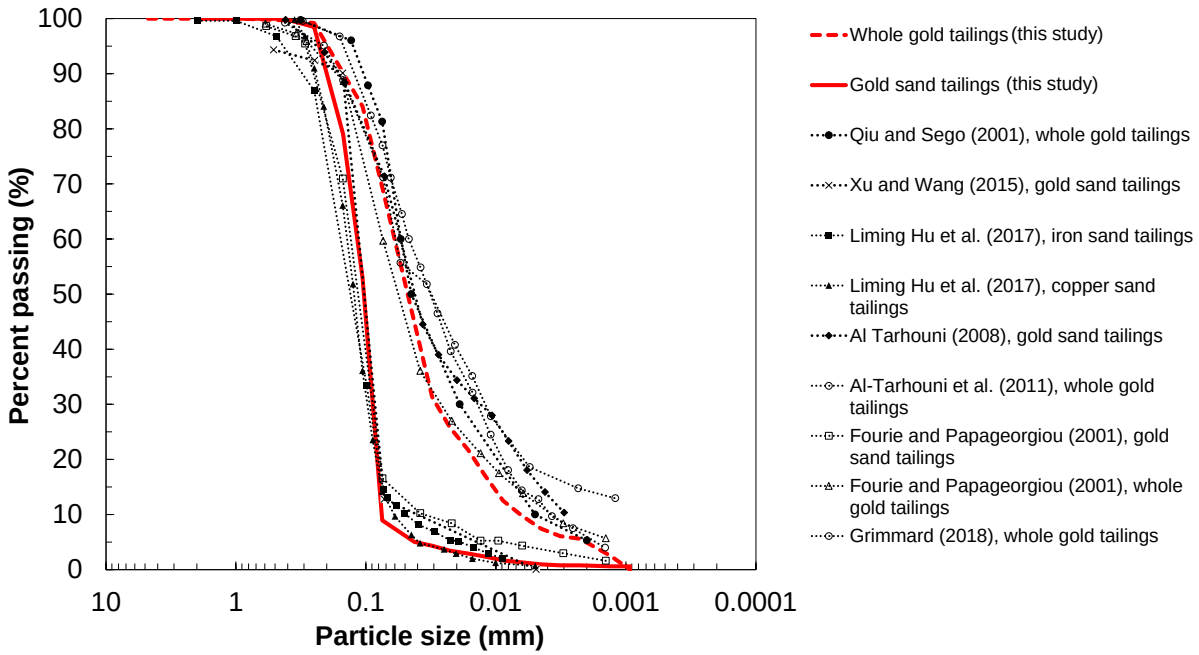

Figure 4-1: Particle size distribution for whole and sand gold tailings tested (red) compared with those of other tailings as reported by various researchers.

Table 4-1: Geotechnical properties of gold mine tailings.

Material	D_{10} (mm)	D_{30} (mm)	D_{60} (mm)	C_u	Clay Content (%)	G_S	e_{min}	e_{max}
Whole tailings	0.007	0.03	0.06	8.6	5	3.28	0.59	1.28
Sand tailings	0.08	0.09	0.12	1.5	--	3.10	0.79	1.35

The mineralogy of the whole tailings and the fines (< #200) was analyzed by means of X-ray diffraction analysis. Figure 4-2 presents the diffraction patterns obtained, which consist of a series of reflections of different intensities at different values of twice the X-ray striking angle (i.e. 2θ)

(Mitchell and Soga 2013). Since minerals have distinct and unique spacings of interatomic planes in three dimensions, identification of the mineral crystal involves the use of the X-ray's wavelength and Bragg's Law to estimate the crystal's distance between parallel atomic planes. Accordingly, the tailings were found to be composed mostly of quartz (55.8%), phlogopite (21.5%), chalcopyrite (4.8%), beryl (3.7%), chlorite (3.6%), and small percentages of magnesite and glaucophane.

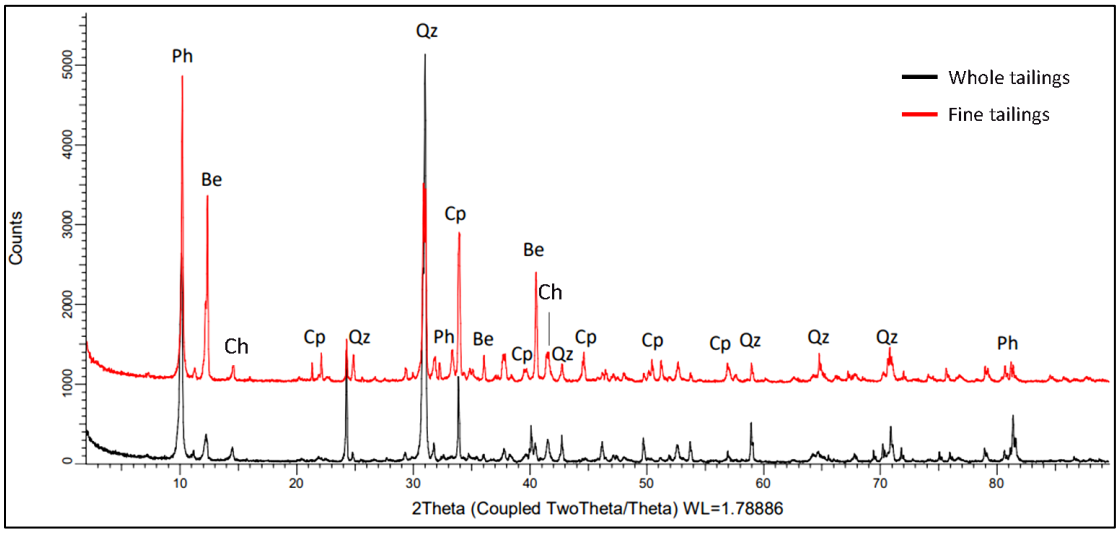

Figure 4-2: X-ray diffraction intensity traces for whole gold tailings (black) and sand gold tailings (red); Qz: quartz, Ph: phlogopite, Cp: chalcopyrite, Be: beryl, and Ch: chlorite.

Particle shape for the whole tailings was analyzed through a scanning electron microscope (SEM), which reproduced enlarged images of the particles by detecting the backscattered (or reflected) electrons from the specimen's surface produced by an electron beam moving in a pattern of horizontal lines (raster) over the specimen (Allen 2015). From the images obtained, the tailings particle shape was determined to generally range from angular to sub-angular as shown in Figure 4-3.

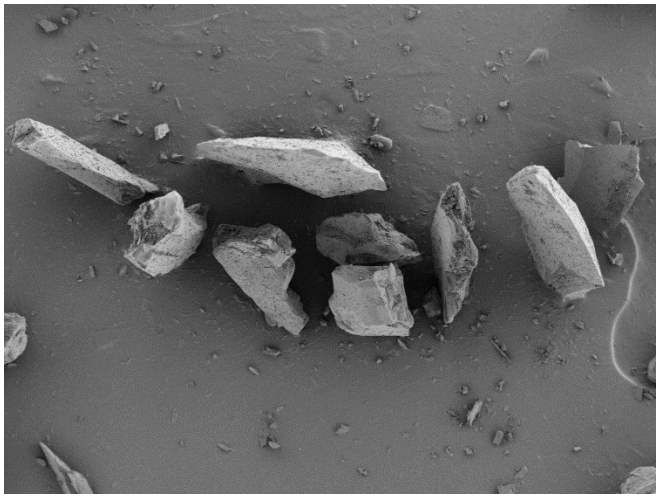

Figure 4-3: SEM images of whole gold tailings displaying angularity of larger sand particles.

4.3. Methods and Equipment

4.3.1. Equipment Used

An advanced direct simple shear device manufactured by GDS Instruments was employed for the DSS tests conducted in the experimental program. Aside from a vertical electro-mechanical actuator employed to apply vertical stresses, the machine also has a horizontal actuator that allows simple shear to be performed. The vertical actuator has a displacement range of approximately 50 mm and a maximum force capacity of 5 kN. The horizontal actuator has a displacement range of 25 mm and a maximum load capacity of 2 kN. Once mounted, test specimens are axially confined between an upper and a lower pedestal, and radially restrained by a stack of Teflon-coated steel rings internally lined with a latex membrane of 0.82 mm in thickness, which seals the sample at the top and bottom using O-rings. The steel rings have an inner diameter of about 71.96 mm and a thickness of 1.05 mm each, and when stacked, they provide a rigid radial boundary for the sample while allowing unrestricted application of horizontal displacement during shear. When assembled, the lower pedestal and the stacked rings serve as the specimen preparation mold. Given the constraints in size provided by the rings' inner diameter and the latex membrane, the specimens are prepared with a diameter of 70.3 mm. Specimen saturation is accomplished by flushing water

through outlet connections in the top and bottom pedestals, which allow the ingress of water through confining porous disks making direct contact with the specimen.

All samples tested in the DSS apparatus were initially loaded under a vertical seating stress of 5 kPa, while flushing them with deaired water. The target consolidation vertical stress, σ'_{vc} was subsequently applied on the specimen until the rate of vertical displacement significantly reduced, indicating the end of primary consolidation. Given the sandy/silty nature of the tailings, all specimens were sheared at a rate of 10% per hour, thus ensuring that failure occurred in a time that exceeded twice the 90% consolidation time in order to prevent the generation of pore water pressure upon shearing (ASTM D6528-17). Drained simple shear tests were conducted by maintaining a constant vertical stress as the shear displacement/load was applied, thus allowing the sample's height to vary as shear strain was increased. Conversely, as drainage was allowed in constant-volume tests, no shear-induced pore water pressure was produced, and the change in vertical stress required to maintain a constant height was taken as the equivalent pore water pressure that would have been generated in a truly undrained test on a saturated sample (Bjerrum and Landva 1966; Tatsuoka et al. 1984; ASTM D6528-17).

A unique type of stress path similar to the one hypothesized to have triggered the static liquefaction collapse of Fundão Dam in Brazil was also investigated in this study. The particular loading conditions attributed to foundation spreading and unloading in this case were applied by conducting drained constant-shear stress tests (CSS-DSS), in which a constant shear stress was applied and maintained, while simultaneously reducing the applied vertical stress (i.e. unloading).

Shear-wave velocity (V_S) measurements were also taken in sand tailings specimens using bender element inserts affixed to supplementary specimen pedestals. The elements consist of small cantilever piezoelectric plates that are shallowly embedded at the top and bottom of the specimen during confinement. The bender elements were controlled using a signal generation software that allowed the on-command triggering of shear waves. A voltage signal was transmitted to one of the bender elements, which subsequently converted this signal to a sinusoidal mechanical vibration with a set wavelength (λ) by means of its piezoelectric properties. The shear wave propagating through the tailings sample was then received by the other bender element and converted back to an electric voltage signal.

Although several methods for interpreting V_S signals have been proposed (Viggiani and Atkinson 1995; Jovičić et al. 1996), the peak-to-peak method was employed here as it has been proven to provide accurate measurements of V_S (Brignoli et al. 1996; Camacho-Tauta et al. 2015). Accordingly, the travel time was estimated to be equal to the time difference between the peaks of the transmitted wave and the first wave received, and the distance travelled by this first wave was taken as the tip-to-tip distance of the bender elements along the specimen (Brignoli et al. 1996), which was maintained to be at least twice λ by using a wave excitation frequency of 33.3 kHz in order to avoid near-field effects (NFE) caused by P-wave reflections and electrical noise. Hence, by consolidating a specimen to various vertical stresses and changing its void ratio, different peak-to-peak travel times and travel distances were obtained for the calculation of V_S.

4.3.2. Sample Preparation

Tailings specimens were reconstituted using two different techniques in order to evaluate the effects of fabric on their shear behaviour. A unique slurry preparation method was developed and adopted in an effort to simulate typical slurry deposition of tailings. Additionally, moist-tamping was employed as it is the most common sample preparation technique because of its ease of use and high control over the specimen's void ratio. Regardless of the method used, all specimens were prepared with a height to diameter (H/D) ratio of less than 0.4, as suggested in the ASTM standard D6528 in order to minimize nonuniformities upon shearing. Each of these sample preparation methods are described in the following paragraphs.

4.3.2.1. Slurry Deposition

Dry tailings samples were mixed with distilled water at a 1:1 ratio by mass inside a plastic bottle in order to obtain a pulp density ($\rho_{pulp}=M_{solid}/M_{total}$) of 50%, similar to that typically produced by thickeners for slurry transportation (Vick 1990). As shown in Figure 4-4, the slurry was pumped into the mold from the plastic bottle using a silicone hose with a 5-mm inner diameter connected to a peristaltic pump. In order to reduce particle segregation due to sedimentation inside the bottle, the plastic bottle was continuously shaken by hand during pumping to assure full suspension of

particles. The depositing end of the hose was slowly raised as specimen height increased, and it was moved in radial and circumferential directions until the desired specimen height was reached.

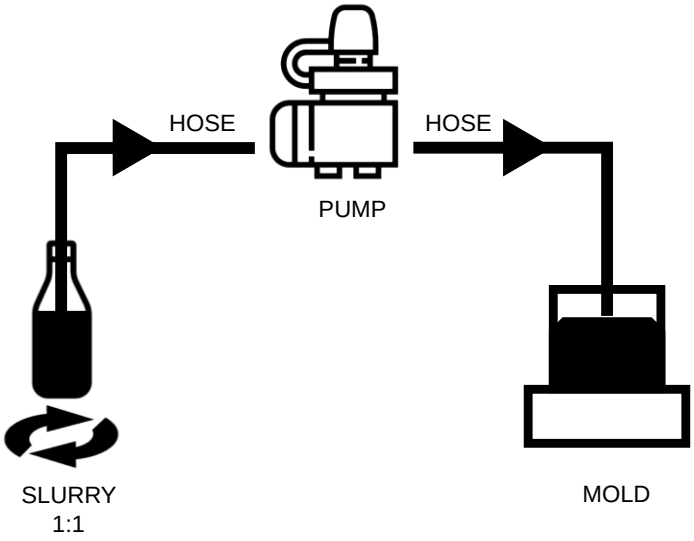

Figure 4-4: Schematic of slurry preparation of tailings specimens.

The pump's rotation was adjusted to 50 RPM in order to yield an initial water content similar to those used for hydraulic deposition and spigotting of tailings in the field. Because of the inherent complexity in controlling the slurry's density during specimen preparation, the void ratio of a given specimen was controlled by consolidating each sample to different vertical stresses prior to shearing. This void ratio was subsequently calculated from the amount of oven-dried tailings recovered from each sample after testing. As shown in Figure 4-5, an average initial water content (w_o) of 42% was used for all specimens tested irrespective of initial specimen height.

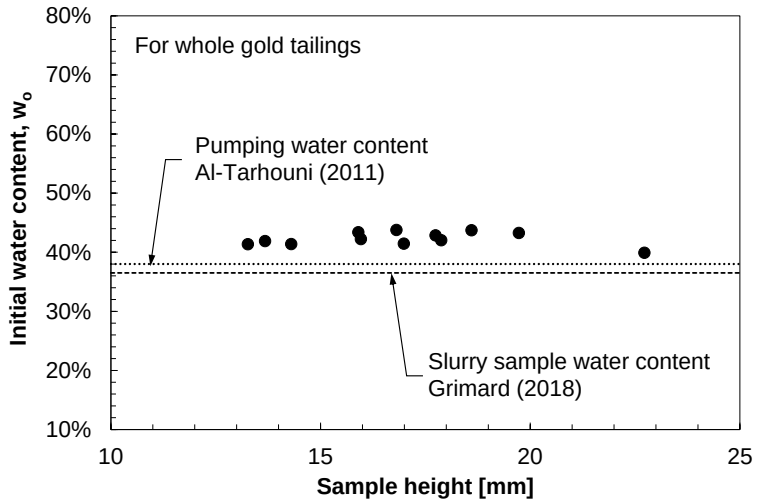

Figure 4-5: Water content of slurry tailings specimens.

4.3.2.2. Moist-tamping

Moist-tamped tailings samples were prepared by mixing dry tailings with a small amount of water, resulting in samples with 5% water content. The moist tailings were subsequently scooped into the mold and tamped to the desired specimen height. The low moisture generates a capillary effect among tailings particles, creating a very loose fabric that was readily molded into the specimen volume. Given the short height of the specimens (≈ 25 mm), single layering of the tailings was deemed prudent as opposed to the conventional use of multiple layers. This idea was later confirmed by observing similar results when testing Fraser River sand following this same procedure with those obtained by Jones (2017), for which the samples were prepared in multiple layers. Lastly, the void ratio of each specimen was controlled by varying either the specimen height or the amount of dry tailings used for sample preparation.

A total of 42 monotonic DSS tests and 17 bender element tests were carried out, which are summarized in Table 2-2. Each test designation code indicates the type of material tested (W: whole tailings; S: sand tailings), the specimen preparation method (SD: slurry; MT: moist-tamped), and the test type (D-DSS: drained direct simple shear; CV-DSS: constant-volume direct simple shear; CSS-DSS: constant-shear stress direct simple shear; BE: bender element). The initial

void ratio (e_c) corresponds to that obtained at end of the consolidation stage, and σ'_{vc} is the vertical stress applied for consolidation.

Table 4-2: Summary of testing parameters using the in the DSS tests.

Test Designation	σ'_{vc} (kPa)	e_c	Test Designation	σ'_{vc} (kPa)	e_c
W/SD/CV-DSS 01	300	0.82	S/MT/CV-DSS 06	300	1.08
W/SD/CV-DSS 02	200	0.85	S/MT/CV-DSS 07	400	1.06
W/SD/CV-DSS 03	200	0.81	S/MT/CV-DSS 08	500	1.02
W/SD/CV-DSS 04	100	0.82	S/MT/CV-DSS 09	100	1.13
W/SD/CV-DSS 05	100	0.83	S/MT/CV-DSS 10	100	1.09
W/MT/CV-DSS 01	500	0.75	S/MT/CV-DSS 11	200	1.10
W/MT/CV-DSS 02	400	0.75	S/MT/CV-DSS 12	200	1.12
W/MT/CV-DSS 03	300	0.78	S/MT/CV-DSS 13	300	1.08
W/MT/CV-DSS 04	200	0.79	S/MT/CV-DSS 14	300	1.07
W/MT/CV-DSS 05	100	0.85	S/MT/CSS-DSS 01	100	1.15
W/MT/CV-DSS 06	50	0.87	S/MT/CSS-DSS 02	100	1.15
W/MT/CV-DSS 07	35	0.90	S/MT/CSS-DSS 03	400	1.06
W/MT/D-DSS 01	300	0.80	S/MT/BE 01	250	1.10
W/MT/D-DSS 02	600	0.72	S/MT/BE 02	300	1.10
W/MT/D-DSS 03	900	0.69	S/MT/BE 03	350	1.10
S/SD/CV-DSS 01	100	1.18	S/MT/BE 04	100	1.00
S/SD/CV-DSS 02	200	1.13	S/MT/BE 05	300	1.10
S/SD/CV-DSS 03	300	1.08	S/MT/BE 06	300	1.10
S/SD/CV-DSS 04	400	1.04	S/MT/BE 07	300	1.00
S/SD/CV-DSS 05	150	1.14	S/MT/BE 08	100	0.97
S/SD/CV-DSS 06	250	1.12	S/MT/BE 09	500	0.97
S/SD/CV-DSS 07	300	1.04	S/MT/BE 10	100	1.10

S/SD/CV-DSS 08	350	1.03	S/MT/BE 11	500	1.00
S/SD/D-DSS 01	300	0.93	S/MT/BE 12	100	1.10
S/SD/D-DSS 02	25	1.12	S/MT/BE 13	400	1.00
S/MT/CV-DSS 01	100	1.16	S/MT/BE 14	750	0.97
S/MT/CV-DSS 02	200	1.10	S/MT/BE 15	400	1.06
S/MT/CV-DSS 03	300	1.08	S/MT/BE 16	600	1.00
S/MT/CV-DSS 04	400	1.07	S/MT/BE 17	700	1.00
S/MT/CV-DSS 05	50	1.19			

4.4. Results

Prior to analyzing their shear behaviour, the normal compression lines (NCL) for both the whole tailings and sands were established. Figure 4-6 compares the NCLs for the whole tailings obtained from the consolidation stages of the DSS tests as well as one-dimensional oedometer tests with those reported by Qiu and Sego (2001) and Al-Tarhouni (2008). Despite differences in initial void ratios, these NCLs are more-or-less parallel with compression index (C_C) 0.13 - 0.14. Similarly, Figure 4-6 also shows the NCL of the sand tailings, exhibiting a comparable slope with a compression index of 0.16, indicative of the consistent moderately compressible nature of both whole and sand tailings.

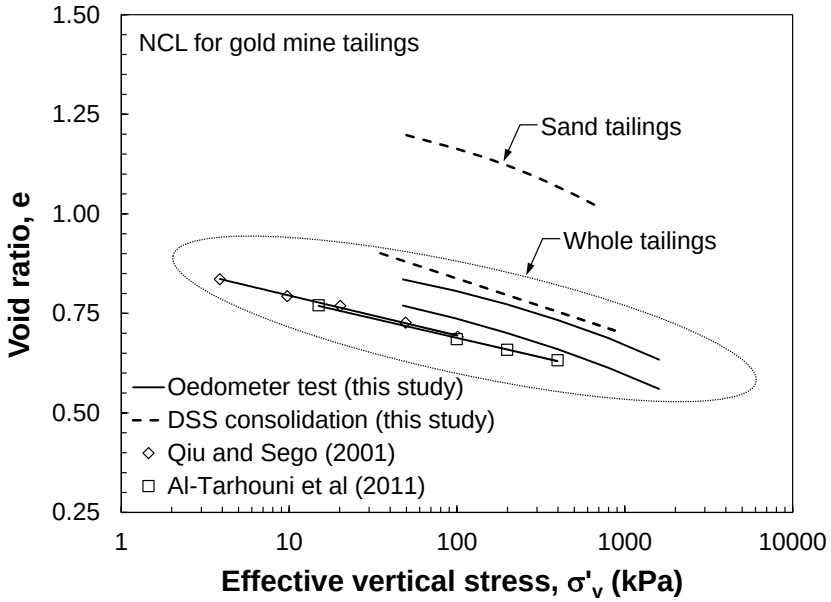

Figure 4-6: Normal compression lines (NCLs) for whole and sand tailings.

Figures 4-7 and 4-8 present stress paths and stress-strain curves for the CV-DSS tests carried out on the whole tailings. The specimens in Figure 4-7 were prepared by slurry deposition at e_c = 0.81 to 0.85 and were consolidated to σ'_{vc} ranging from 100 -300 kPa. Typical liquefying behaviour is entailed by the strain softening and strength loss that occur when the applied shear stress exceeds the undrained yield strength, s_u(yield). However, as shown in the figure, all specimens display stable strain-hardening shearing behaviour. This dilative response prevails in all samples after a shear strain of about 5%, corresponding to a phase-transformation friction angle of 27º. Similarly, Fourie and Papageorgiou (2001) and Qiu and Sego (2001) also report weak strain-softening and dilative behaviour in hydraulically deposited tailings samples. Within the shear-strain limits of the DSS tests, a peak friction angle (ϕ'_{max}) of 32º is reached at the end of the tests. Note that $\phi'_{max} > \phi'_{PT}$ due to dilatancy.

Unlike slurry-deposited specimens, moist-tamped samples of the whole tailings (prepared at e_c = 0.75 to 0.85) experienced strain-softening behaviour as shown in Figure 4-8, despite some showing weak strain-hardening at large strains (γ > 5%). For these specimens, liquefaction and undrained yielding occurred at an average friction angle (ϕ'_{yield}) of about 16º. Similar to the slurry-deposited

samples, $\phi'_{PT} = 27^o$ is mobilized at phase transformation states. Nevertheless, a slightly lower $\phi'_{max} = 31^o$ is reached because of the weaker dilation in these samples.

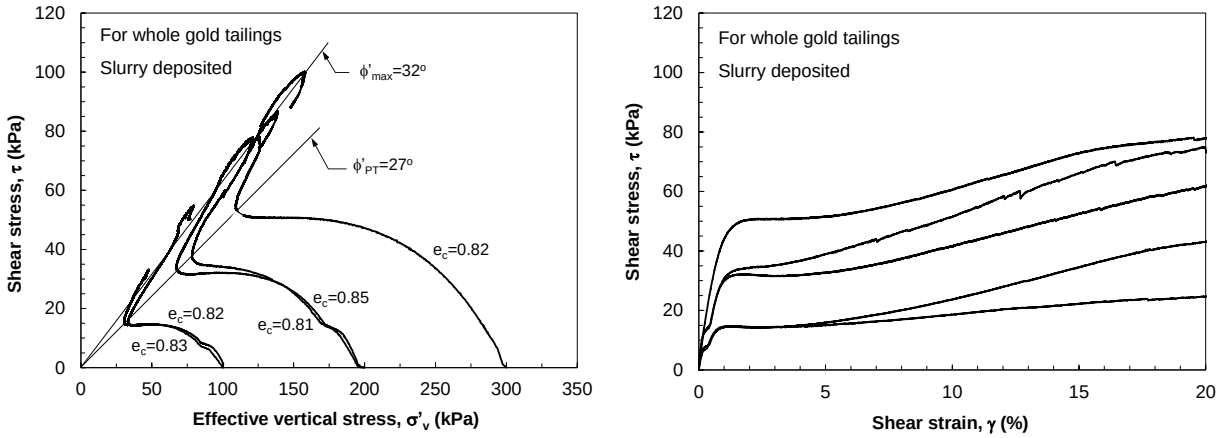

Figure 4-7: Stress paths and stress-strain curves of constant-volume DSS tests on slurry-deposited whole gold tailings.

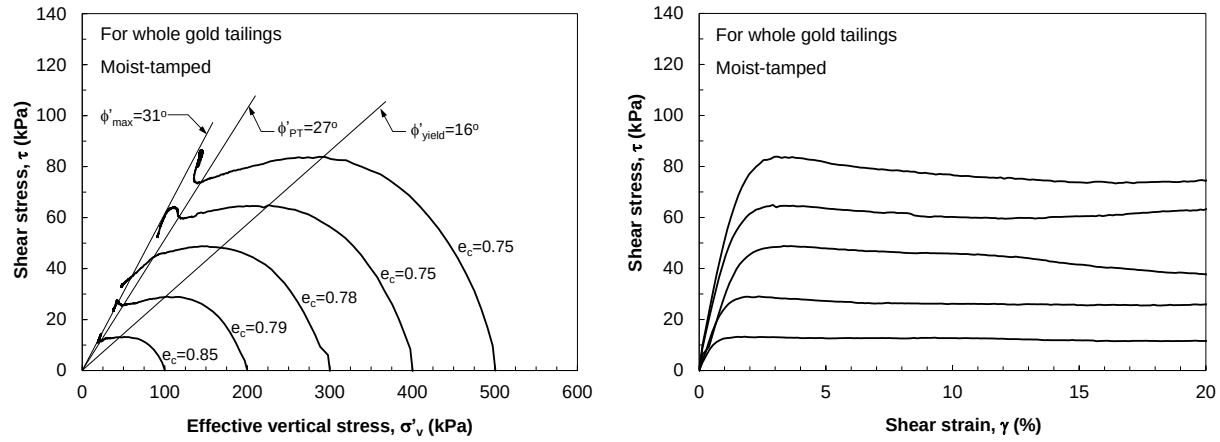

Figure 4-8:Stress paths and stress-strain curves for constant-volume DSS tests on moist-tamped whole gold tailings.

As shown in Figure 4-7 and 4-8, there was a significant difference between the shearing behaviours of whole tailings samples prepared by moist-tamping and slurry deposition at nearly similar void ratios.

A third series of constant-volume DSS tests were carried out on sand tailings but at larger void ratios (e_c = 1.02 to 1.19) to induce static liquefaction behaviour. Stress paths and stress-strain plots of these tests are shown in Figures 4-9 and 4-10. According to the figures, the triggering of static liquefaction occurred at shear strains of about 1 to 3% and at an average $\phi'_{yield}=14^o$. All samples exhibited a strain-softening behaviour with no dilation. As shown, this strain softening produced after triggering undrained strength loss continues with further shear displacement until an undrained post-liquefied strength, S_u(liq) is reached along the critical state line (CSL). Critical states were ultimately reached at the end of shearing, with a corresponding $\phi'_{cs} = 29^o$ for slurry-deposited samples, and $\phi'_{cs} = 27^o$ for moist-tamped – a +/-2^o difference between the two fabrics as also reported by Tatsuoka (1987). Note that although an average ϕ'_{yield} is prescribed in Figures 4-9 and 4-10, the variation of ϕ'_{yield} with e_c is discussed later in this chapter.

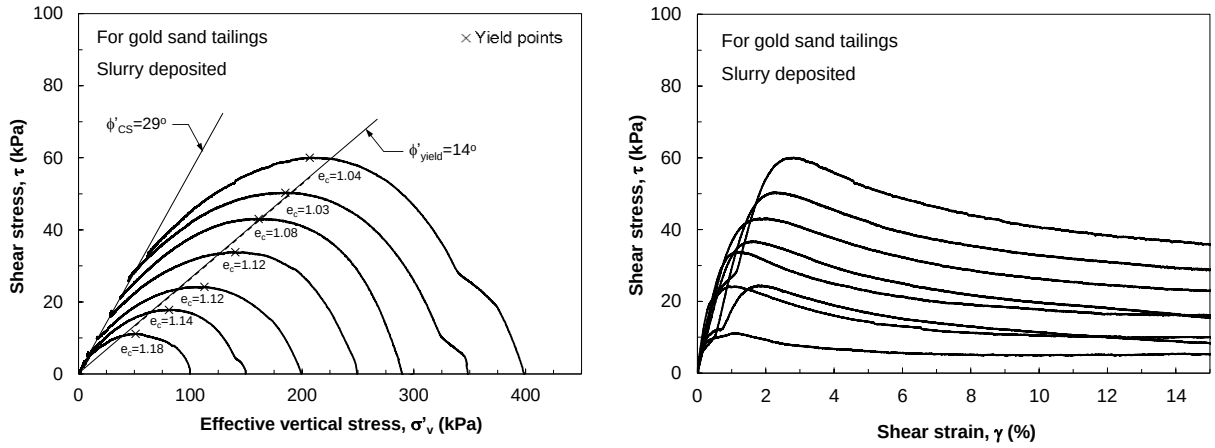

Figure 4-9: Stress paths and stress-strain curves for constant-volume DSS tests on slurry-deposited gold sand tailings.

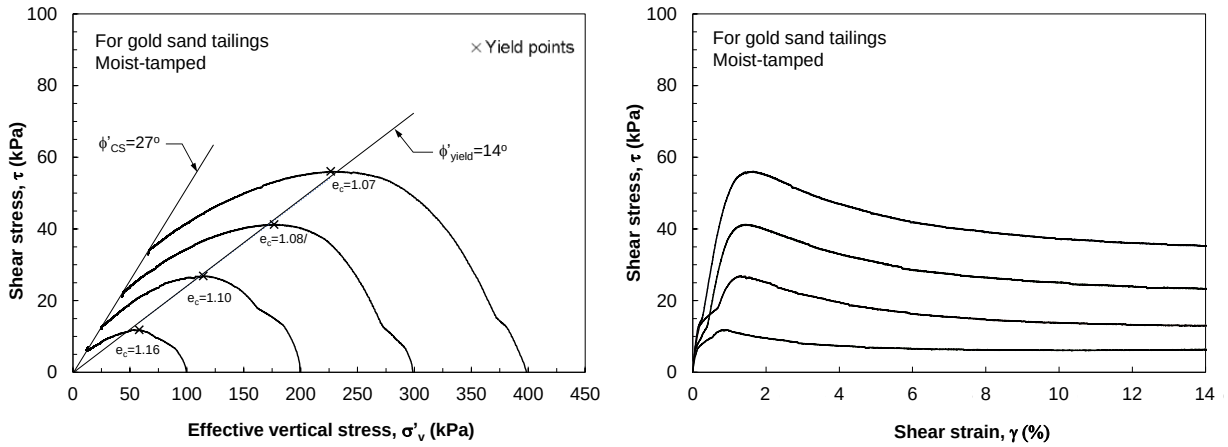

Figure 4-10: Stress paths and stress-strain curves for constant-volume DSS tests on moist-tamped gold sand tailings.

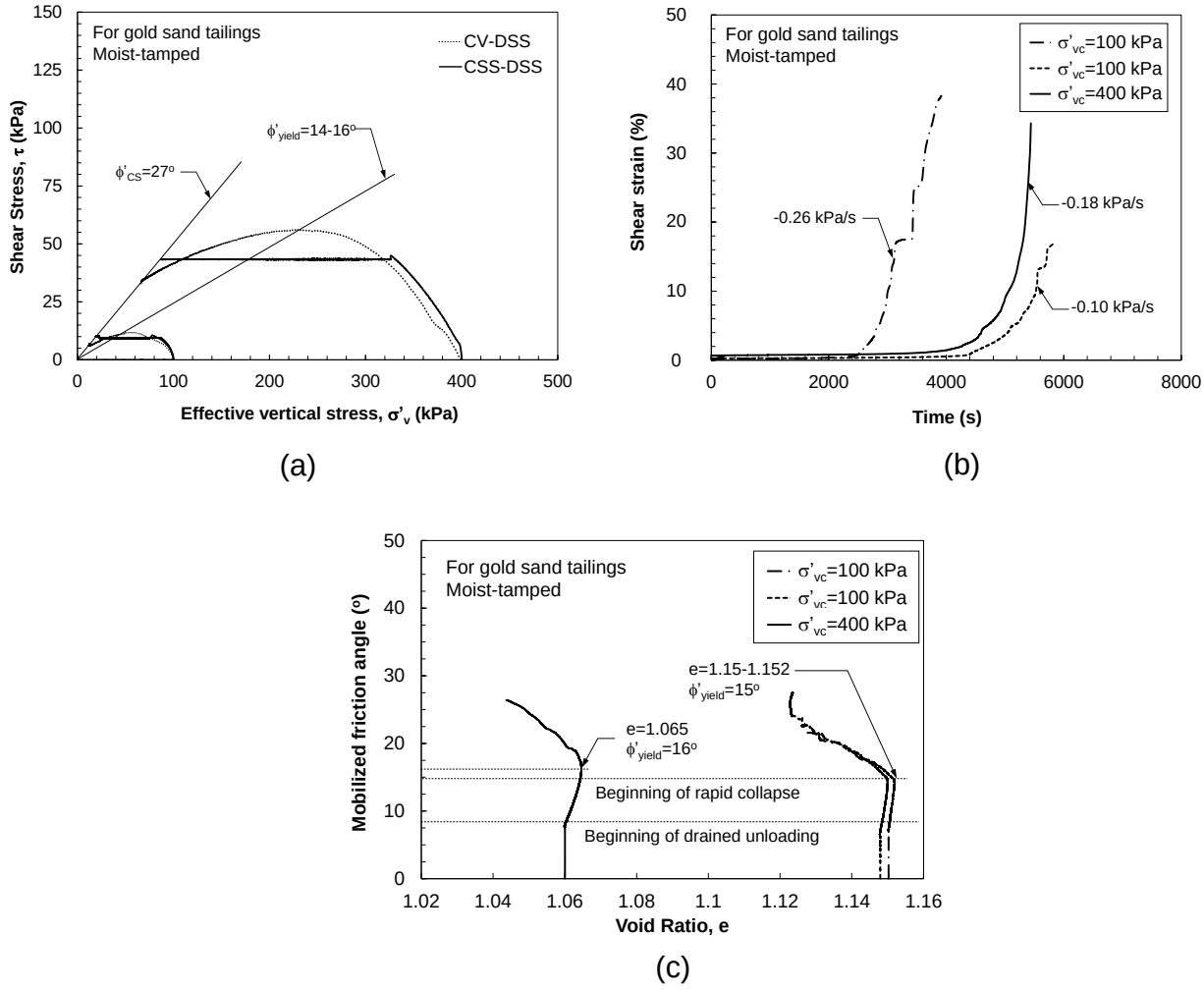

Figure 4-11: (a) Stress paths, (b) Shear-strain time history, and (c) void ratio versus mobilized friction angle for drained constant shear stress DSS tests on moist-tamped gold sand tailings specimens.

Besides constant-volume DSS tests, a limited number of drained constant-shear-stress DSS tests were also carried out on moist-tamped sand tailings to replicate the stress path of several deformation-induced liquefaction failures (e.g., the Fundão dam, Nerlerk Berm). In these tests, the specimens were first consolidated to a certain σ'_{vc} and an initial shear stress (τ_c). They were subsequently sheared by reducing the total vertical stress while maintaining a constant τ_c as shown in Figure 4-11(a). Despite the drained conditions imposed on the specimens tested (by allowing changes in volume), liquefaction behaviour was exhibited by a rapid acceleration of shear-strain

(Fig. 2-11b) and a sudden drop in void ratio (Fig. 2-11c). Yielding is defined for these stress paths when volumetric behaviour changes from dilation to contraction (in Fig. 2-11c), which corresponds to the crossing of the instability line (IL) – the locus of yield points that projects as a straight line down to the origin of the stress path – at ϕ'_{yield} = 14° to 16°, comparable to those obtained from the constant-volume DSS tests. The difference in time required to trigger yielding portrayed in Figure 4-11(b) is simply due to the application of different rates of vertical stress reduction, which was found to have a negligible effect as the two similar specimens consolidated to 100 kPa showed the same ϕ'_{yield}. This observation suggests that triggering of liquefaction by constant-volume (i.e. undrained) loading and effective stress reduction are coupled by the slope of the instability line (i.e. ϕ'_{yield}), and strain-softening is ensued when the instability line is crossed regardless of the stress path followed.

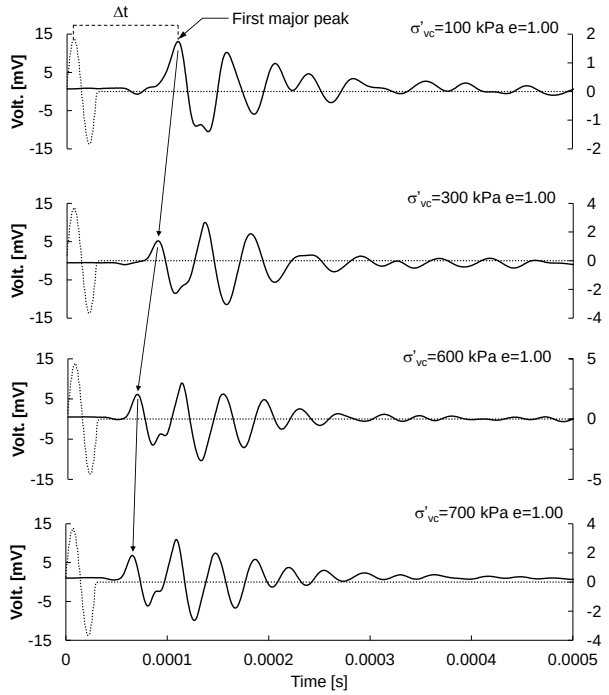

Figure 4-12: Variations in travel time with increasing σ'_{vc} measured in BE tests on gold sand tailings specimens for e_c = 1.00

In order to relate the laboratory test results to an in-situ measurement, shear wave velocity (V_S) was measured in the tailings samples consolidated at different σ'_{vc} to a certain e_c. V_S can be readily measured with several in-situ testing techniques including downhole, cross-hole, multichannel analysis of surface waves, or seismic CPT methods. V_S is often expressed as a function of e_c and σ'_{vc} as below (Hardin and Richart Jr. 1963):

(Eq. 4-1) $$V_S = f(e_c)\sigma'_{vc}{}^{\beta}$$

In which, β is the stress normalization exponent and $f(e_c)$ is the void ratio function.

An overburden-stress normalized V_S can be subsequently determined in order to account for the effect of σ'_{vc} as below (Robertson et al.1995):

(Eq. 4-2) $$V_{S1} = V_S \left(\frac{P_a}{\sigma'_{vc}}\right)^{\beta}$$

Where $P_a \approx 100$ kPa.

Figure 4-12 shows the incipient and received shear wave signals (at an input frequency of 33.3 kHz) for a series of BE tests on specimens with $e_c = 1.00$ and consolidated to $\sigma'_{vc} = 100$ - 700 kPa. As illustrated in the figure, the V_S travel time decreased with increasing σ'_{vc}, demonstrating the high dependency of V_S on effective stress. Figure 4-13 summarizes V_S profiles with σ'_{vc} at different e_c ($\approx$ 1.10, 1.00, 0.97), and according to this figure, the stress normalization exponents (β) fitted by a power function reduces for denser samples from $\beta = 0.23$, 0.18, and 0.17 for $e_c \approx 1.10$, 1.00, and 0.97, respectively. This observation is further shown in Figure 4-14, in which the exponential correlation between β and e_c illustrates the dependency of the sand tailings' V_S on density. Note that the β exponents presented in the figure compare relatively well with that typically used for silica sands (0.25), likely due to the specific mineralogy or shape of the sand tailings particles. Additionally, V_S measurements in gold tailings samples (with FC = 76%) by Grimard (2018) are shown in Figure 4-13, which seem to agree with those measured in this study at $e_c = 1.10$.

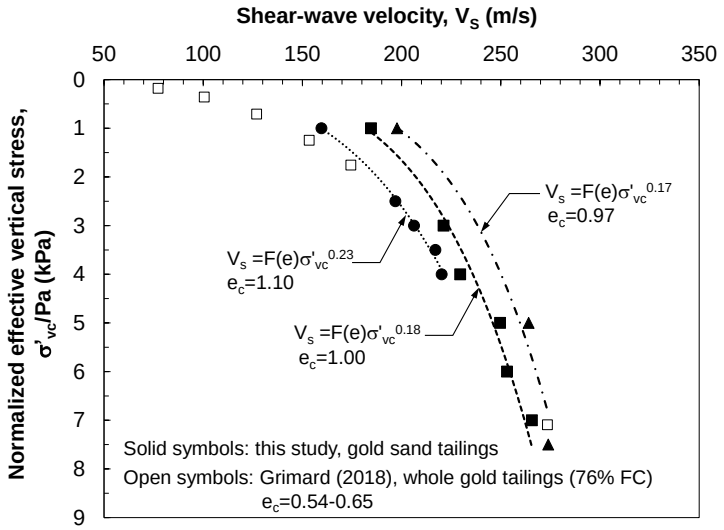

Figure 4-13: Variation of V_s with σ'_{vc}/Pa for gold sand tailings of this study as well as those for other gold tailings by Grimard (2018).

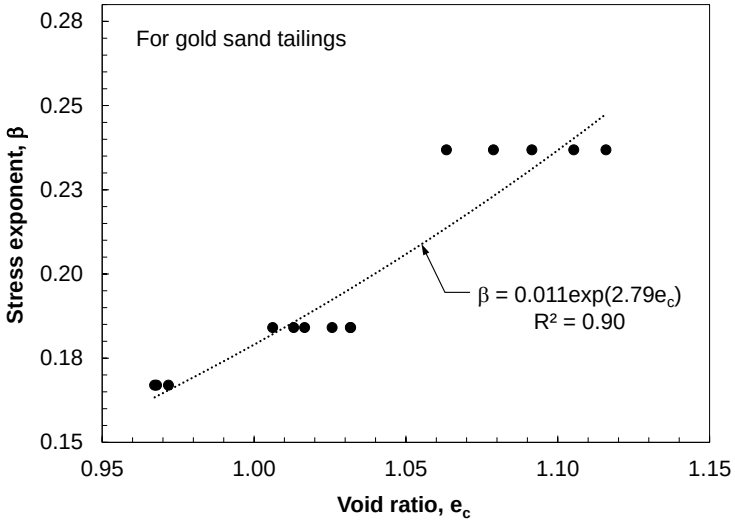

Figure 4-14: Variation of β exponent with e_c for gold sand tailings in this study

4.5. Interpretation and Discussion of Results

4.5.1. Effects of Fabric

As shown earlier, very contrasting shear behaviours were observed in the constant-volume DSS testing of whole gold tailings using the two different specimen preparation techniques. Slurry deposited whole tailings exhibited little yielding and showed incessant dilation, whereas moist-tamped tailings underwent strain-softening before showing dilation towards the end of shearing. Both types of behaviour, however, seem to conform to the findings and observations made by other researchers (Fourie and Papageorgiou 2001; Fourie et al. 2001; Papageorgiou 2004; Fourie and Tshabalala 2005), and the contrast can be attributed to the different fabric produced by each preparation method. Although slurry preparation may be considered to produce a uniform soil fabric similar to that found in-situ (Chang 2009), this technique often results in segregation when used in silty or well-graded soils by maintaining fine particles in suspension (Kuerbis et al.1988) and the void ratios attainable in a laboratory are much lower than those possible in-situ (Jeffries and Been 2016). Distinctly, the capillary effect in moist-tamping forms a fabric with flocks of small particles acting as bridges between larger ones (Chang 2009), resulting in very loose soil structures susceptible to strain-softening in undrained shear conditions (Ishihara1993). Hence, despite the effort made to reduce segregation by preventing the particles from settling during slurry preparation, the depositional method still inhibited the formation of a metastable structure in the whole tailings, rendering any comparison of liquefied behaviour with moist-tamped specimens unfeasible. Nevertheless, it can be highlighted that the same values of average ϕ'_{PT} for both depositional methods were observed. Likewise, as shown in Figure 4-15(a), if the void ratios and effective vertical stresses of slurry prepared specimens at phase-transformation states are plotted, the datapoints lie within the experimental scatter of the CSL obtained from moist-tamped specimens and are also comparable to those reported by Papageorgiou (2004) for TxC tests on Merriespruit whole gold tailings (with FC = 60%), for which σ'_v was estimated to be equal to σ'_1. Figure 4-15(b) further compares this same CSL in e-p' (assuming $K_0 = 1 - \sin \phi'_{max} = 0.48$ for DSS tests) space with those described by Grimard (2018) and Bedin et al. (2012) from TxC tests, highlighting the resemblance in slope, but exhibiting vertical offsets plausibly due to the difference in FC.

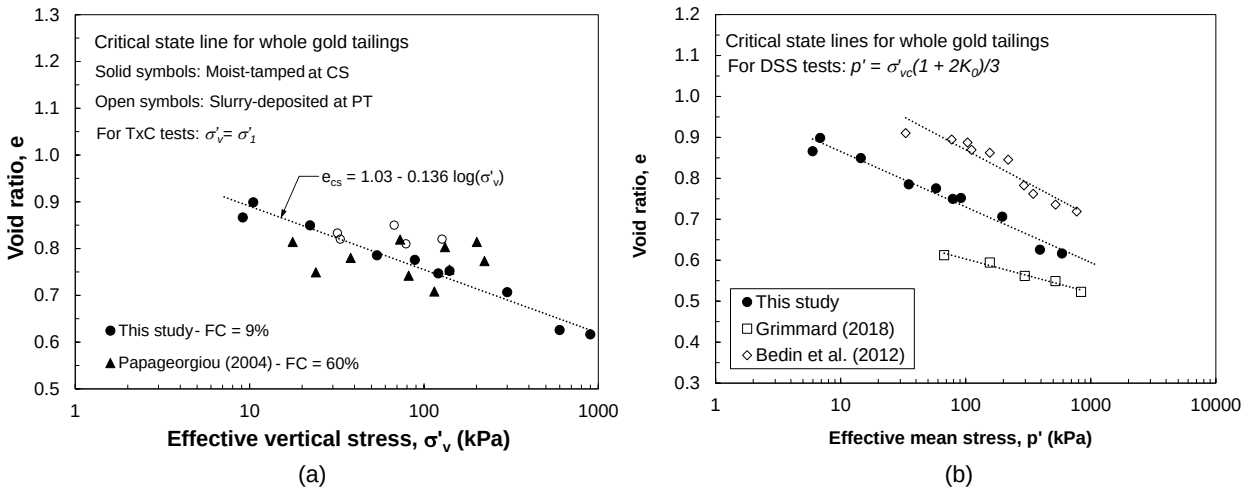

Figure 4-15: (a) Critical state lines for the whole gold tailings obtained from experiments on moist-tamped and slurry deposited specimens; (b) Comparison of obtained CSL with those from TxC on tailings (Grimard 2018; Bedin et al. 2012).

Given the lower FC of gold sand tailings, the effects of fabric on their liquefaction behaviour can be more readily evaluated than on the whole tailings. Moreover, since particle segregation upon deposition and/or the use of spray-bars and cycloning generate a sandier beach that serves as foundation for subsequent upstream raising of impoundments, the remaining of this study focuses on the behaviour of sand tailings. Unlike the results of whole tailings, both preparation methods produced soils structures that strain-softened and reached critical state without any signs of dilation in sands. Consistent with previous observations by Arthur and Menzies (1972), ϕ'_{CS} measured for both types of fabrics is essentially the same, with slurry-deposited specimens exhibiting an average $\phi'_{CS} = 29^o$ and moist-tamped specimens $\phi'_{CS} = 27^o$ (see Fig. 2-16a). As also observed by Jeffries and Been (2016), s_u(yield) (hence also ϕ'_{yield}) and s_u(liq) are very similar notwithstanding the different depositional methods used (see Fig. 2-16b). Furthermore, as shown in Figure 4-17(a), a small difference in the location of the CSL for both fabric types can be deduced from the results obtained. Nevertheless, a single CSL can be assumed for practical purposes, as such a small difference is seen to be blurred by experimental scatter in the data. The single CSL is hence described by the following relationship:

(Eq. 4-3) $$e_{cs} = 1.29 - 0.131 \log \sigma'_{vc}$$

The uniqueness of this CSL is further illustrated in Figure 4-17(a), in which the critical states of moist-tamped specimens tested under vertical stress relief paths is shown to coincide with the CSL obtained from undrained tests. Figure 4-17(b) further compares this established CSL for the gold sand tailings in e-Log(p') space with the CSL determined by Fourie and Tshabalala (2013) for Merriespruit gold sand tailings (FC = 20%) and demonstrates their similarity in slope, while the vertical offset plausibly results from the 10% difference in FC between the two tailings samples.

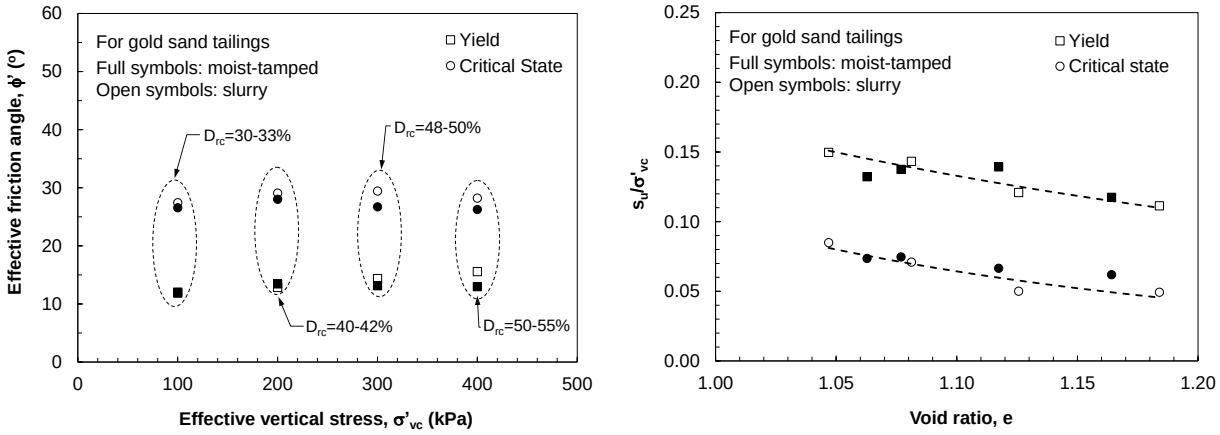

(a) (b)

Figure 4-16: (a) Comparison of ϕ'_{yield} and ϕ'_{CS} measured in slurry-deposited and moist-tamped DSS specimens with similar densities and stress states; (b) Diagram showing trends of S_u/σ'_{vc} with e_c for different sample preparation methods.

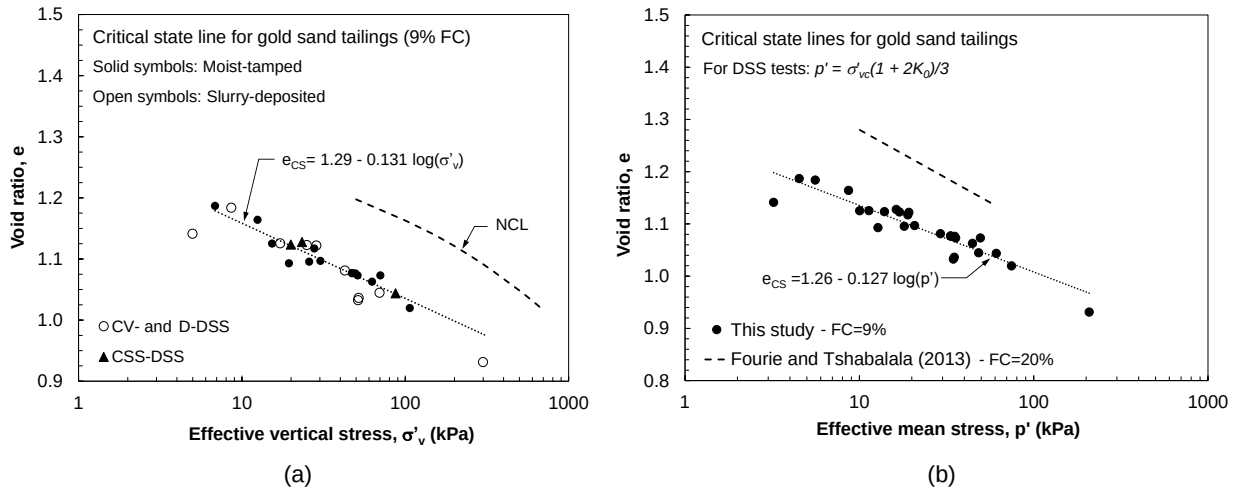

Figure 4-17: (a) Critical state line established for gold sand tailings using moist-tamped and slurry-deposited samples; (b) Comparison of the CSL established for the gold sand tailings of this study with that for Merriespruit sand tailings from TxC tests (Fourie and Tshbalala 2013).

4.5.2. Post-Liquefied Shear Behaviour

Figure 4-18 presents general trends of yielding and post-liquefaction undrained strength ratios, i.e. $S_u(yield)/\sigma'_{vc}$ and $S_u(liq)/\sigma'_{vc}$, as well as ϕ'_{yield} with changes in e_c observed for the gold tailings tested in this study. All three of these strength parameters exhibit increasing trends with decreasing e_c, thus indicating the strengthening of sand tailings with density. As shown in Figure 4-18(a), undrained strength ratios from moist-tamped whole tailings specimens from this and other studies (Al-Tarhouni 2001; Papageorgiou 2004; Morgenstern et al. 2016) also compare favourably with the trends indicated by the sand tailings. Figure 4-18(b) further shows the values of ϕ'_{yield} obtained for gold sand and whole tailings and compares them with those of Fundão iron sand tailings reported by Morgenstern et al. (2016). As shown, a well-defined trend of ϕ'_{yield} for e_c = 0.70 - 1.2 can be established irrespective of FC and liquefaction triggering mechanism (i.e. test type), with ϕ'_{yield} ranging from approximately 12^o to 17^o.

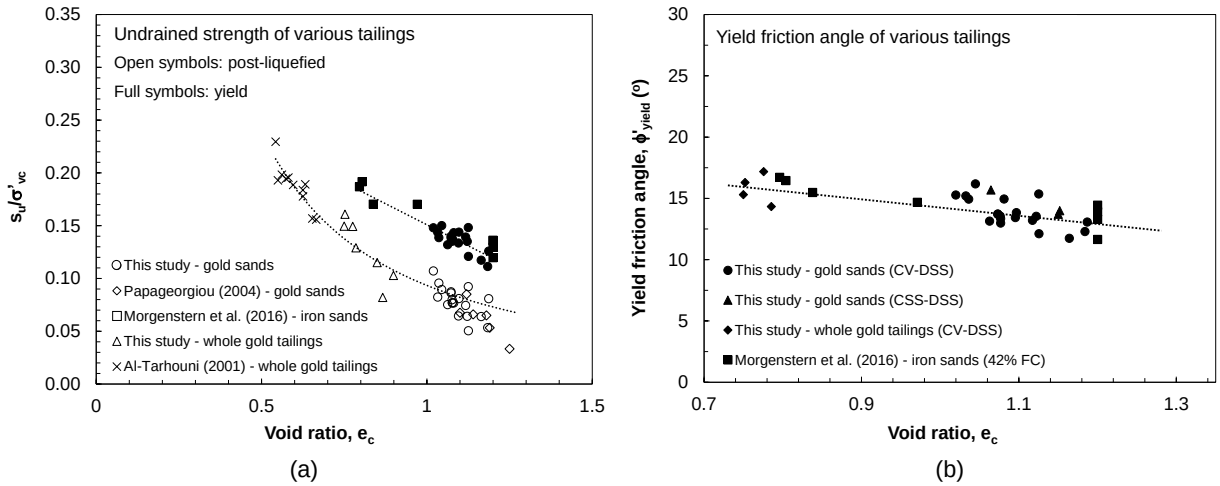

Figure 4-18: Variations of (a) $S_u(yield)/\sigma'_{vc}$ and $S_u(liq)/\sigma'_{vc}$, and (b) ϕ'_{yield} with e_c for a variety of tailings.

Given that the state of a soil element is better represented by the state parameter, Figure 4-19 presents the trends in $S_u(yield)/\sigma'_{vc}$ and $S_u(liq)/\sigma'_{vc}$, with changes in ψ for the gold sand tailings tested in this study compared with those tested by Papageorgiou (2004). Similar comparisons with other sand tailings were not possible, as the required critical state parameters (Γ and λ) were not readily available. The following relationships are fitted for the gold sand tailings tested in this study:

(Eq. 4-4) $$S_u(yield) = -0.334(\psi) + 0.174$$

(Eq. 4-5) $$S_u(liq) = -0.504(\psi) + 0.136$$

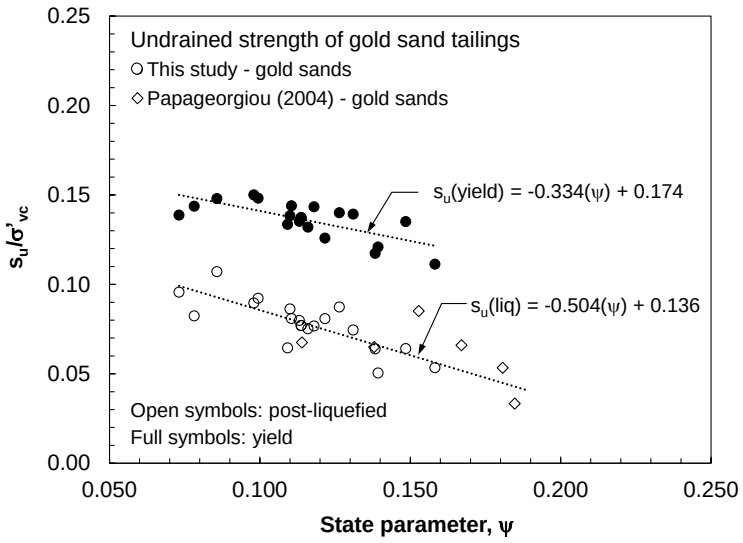

Figure 4-19: Variations of S_u(yield)/σ'_{vc} and S_u(liq)/σ'_{vc} with ψ for the gold sand tailings in this study and those by Papageorgiou (2004).

An observation can also be made with regards to change in the sand tailings' brittleness, expressed as the brittleness index I_B=(S_u(yield)- S_u(liq))/ S_u(yield) x 100%, with changes in the state parameter. Figure 4-20 shows the decreasing trend in the magnitude of I_B with decreasing values of the state parameter for the gold sand tailings, demonstrating the reduction in sudden strength loss as the state of a tailings element approaches critical state.

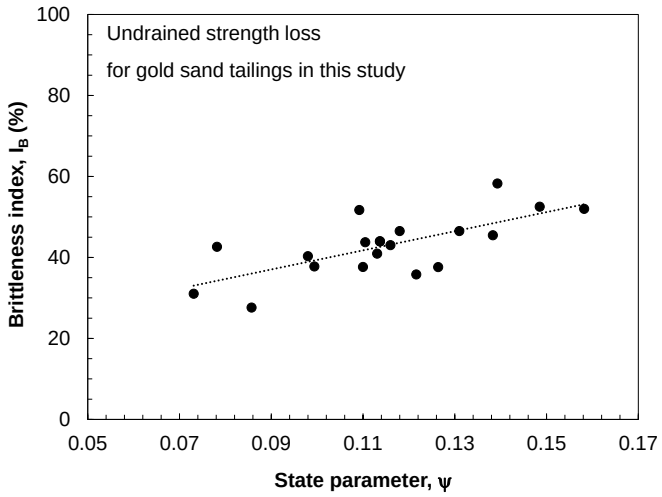

Figure 4-20: Variations of I_B with ψ for the gold sand tailings in this study.

After confirming the comparability of the results obtained for gold sand tailings with those reported by other investigators in the preceding figures, these same results are presented in Figure 4-21 in terms of the ratio of state parameter and the CSL slope (ψ/λ_{10}), calculated using the CSL parameters previously established. Sadrekarimi (2013) made the observation that $Su(liq)/\sigma'_{vc}$ of several sands exhibit a unique trend with ψ/λ_{10}. Accordingly, Figure 4-21 shows that similar trends exist not only for $S_u(liq)/\sigma'_{vc}$, but also for $s_u(yield)/\sigma'_{vc}$ and ϕ'_{yield} with ψ/λ_{10}. The following relationships are consequently fitted for the gold sand tailings tested in this study:

(Eq. 4-6) $$\frac{S_u(liq)}{\sigma'_{vc}} = 0.20\exp(-0.429\,\psi/\lambda_{10})$$

(Eq. 4-7) $$\frac{S_u(yield)}{\sigma'_{vc}} = 0.21\exp(-1.112\,\psi/\lambda_{10})$$

(Eq. 4-8) $$\phi'_{yield} = 19.4\exp(-0.392\,\psi/\lambda_{10})$$

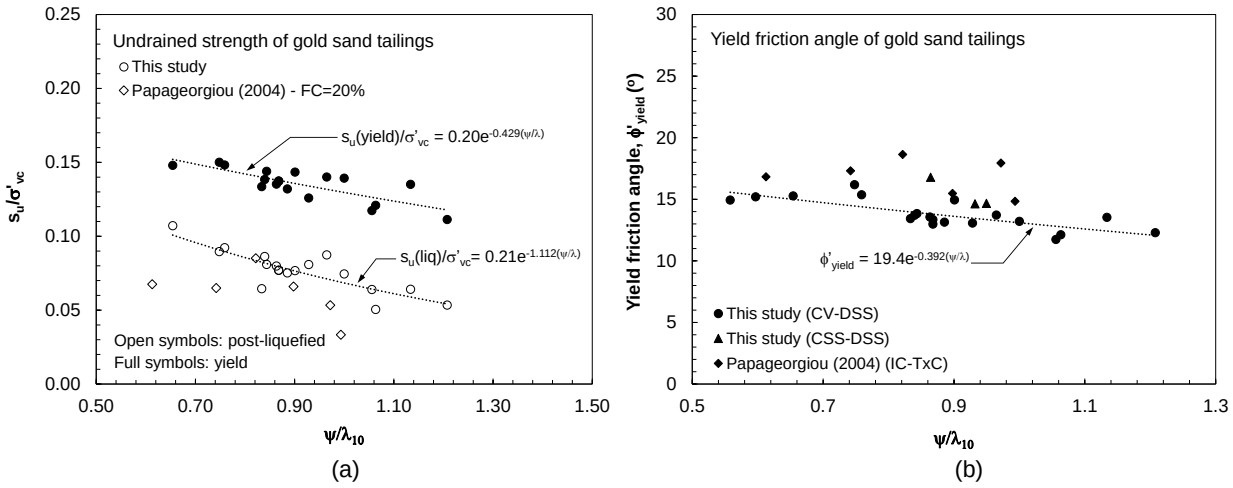

Figure 4-21: Variations of (a) $S_u(yield)/\sigma'_{vc}$ and $S_u(liq)/\sigma'_{vc}$, and (b) ϕ'_{yield} with ψ/λ_{10} for gold sand tailings.

4.5.3. Shear-wave Velocity

As previously discussed, and described by Equation (5), V_S is dependent on e_c and σ'_{vc}. As shown in Figure 4-13, the effect of σ'_{vc} was described by a power function for each e_c. Several researchers (Hardin and Richart Jr. 1963, Robertson et al. 1995) have suggested different functions to express the effect of void ratio on V_S. Figure 4-22 shows that the effect of e_c on the stress-normalized V_S/σ'_{vc} can be described by a linear function for the gold sand tailings. According to this figure, linear trends have also been used by several other studies (de Alba et al. 1984; Huang et al. 2004; Grimard 2018) to show the effect of e_c on V_S for sands and tailings. Nevertheless, a much steeper trend is observed in this study, indicating a stronger effect of e_c on V_S measured in the gold sand tailings of this study, perhaps because of their angular particle shapes and greater compressibility (C_C= 0.16 in Fig. 2-6).

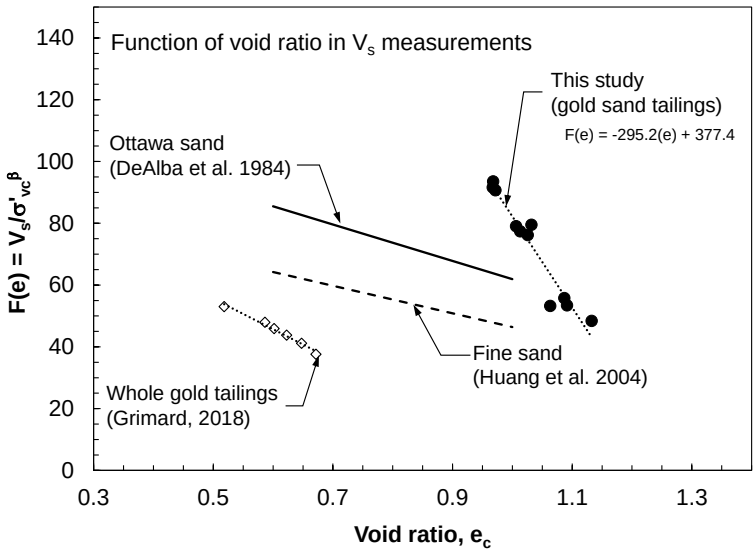

Figure 4-22: Variation of F(e) with consolidation void ratio (e_c) for gold sand tailings and comparison with correlations derived by others for similar materials.

Based on Figures 4-13, 4-14, and 4-22, V_S of the gold sand tailings can be predicted from the following equations if σ'_{vc} and e_c or ψ are known:

(Eq. 4-9) $$V_S(m/s) = (377.4 - 295.2e_c)\sigma'^{[0.011\exp(2.79e_c)]}_{vc}$$

(Eq. 4-10) $$V_S(m/s) = (38.7\log_{10}\sigma'_{vc} - 295.2\psi - 3.41)\sigma'^{[0.011\exp(2.79\psi+3.60-0.365\log_{10}\sigma'_{vc})]}_{vc}$$

In the following paragraphs, the laboratory test results are processed on order to establish empirical correlations for static liquefaction analysis of gold sand tailings.

4.5.4. Liquefaction Analysis

Robertson et al. (1995) introduced an analytical relationship between V_S and ψ. This same relationship is established below to conform with the vertical stress measured in a DSS tests:

(Eq. 4-11) $$\psi = \left(\frac{A}{B} - \Gamma\right) - \left(\frac{V_S}{B\sigma'^{\beta}_{vc}} - \lambda_{10}\log_{10}\sigma'_{vc}\right)$$

in which A and B are the intercept and slope of the void ratio function shown in Figure 4-15. A V_S-based liquefaction susceptibility boundary can be established by plotting the above equation for $\psi = 0$. Figure 4-23(a) presents this boundary for the gold sand tailings tested in this study using parameters A = 377.4, B = -295.2, $\Gamma = 1.29$, $\lambda_{10} = 0.131$, and an average $\beta = 0.20$. Figure 4-23(a) also shows V_S predicted using Equation (16) for the specimens of Figures 4-9 to 4-11. These data plot in the contractive region (i.e. below the boundary) of Figure 4-23(a), indicative of their observed susceptibility to strain-softening shown in Figures 4-9 to 4-11. Figure 4-23(b) further compares this liquefaction susceptibility boundary established for the gold sand tailings with the laboratory V_S measurements reported by Shnaid et al. (2013) for whole gold tailings from a Brazilian mine, and those reported by Vidich et al. (1998) from a seismic cone penetration test (SCPT) carried out in the beach section of a gold mine tailings dam in Nevada, USA. With respect to the V_S data measured by Shnaid et al. (2013), the boundary seems to accurately indicate the susceptibility to liquefaction of those specimens reported to have strain-softened, as well as the dilative behaviour of those that showed signs of strain-hardening. In the same way, the boundary appears to agree with the conclusion reached by Vinich et al. (1998) in the case of the tailings dam, whereby the beach tailings were deemed most likely to behave in a dilative manner. It must be highlighted, however, that each material has its distinct properties, and as such, a liquefaction susceptibility boundary for each must be determined to accurately assess static liquefaction risk. Nevertheless, in the absence of advanced testing for determining the parameters of Equations (7), (15), and (16), the boundary of Figure 4-23 could be used as a preliminary guideline to identify liquefiable tailings deposits.

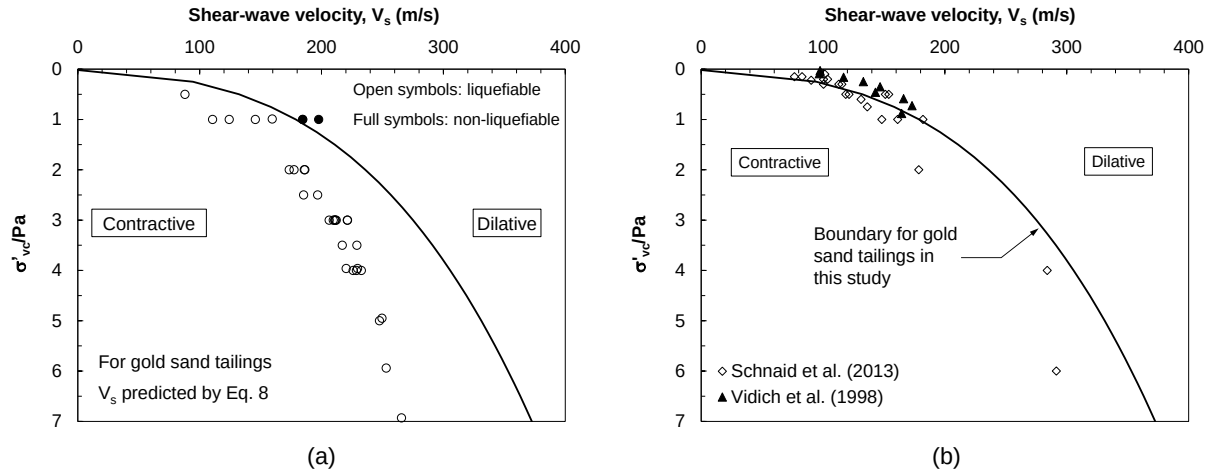

Figure 4-23: Comparison of the V_S-based contractive-dilative boundary for gold sand tailings with (a) V_S predicted for the specimens of Figures 4-4 to 4-6, and (b) V_S measured in laboratory (Schnaid et al. 2013) and field SCPT (Vidich et al. 1998) tests in gold mine tailings.

Since both strength and V_S of cohesionless materials are primarily controlled by the stress state and void ratio, it is also reasonable and practical to combine the experimental results obtained in order to establish empirical correlations between these parameters. Figure 4-24 shows the undrained strength ratios and ϕ'_{yield} from the DSS tests versus V_{S1} estimated from Equations 10-12 and 6 for the gold sand tailings of this study. The following empirical relationships are subsequently established between V_{S1} and tailings shear strength at yielding and post-liquefaction:

(Eq. 4-12) $$\frac{S_u(liq)}{\sigma'_{vc}} = 0.05\exp(0.003V_{s1})$$

(Eq. 4-13) $$\frac{S_u(yield)}{\sigma'_{vc}} = 0.11\exp(0.002V_{s1})$$

(Eq. 4-14) $$\phi'_{yield} = 9.14\exp(0.003V_{s1})$$

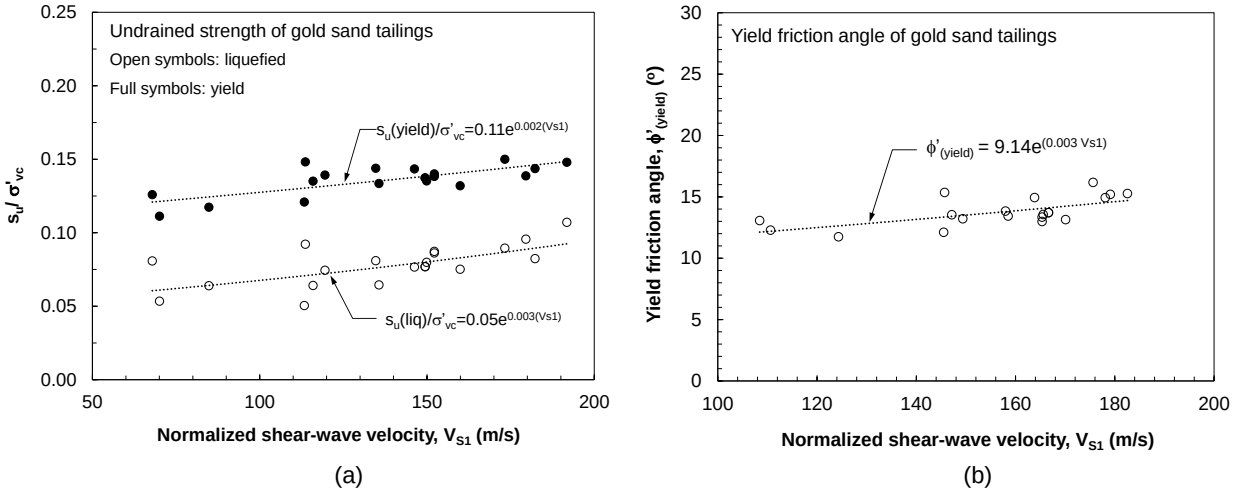

Figure 4-24: Variations of (a) $S_u(yield)/\sigma'_{vc}$ and $S_u(liq)/\sigma'_{vc}$, (b) ϕ'_{yield} with V_{S1} for the gold sand tailings tested in this study.

In a static liquefaction analysis, $S_u(yield)/\sigma'_{vc}$ or ϕ'_{yield} can be used (e.g. in a limit equilibrium analysis) to determine the triggering of static liquefaction for contractive tailings identified through Figure 4-24. The risk of a liquefaction flow failure (or a factor of safety) can then be established by using the post-liquefaction undrained strength, $S_u(liq)$, for the liquefied tailings.

4.6. Conclusions

Mine tailings are unique materials with distinctive properties that are dependent on the mineral extraction processes as well as the ores' mineralogy. Common hydraulic deposition of tailings produces a uniform soil fabric with heterogeneous gradations throughout storage impoundments, with coarser particles settling near the points of discharge and fines accumulating in the decant pool. This particle segregation is sometimes purposely generated by cycloning of sands prior to deposition or the use of spray-bars in order to use this same material for subsequent raising of the dam. If saturated, these loose sand tailings have been found to be susceptible to static liquefaction, and many dam collapses have occurred as a result. Conclusions from the experimental program conducted in this study on moist-tamped and slurry deposited specimens suggest that the effect of fabric on the undrained shear behaviour of gold sand tailings is negligible for practical purposes.

The same cannot be said about the whole (or as-milled) tailings, as the higher silt content produced a more uniform gradation that fostered particle suspension during hydraulic preparation of specimens in the laboratory, ultimately inhibiting the generation of a liquefiable metastable structure and exhibiting dilative behaviour upon shearing. Unlike the results on whole tailings, both moist-tamping and slurry deposition of sand tailings produced soils structures that strain-softened and reached critical state without any signs of dilation.

Based on the critical state framework, an empirical method correlating shear-wave velocity of gold sand tailings with their susceptibility to static liquefaction and their undrained strength was developed from an extensive experimental program comprised of bender element and direct simple shear tests. The method's accuracy was confirmed by comparing liquefaction susceptibility assessments made by other researchers on fairly similar tailings. It is thus concluded that as long as critical state parameters and shear wave velocity data are available, the presented method can be used to evaluate the liquefaction potential of a tailings profile based on V_S measurements taken, and their undrained strength can be estimated for use in slope stability analyses.

As a final point, it must be highlighted that due to the various properties of the many types of tailings, individual parameters used in the analytical method are solely applicable to the tailings being evaluated. Hence, any attempts to extend the results to other hard rock tailings is not encouraged and must be considered very carefully. Moreover, although clear trends with high correlation coefficients were established for the correlations presented to characterize the shear behaviour of the tailings, there remains a small level of uncertainty in the repeatability of the results.

4.7. References

Airey, D., and Wood, D. (1987). An evaluation of direct simple shear tests on clay. *Geotechnique*, Vol 37, No. 1, pp. 25-35.

Airey, D., Budhu, M., and Wood, D. (1985). Some aspects of the behaviour of soils in simple shear. In E. P. Butterfield, *Development in Soil Mechanics and Foundation* (pp. Vol. 2, pp. 185. Elsevier.

Alarcon-Guzman, A., Leonards, G., and Chameau, J. L. (1988). Undrained monotonic and cyclic strength of sands. *Journal of Geotechnical Engineering,* 114(10), 1089-1109.

Allen, T. (2015). *Microscopy: A Very Short Introduction.* Oxford, UK: Oxford University Press.

Al-Tarhouni, M. (2008). *Liquefaction and Post-liquefaction Behaviour of Gold Mine Tailings under Simple Shear Loading.* Ottawa: Carleton University.

Al-Tarhouni, M., Simms, P., and Sivathayalan, S. (2011). Cyclic behaviour of reconstituted and desiccated-rewet thickened gold tailings in simple shear. Canadian Geotechnical Journal, 48(7),1044.

Arthur, J. and Menzies, B. (1972): Inherent anisotropy in a sand. *Geotechnique, vol. 22*, pp. 115-128.

ASTM D6528-17, A. (2017). Standard Test Method for Consolidated Undrained Direct Simple Shear Testing of Fine Grain Soils. *ASTM International*.

ASTMD422-63. (2007). *Standard Test Method for Particle-Size Analysis of Soils.* ASTM. doi:10.1520/D0422-63R07E02

ASTMD4253—16. (2016). Standard Test Methods for Maximum Index Density and Unit Weight of Soils Using a Vibratory Table1. *ASTM*. Retrieved from https://doi-org.proxy1.lib.uwo.ca/10.1520/D4253-16

ASTMD4254—16. (2016). Standard Test Methods for Minimum Index Density and Unit Weight of Soils and Calculation of Relative Density1. *ASTM*. Retrieved from https://doi-org.proxy1.lib.uwo.ca/10.1520/D4254-16

ASTMD6528-17. (2017). Standard Test Method for Consolidated Undrained Direct Simple Shear Testing of Fine Grain Soils. *ASTM*. Retrieved from https://doi-org.proxy1.lib.uwo.ca/10.1520/D6528-17

ASTMD854—14. (2014). Standard test methods for specific gravity of soil solids by water pycnometer. *ASTM*. Retrieved from https://doi-org.proxy1.lib.uwo.ca/10.1520/D0854-14

Bedin, J., Schnaid, F., Da Fonseca, A. V., and Costa Filho, L. M. (2012). Gold Tailings Liquefaction under Critical State Soil Mechanics. *Gotechnique 62*, No. 3, 263–267 .

Been, K., and Jeffries, M. G. (1985). A state parameter for sands. *Geotechnique*, 35(2), 99-112.

Been, K., Jeffries, M. G., and Hachey, J. E. (1991). The critical state of sands. *Geotechnique*, 41(3), 365-381.

Bjerrum, L., and Landva, A. (1966). Direct simple shear test of Norwegian quick clay. *Geotechnique*, 16(1): 1-20.

Blight, G. (2010). *Geotechnical Engineering for Mine Waste Storage Facilities.* London, UK: Taylor and Francus Group.

Blight, G., and Steffen, D. (1979). Geotechnics of Gold Mine Waste Disposal. *Current Geotechnical Practice in Mine Waste Disposal, ASCE*, pp. 1-52.

Brignoli, E., Gotti, M., and Stokoe, K. (1996). Measurement of Shear Waves in Laboratory Specimens by Means of Piezoelectric Transducers. *Geotechnical Testing Journal, Vol. 19, No. 4*, 384-397. Retrieved from https://doi-org.proxy1.lib.uwo.ca/10.1520/GTJ10716J.

Camacho-Tauta, J. F., CASCANTE, G., VIANA DA FONSECA, A., and A, S. J. (2015). ime and frequency domain evaluation of bender element systems. *Geotechnique*, 65:548-562.

Casagrande, A. (1936). Characteristics of cohesionless soils affecting the stabilityof earth fills. *Journal of Boston Society of Civil Engineers*, 23, 257-276.

Chang, N. (2009). *The Effect of Fabric on the Behaviour of Gold Tailings.* Hatfield: University of Pretoria.

Chang, N., Heymann, G., and Clayton, C. (2011). *The effect of fabric on the behaviour of gold tailings.* Géotechnique 2011 61:3, 187-197.

Dobry, R., Vasquez-Herrera, A., and Ramly, M. (1985). Liquefaction flow failure of silty sand by torsional cyclic tests. *Advances in the art of testing soils under cyclic conditions* (pp. 29-50). Detroit, MI: ASCE.

Dyvik, R., Berre, T., Lacasse, S., and Raadim, B. (1987). Comparison of truly undrained and constant volume direct simple shear tests. *Geotechnique*, 37(1): 3-10.

East, D., Ransone, J., and Cincilla, W. (1988). Testing of the Homestake mine tailings deposit. *Proceedings 2nd International Conference on Case Histories in Geotechnical Engineering*, (pp. pp. 495-502).

Fourie, A. B., Blight, G. E., and Papageorgiou, G. (2001). Static liquefaction as a possible explanation for the Merriespruit tailings dam failure. *Canadian Geotechnical Journal*, 8(4), 707–719.

Fourie, A., and Papageorgiou, G. (2001). Defining an appropriate steady state line for Merriespruit gold tailings . *Canadian Geotechnical Journal*, 38, 4: pp.695-706.

Fourie, A. B., and Tshabalala, L. (2005). Initiation of static liquefaction and the role of K^sub 0^ consolidation. *Canadian Geotechnical Journal*, 42(3), 892-906. Retrieved from https://www-lib-uwo-ca.proxy1.lib.uwo.ca/cgi-bin/ezpauthn.cgi?url=http://search.proquest.com.proxy1.lib.uwo.ca/docview/213356536?accountid=15115

Galindon da Fonseca, P., and Galindo da Fonseca, I. (2016). Brazil's Greatest Environmental Catastrophe – Samarco's Fundão Tailings Dam –. *Environmental Policy and Law*, 46/5: 334-337.

Hamel, J., and Gunderson, J. (1973). Shear Strength of Homestake Slimes Tailings. *J. of Soil Mech. and Fdn. Div., ASCE*, Vol. 99, No. SM5, pp. 247-234.

Hardin, B. O., and Richart Jr., F. E. (1963). Elastic wave velocities in granular soils. *Journal of Soil Mechanics and Foundation Division, ASCE*, 89(1), 33 - 65.

Ishihara, K. (1993). Liquefaction and flow failure during earthquakes. *Geotechnique* 43, No. 3, 351–415.

Jeffries, M. G., and Been, K. (1987). Use of critical state representations of sand in the method of stress characteristics. *Canadian Geotechnical Journal*, 24: 441-446.

Jeffries, M., and Been, K. (2016). *Soil Liquefaction -- A Critical State Approach, 2nd Ed.* Boca Raton: Taylor and Francis Group.

Jones, S. (2017). *Liquefaction Susceptibility Analysis of Fraser River sand in Miniature Cone Penetration Tests and Cyclic Direct Simple Shear Tests.* Electronic Thesis and Dissertation Repository. Retrieved from https://ir.lib.uwo.ca/etd/4782

Jovičić, V., and Coop, M. (1998). The Measurement of Stiffness Anisotropy in Clays with Bender Element Tests in the Triaxial Apparatus. *Geotechnical Testing Journal Vol. 21, No. 1*, 3-10. Retrieved from https://doi-org.proxy1.lib.uwo.ca/10.1520/GTJ10419J

Kuerbis, R., Negussey, D., and Vaid, Y. (1988). Effects of gradation and fines content on the undrained response of sands. In E. b. Vick, *Hydraulic fill structures* (pp. 330-345). ASCE.

Mitchell, J. K., and Soga, K. (2013). *Fundamentals of soil behaviour, 3rd ed.* Hoboken, NJ: John Wiley and Sons.

Morgenstern, N. R., Vick, S. G., Viotti, C. B., and Watts, B. D. (2016). *Fundão Tailings Dam Review Panel: Report on the Immediate Causes of the Failure of the Fundão Dam.*

Olson, S.M. and Stark, T.D. (2003). Yield Strength Ratio and Liquefaction Analysis of Slopes and Embankments. *Journal of Geotechnical and Geoenvironmental Engineering – ASCE, Vol. 129, No. 8.* DOI: 10.1061/ASCE1090-02412003129:8727

Papageorgiou, G. (2004). *Liquefaction Assessment and Flume Modelling of the Merriespruit Gold and Bafokeng Platinum Tailings.* Johannesburg: University of the Witwatersrand.

Pettibone, H., and Kealy, C. (1971). *Engineering Properties of Mine Tailings.* ASCE.

Pitman, T. D., Robertson, P. K., and Sego, D. C. (1994). Influence of fines on the collapse of loose sands. *Canadian Geotechnical Journal*, 31(5): 728-739. Retrieved from https://doi-org.proxy1.lib.uwo.ca/10.1139/t94-084

Qiu, Y., and Sego, D. (2001). Laboratory Properties of Mine Tailings. *Canadian Geotechnical Journal*, 38:pp. 183-190.

Robertson, P. K. (2010). Estimating soil unit weight from CPT. *2nd International Symposium on Cone Penetration Testing.* Huntington Beach, CA.

Robertson, P. K., Sego, D. C., and Cunning, J. C. (1995). Shear Wave Velocity to Evaluate in Situ State of Cohesionless Soils. *Canadian Geotechnical Journal 32*, no. 5: 848-858.

Roscoe, K., Schofield, A. N., and Wroth, C. P. (1958). On the yielding of soils. *Geotechnique*, 8(1), 22-53.

Sadrekarimi, A. (2013). Influence of fines content on liquefied strength of silty sands. *Soil Dynamics and Earthquake Engineering* 55 (2013) 108–119. DOI: http://dx.doi.org/10.1016/j.soildyn.2013.09.008

Sadrekarimi, A. (2016). Static Liquefaction Analysis Considering Principal Stress Directions and Anisotropy. *Geotech Geol Eng*, 34:1135–1154. doi:10.1007/s10706-016-0033-7

Sadrekarimi, A., and Olson, S. M. (2012). Effect of Sample-Preparation Method on Critical-State Behaviour of Sands. *Geotechnical Testing Journal*,, ol. 35, No. 4, 2012, pp. 548-562. Retrieved from https://doi-org.proxy1.lib.uwo.ca/10.1520/GTJ104317

Schnaid, F., Bedin, J., Viana da Fonseca, A., and de Moura Costa Filho, L. (2013). Stiffness and Strength Governing the Static Liquefaction of Tailings. *Journal of Geotechnical and Geoenvironmental Engineering*, Vol. 139, No. 12, pp. 2136-2144.

Schofield, A., and Wroth, C. P. (1968). *Critical state soil mechanics.* London, UK: McGraw Hill.

Seed, H.B. 1987. Design problems in soil liquefaction. *Journal of Geotechnical Engineering Division*, ASCE, 113(8): 827-845.

Sladen, J. A., D'hollander, R. D., Krahn, J. (1986). Liquefaction of sands, a collapse surface approach, *can geotech J* V22, N4, nov 1985, P564–P578. *International Journal of Rock Mechanics and Mining Sciences and Geomechanics Abstracts*, 23(4), 138-138. doi:10.1016/0148-9062(86)90748-5

Soderberg, R., and Busch, R. (1977). *Design Guide for Metal and Nonmetal Tailings Disposal.* U.S. Bureau of Mines.

Stark, T.D., Olson, S.M., Kramer, S.L., and Youd, T.L. (1998). Shear strength of liquefied soils. In *Proceedings of the Workshop on Post-Liquefaction Shear Strength of Granular Soils*, University of Illinois at Urbana-Champaign, Urbana, Illinois, 17-18 April 1997, 288 p. (Available only on the World Wide Web at http://mae.ce.uiuc.edu/info/resources.html.)

Tatsuoka, F., Sasaki, T. and Yamada, S.(1984). Settlement in Saturated Sand Induced by Cyclic Undrained Simple Shear. *Proceedings, 8th World Conference on Earthquake Engineering, San Francisco*, Vol. 3, pp. 95-102, July 1984.

Tatsuoka, F. (1987). Strength and dilatancy of sands: Discussion. *Geotechnique*, 37(2), 219-225.

Terzaghi, K., Peck, R., and Mesri, G. (1996). *Soil Mechanics in Engineering Practice, 3rd Ed.* John Wiley and Sons.

U.S. Geological Survey. (1857). *Introduction to Geology and Resources of Gold, and Geochemistry of Gold.* Denver: U.S. Department of the Interior.

Van Niekerk, H. J., and Viljoen, M. J. (2005). Causes and consequences of the merriespruit and other tailings-dam failures. *Land Degradation and Development*, 16(2), 201-212.

Vermeulen, N. (2001). *The Composition and State of Gold Tailings.* Pretoria: University of Pretoria.

Vick, S. G. (1990). *Planning, Design, and Analysis of Tailings Dams.* John Wiley and Sons.

Vidich, S. D., Beckwith, G. H., and Keaton, J. R. (1998). Liquefaction assessment of mine tailings dams. In P. K. Robertson, and P. W. Mayne (Ed.), *The first international conference on site characterization -- ISC'98. 1*, pp. 543-548. Atlanta, GA: A.A. Balkema.

Viggiani, G., and Atkinson, J. H. (1995). Interpretation of bender element tests. *International Journal of Rock Mechanics and Mining Sciences and Geomechanics Abstracts*, 32(8), A373-A373. doi:10.1016/0148-9062(95)99498-M

Wagener, F., Strydom, K., Craig, H., and Blight, G. (1997). The tailings dam flow failure at Merriespruit, South Africa: Causes and consequences. *International conference; 4th, Tailings and mine waste; 1997*, pp. 657-666. Fort Collins, CO: A. Balkema

Chapter 5

5. Study on the Effects of MICP Treatment on the Monotonic and Cyclic shear behaviour of Fraser River sand

5.1. Introduction

5.1.1. Problem Statement and Objective

Fraser River sand is an alluvial deposit found in the Fraser River Delta. Located in the lower mainland of British Columbia, Canada. This area is of substantial economic importance, as it covers the city of Vancouver, and it is also vulnerable to earthquakes due to its location between tectonic plate boundaries. Because young sediments (Holocene) in the delta form a large zone susceptible to seismic liquefaction (Watts et al. 1992), the seismic stability of structures in the region is a serious concern. Additionally, the presence of methane gas at shallow depths in the delta has been found to induce dynamic pore pressures during tidal drawdown that trigger recurrent flow liquefaction failures (Christian et al. 1997; Chillarige 1995). This study aims to demonstrate the effectiveness of an MICP treatment in improving the static and cyclic undrained shearing behaviour of Fraser River sand by employing *Sporosarcina ureae* as the ureolytic bacterial strain. This is the first time that the application of MICP is studied for the Fraser River sand, which is done in order to observe and contrast the method's effectiveness in a natural sand (with its diverse mineralogy and more natural particle shape and size distribution) with that in artificial sands studied by many other researchers. With the objective of better understanding the treatment's effects, only a single application of the treatment is studied, and the improvements are quantitatively compared and analyzed within a critical state framework.

5.2. Materials and Methods Used

5.2.1. Microorganism and Cementation Reagents

Sporosarcina ureae (ATCC 13881) was used in this study for the treatment of Fraser River sand through MICP. *S. ureae* is an endospore-forming, urease-positive, motile, strictly aerobic bacterium, with optimum growth temperature and pH of 25^{o}C and 7, respectively (Whitman 2009). This species is commonly found in soil and can tolerate pH levels of up to 10. Cells are round or oval with a diameter of approximately 1.0 - 2.5 μm and may grow individually, in pairs, tetrapads, or in packets of eight or more cells due to division in two or three perpendicular planes. As shown in Figure 5-1(a), colonies are creamy in colour, turning yellowish in a nutrient agar medium. As with all bacterial cells, *S. ureae* possesses small bristle-like external fimbriae, responsible for the mutual clinging of cells as a biofilm in a liquid (see Fig. 3-2b) or as microbial colonies (Fig. 3-2a) on solids (Park-Talaro 2008). As a crucial requirement in MICP treatment, the urease in *S. ureae* has been found to be remarkably active with an enzymatic activity greater than 9300 μmol urea hydrolyzed per minute for each milligram of protein at an optimal pH of 7.5 (McCoy et al. 1992).

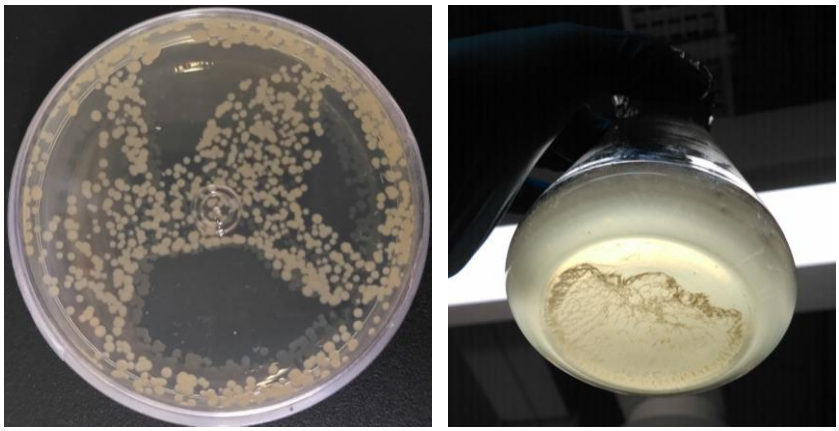

(a) (b)

Figure 5-1: *Sporosarcina ureae* cultured in (a) solid and (b) liquid media.

For the preparation of growth media and chemical reagents, all equipment and individual solutions were autoclaved for 25 minutes (with the exception of urea solution, which was filter-sterilized)

in order to prevent contamination with unwanted foreign species. Given that *S. ureae* has been observed to grow well on peptone-containing media (Goldman and Wilson 1977), nutrient agar and broth containing 22% peptone and 13% beef extract were used as solid and liquid growth media, respectively. Colonies were first plated on petri-dishes (5.5 cm dia.) with nutrient agar (23 g/L) and incubated for a period of 24 hours at a temperature of 25^{o}C. To prepare bacterial stock, single colony was subsequently inoculated in 30 mL of nutrient broth (8 g/L) with pH = 7.17 and incubated at 25^{o}C without agitation.

Bacterial growth was continuously monitored by means of a UV-Vis spectrophotometer (HACH DR6000). An absorbance spectrophotometer is an instrument that measures the amount of light a solution absorbs by comparing the intensity of incident light reaching the sample with the intensity of light passing through it. Because particles in suspension inside a given compound cause the scattering of light, a spectrophotometer is used to estimate the number of cells in suspension for microbiological applications. A higher bacterial concentration in a liquid culture results in a higher absorbance of light. In this case, absorbance is referred to as Optical Density (OD_{λ}), where λ is the wavelength of light used for measurements. Because organic materials have a higher optical density at light with λ = 600 ηm, readings are commonly taken as OD_{600}. Measurements of a sample relative to a blank reference liquid containing everything in the sample except the cells being analyzed (i.e. plain media vs. inoculated media) provides an estimate of the cell concentration in the liquid, which can be used to estimate the growth phase of the population cell.

In order to determine the amount of time required to reach a stationary growth phase for *S. ureae* and measure the maximum cell density, a series of 1-mL resuspended culture volume was placed in 1.5-mL polystyrene cuvettes and tested in the spectrophotometer at various time intervals. Since only the OD of the multiplying suspended particles was of interest, a sample of the pure nutrient broth was used as a blank. By measuring OD_{600} at different time intervals, the stationary growth phase for *S. ureae* was reached approximately 7 days (10,000 min.) after inoculation, as shown in Figure 5-2, with OD_{600} = 1.2 by the two distinct trials. Cell concentration at the stationary phase was found to be 5×10^{5} colony forming units (CFU) per mL by means of serial dilution – a statistical procedure to estimate the number of viable bacterial cells in a liquid culture. This cell density falls within the range of CFU and viable cell counts used by other researchers investigating the

effectiveness of MICP (Lee et al. 2012; Martinez 2013; Buikema 2015; Sharmaa and Ramkrishnan 2016).

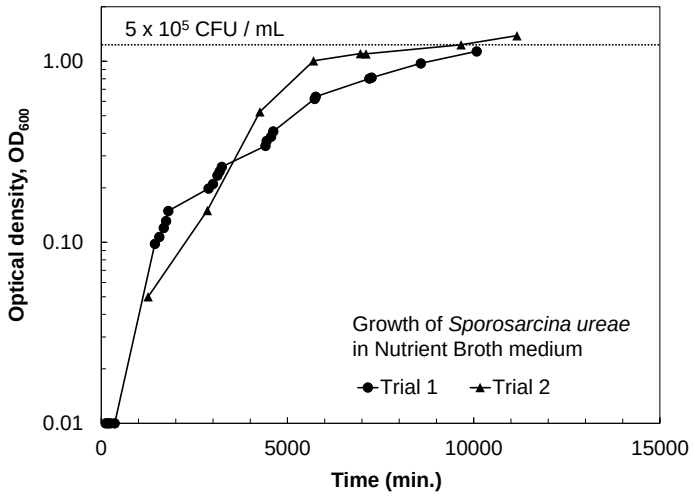

Figure 5-2: Growth curve for *Spororsarcina ureae* in liquid medium without agitation.

As previously described in Equations (1) to (6), the biochemical reactions involved in urea hydrolysis increase the local pH in the solution due to the generation of hydroxide ions (OH^-) and ammonium ($NH4^+$). Therefore, pH measurements can be used to monitor the progress of urease activity (Stocks-Fischer et al. 1999; Gat et al. 2014). Figure 5-3 presents the observed changes in pH with respect to time, measured using a digital pH meter (Mettler Toledo) after combining 15 mL of *S. ureae* bacterial stock (inoculum size: 5 x 10^5 CFU/mL) with 15 mL of urea at two different concentrations. The mixtures were maintained at a room temperature of 22º C. As shown in Figure 5-3, the initial pH of the harvested stock was 8.4, and for both trials, a limiting pH value of approximately 9.2 was reached after 48 hours. This suggests that the urea concentration was not a limiting factor in enzymatic activity. Instead, the continuously increasing pH caused the rate of urea hydrolysis to decrease, reaching a stagnant point at pH > 9. Similar observations are also reported by Stocks-Fischer et al. (1999), Gorospe et al. (2013) and Feng and Montoya (2016) using other types of ureolytic bacteria.

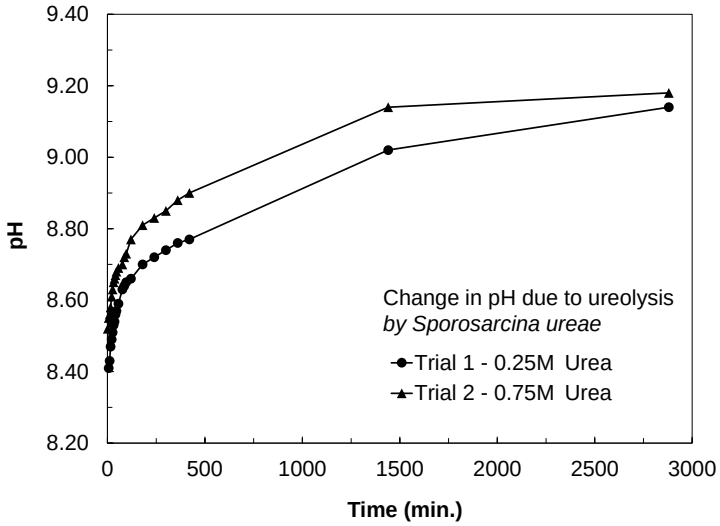

Figure 5-3: Changes in pH during urea hydrolysis for two different concentrations of urea.

Given that ureolysis reactions are largely controlled by the type of microorganism, the mole ratios in Equations (1) to (6) cannot be used to estimate reagent concentrations required to yield a predetermined concentration of precipitated $CaCO_3$ (i.e. 1 mole of urea will not result in 1 mole $CaCO_3$). Therefore, the experimental optimization program shown in Figure 5-4 was developed to establish treatment reagent concentrations which would enhance the precipitation of $CaCO_3$. A standard urea solution was prepared and filter-sterilized at a concentration of 0.5 M (or 3% by volume) to also enhance the growth of *S. ureae* during urea hydrolysis (Whitman 2009). Note that urea was not added to the growth medium, as the two processes of population growth and urea hydrolysis would have occurred simultaneously, altering the OD_{600} meant to serve only as an index of growth. As part of the optimization program, three separate laboratory tests were conducted in similar autoclaved Erylenmeyer flasks containing 30 mL samples of *S. ureae* stock mixed with 30 mL of 0.5 M urea solution and maintained at room temperature. The pH measured after the first hydrolysis cycle (48 hours) averaged 9.2 for all three tests. In the first stage, Test 1 was driven to induce $CaCO_3$ precipitation by mixing in 30 mL of autoclaved 0.75 M $CaCl_2$. Calcium chloride was chosen as the calcium source as it would precipitate the most stable form of $CaCO_3$ (De Yoreo and Vekilov 2003; Favre et al. 2009; Gorospe et al. 2013).In Tests 2 and 3, the pH of stock mixtures was reduced by adding 5 mL of autoclaved 0.8 M (or 5% by volume) acetic acid to each test, in order to reactivate enzymatic activity and begin a new hydrolysis cycle. Two days later, the amount

of $CaCO_3$ precipitate in Test 1 was filtered from solution, air-dried, and compared with the theoretical chemical yield, resulting in 56% yield. In the second stage, Test 2 was driven to induce $CaCO_3$ precipitation by mixing in 30 mL of autoclaved 0.75 M $CaCl_2$, while the pH of stock mixture for Test 3 was reduced a second time by adding 5 mL of 5% acetic acid. After another 48-hour period, the amount of $CaCO_3$ precipitated in Test 2 was weighed and compared with the theoretical chemical yield, resulting in 83% yield. Finally, Test 3 was driven to induce $CaCO_3$ precipitation by mixing in 30 mL of autoclaved 0.75 M $CaCl_2$. As with the previous tests, the amount of $CaCO_3$ precipitated in Test 3 was weighed and compared with the theoretical chemical yield, resulting in 72% yield.

Based on the observed results, the reagent concentrations used in Test 2 and summarized in Table 3-1 served as the basis for the cementation treatment applied to the sand specimens in this study. The hydrolyzed urea stock contained the cultured stock along with the compounds produced after two cycles (96 hours) of urea hydrolysis. The precipitation reagent contained calcium chloride, complemented with 2/3 by volume of dissolved urea in order to foster further carbonate precipitation after application.

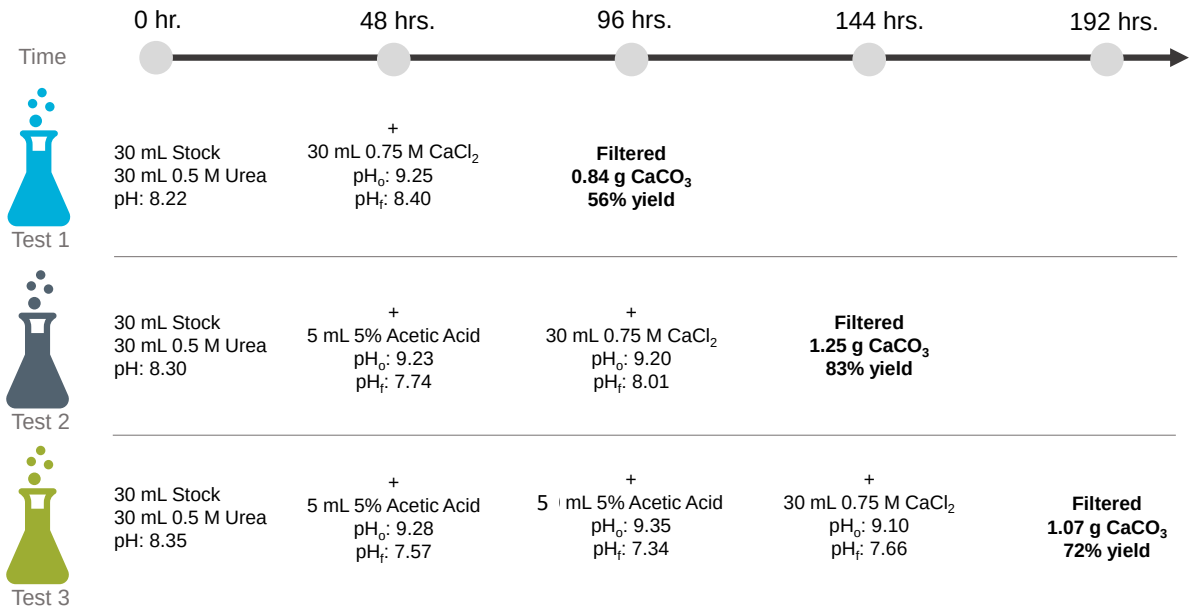

Figure 5-4: Laboratory program for the biomineralization of $CaCO_3$.

Table 5-1: MICP treatment reagents employed.

Reagent	Contents
Hydrolyzed urea stock	15 mL Bacterial stock (5 x 10^5 CFU/mL of *S. ureae*) + 15 mL 0.5 M urea + 5 mL 0.8 M acetic acid
Precipitation reagent	30 mL 0.75 $CaCl_2$ + 20 mL urea

The mineralogy of the $CaCO_3$ precipitate was also analyzed using a powder X-ray diffractometer (Rigaku RINT 2500) with Cu-K radiation (λ = 1.54 Å) to confirm that stable forms of calcium carbonate were produced. Figure 5-5 presents the diffraction pattern, consisting of a series of reflections of varying intensities at different values of twice the X-ray striking angle (i.e. 2θ) (Mitchell and Soga 2013). Because minerals have distinct and unique spacings of interatomic planes in three dimensions, identification of the mineral crystal involves the use of the X-ray's wavelength and Bragg's Law to estimate the crystal's distance between parallel atomic planes. According to Figure 5-5, the mineral phases identified in the precipitate are calcite (62%) and vaterite (38%), the most common phases of $CaCO_3$ polymorphs produced in MICP (Gonzalez-Munoz et al. 2010; Rodriguez-Navarro et al. 2007). The amounts of each phase (i.e. % by weight) were estimated from a Reference Intensity Ratio (RIR) anlaysis of the diffraction pattern, which involved the comparison of intensity peak scaling factors with those of predetermined standards in the reference database employed (Putz 2019).

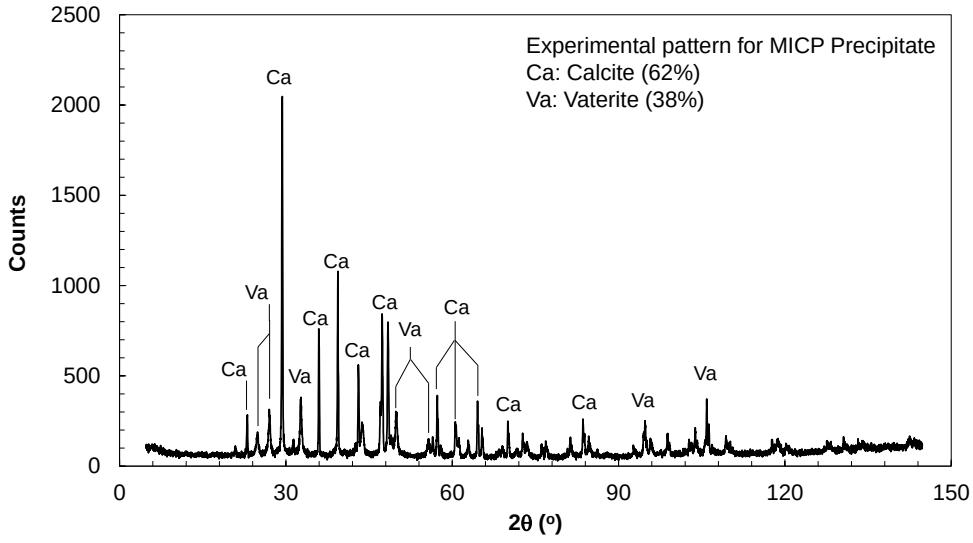

Figure 5-5: XRD trace of the biomineralized precipitate identifying calcite and vaterite as the $CaCO_3$ phases present.

5.2.2. Soil and Cementation Method

Given the interest in the liquefaction behaviour of Fraser River sand (FRS) over the last few decades (Shozen 1991;Vaid and Sivathalayan 1996, 1998; Vaid et al. 2001) due to its vulnerable location between the North America and Pacific tectonic plates, samples of this alluvial material were used in this study to assess the effectiveness of MICP for the mitigation of static and cyclic liquefaction. Originally tested by Jones (2017), FRS samples were obtained from an excavation site in Richmond, British Columbia near the north arm of the Fraser River. Figure 5-6 shows an SEM image of the sand particles, exhibiting their generally sub-angular to angular shape. X-Ray diffraction analysis describe the sand's mineralogical composition as 55% orthoclase feldspar, 35% quartz, and 10% muscovite (Jones 2017).

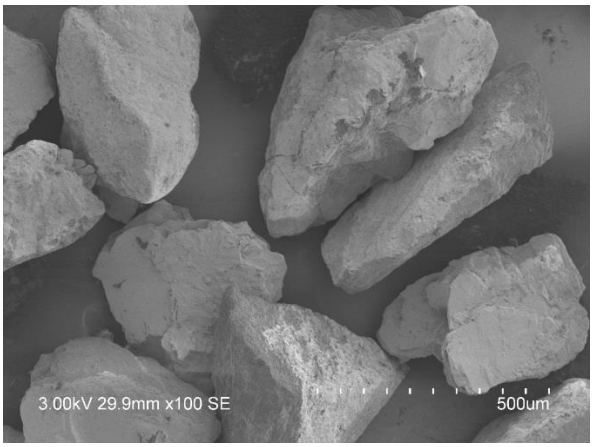

Figure 5-6: SEM image of Fraser River sand particles showing angular to subangular shape. Adapted from Jones (2017)

Sieve analysis on FRS were conducted to determine its particle size distribution in compliance with ASTM D-422 standard procedure. The average gradation is shown in Figure 5-7, which classifies the material as a poorly-graded sand (SP) per the Unified Soil Classification System (USCS). As also shown, this gradation curve compares reasonably well with those of other FRS samples tested by other researchers (Shozen 1991; Robertson et al. 2000). Furthermore, with a D_{10} = 0.15 mm, the organism-to-particle size ratio of *S. ureae* and FRS ranges from 1:150 to 2.5:150, falling within the bounded region in Figure 3-1 for the suitability of microbiological treatment. Table 3-2 summarizes the physical properties and index characteristics of this sand which were determined following ASTM standard procedures.

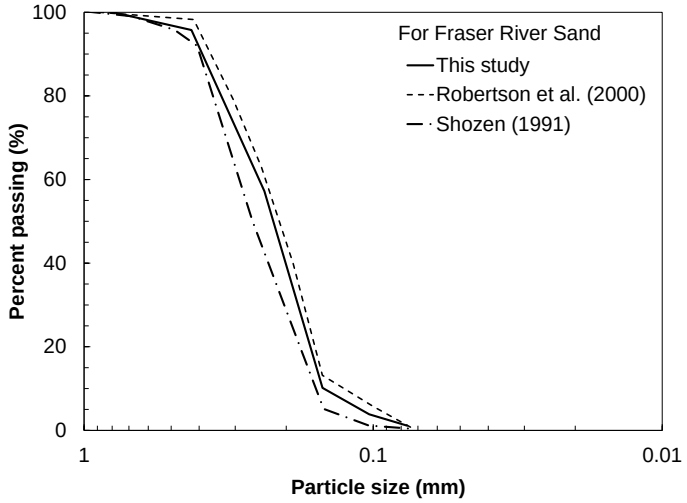

Figure 5-7: Gradation curve for the Fraser River sand samples used in this study compared with those used by other researchers.

Table 5-2: Fraser River sand Properties.

D_{10} (mm)	0.15
D_{30} (mm)	0.18
D_{60} (mm)	0.22
C_u	1.47
Clay content (%)	<1
USCS	SP
G_s	2.69
e_{min}	0.63
e_{max}	0.96

Untreated specimens were prepared by mixing dry sand with 5% by weight of distilled water. The moist sand was subsequently scooped and tamped to the desired specimen height inside the DSS mold. The mold used consists of a bottom steel pedestal that supports a stack of Teflon-coated steel rings internally lined with a latex membrane (0.82 mm thick). The steel rings have an inner diameter of about 71.96 mm and a thickness of 1.05 mm each. Moisture in the sand structure creates a capillary effect among sand particles, producing a very loose fabric that can be readily

molded. The void ratio of each specimen was controlled by varying either the specimen height or the weight of dry sand inside the specimen. Given the constraints in size provided by the rings' inner diameter and the latex membrane, all specimens were prepared with a diameter of 70.3 mm.

FRS specimens for biological treatment were prepared in a similar manner to those for untreated testing. For these specimens, however, the dry sand was mixed with 10% by weight of hydrolyzed urea stock to ensure that the cells were evenly distributed inside the specimen. Moist-tamping was employed to soak the sand instead of flushing, as the finely porous disks in the upper and lower pedestals that ultimately confine the specimen would act as filters, thus impeding a high concentration of cells from reaching the sand. Figure 5-8 shows a moist-tamped FRS specimen prepared for MICP treatment inside the latex-lined DSS mold prior to testing.

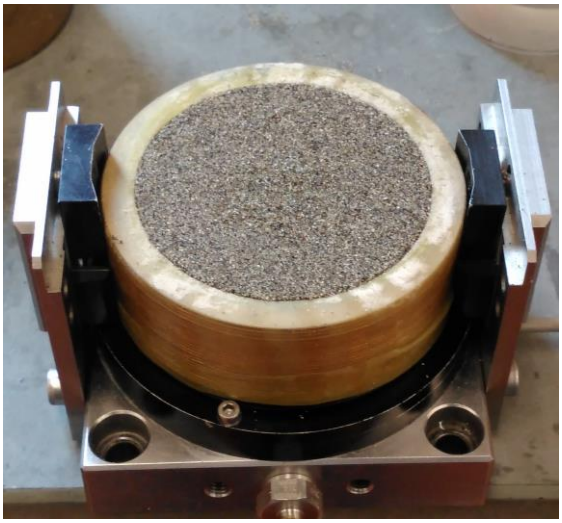

Figure 5-8: Treated moist-tamped Fraser River sand specimen inside DSS mould.

5.2.3. Direct Simple Shear and Bender Element Tests

Laboratory shear tests were conducted at the University of Western Ontario using an advanced direct simple shear (DSS) device (manufactured by GDS Instruments) equipped with bender elements for the measurement of shear-wave velocity (V_S).

The DSS device includes a vertical electro-mechanical actuator for applying vertical stresses, and a horizontal actuator that allows the application of simple shear to a soil specimen. The vertical

actuator has a displacement range of 50 mm and a maximum force capacity of 5 kN. The horizontal actuator has a displacement range of 25 mm with a maximum load capacity of 2 kN. When mounted, the test specimens are axially confined between upper and lower pedestals of the DSS mold as shown in Figure 5-9. A stack of Teflon-coated stainless-steel rings provide a rigid radial boundary for the specimens while allowing unrestricted application of horizontal displacement during shear. Specimen saturation is accomplished by flushing fluid through inlet and outlet connections in the top and bottom pedestals, allowing ingress of the fluid through sintered porous disks through the specimen. A latex membrane, secured by O-rings at the top and bottom pedestals, prevents the leakage of saturation fluid.

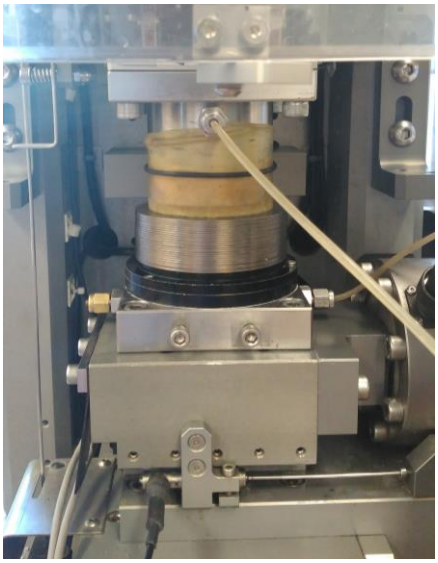

Figure 5-9: Fraser River sand specimen inside DSS device during saturation stage.

Shear-wave velocity (V_S) measurements of sand specimens were taken using bender element (BE) inserts affixed to supplementary DSS pedestals. The elements consist of small cantilever piezoelectric plates that are shallowly embedded at the top and bottom of the specimen during confinement. The bender elements are controlled using a signal generation software that allows the on-command triggering of shear waves. A voltage signal is transmitted to one of the bender elements, which subsequently converts this signal to a sinusoidal mechanical vibration with a set wavelength (λ) by means of its piezoelectric properties. The shear wave propagating through the

sample is then received by the other bender element and converted back to an electric voltage signal.

Untreated sand specimens tested in the DSS device were initially loaded under a vertical seating stress of 5 kPa and saturated with de-aired water by means of a differential pressure head system at a rate of approximately 0.83 mL/min. These samples were subsequently consolidated to a target vertical stress, σ'_{vc}, until the rate of vertical displacement was significantly reduced, thus indicating the end of primary consolidation. Conversely, the MICP treated specimens were consolidated to the target σ'_{vc} prior to saturation with the precipitation reagent, as the instantaneous cementation reaction involved produced by the treatment was noticed to affect the specimens' normal consolidation behaviour. Once the vertical deformation appeared to have stabilized (reaching the end of primary consolidation), the samples were slowly saturated with approximately 40 mL of the precipitation reagent by means of a differential pressure head system at a rate of approximately 0.83 mL/min. Full saturation was reached once air bubbles were no longer visible leaving the outlet of the pedestal, and the volume change was re-stabilized.

Shear-wave velocity (V_S) measurements were taken by means of bender elements in a series of untreated and MICP treated specimens as a non-destructive method to compare and monitor MICP cementation. For the untreated samples, V_S was measured soon after the consolidation stage, when changes in vertical displacement had stabilized. For MICP-treated samples, V_S measurements were taken after the specimens were fully saturated with the precipitation reagent, and the changes in V_S produced by cementation were monitored for 48 hours, after which V_S was observed to stabilize.

Several methods for interpreting the shear wave signal have been proposed (Viggiani and Atkinson 1995; Jovičić and Coop 1998), with the peak-to-peak method proven to provide accurate measurements of V_S (Brignoli et al. 1996; Camacho-Tauta et al. 2015). In this method, which is used in this study, the travel time (Δt) is defined as the time difference between the peaks of the incipient wave and the first received wave. The shear wave travel distance (Δh) is taken as the tip-to-tip distance between the bender elements along the specimen height (Brignoli et al. 1996). In order to minimize near-field effects (NFE) caused by P-wave reflections and electrical noise, a shear wavelength (λ) of less than $\Delta h/2$ was generated by producing shear waves with an excitation

frequency of 33.3 kHz. Hence, by consolidating a specimen to various σ'_{vc} and e_c, different V_S (= $\Delta h/\Delta t$) values were measured.

Due to the free-draining nature of the sand, no excess pore pressure was generated during the monotonic shearing, and a shearing rate of 10% per hour was adopted. Since pore-water pressure is not measured by the DSS device and drainage is allowed, shearing was carried out under a constant-volume condition in order observe the undrained shearing behaviour of the sand specimens. In these tests, no shear-induced pore water pressure was produced, and the changes in vertical stress required to maintain a constant height were taken as the equivalent pore water pressure that would have been produced in a truly undrained test on a saturated sample (Bjerrum and Landva 1966; Finn and Vaid 1977; Dyvik et al. 1987; Vaid and Sivathayalan 1996; ASTM D6528-17). Although specimens were sheared to strains (γ) exceeding 20%, the results are reported here for shear strains of up to 15% to minimize the effect of stress and strain nonuniformities within the specimen at high strain levels (Airey et al. 1985; Airey and Wood 1987).

Cyclic direct simple shear tests were carried out on specimens consolidated to different average D_{rc} = 65, 52, and 22% at σ'_{vc} = 100 kPa. Similar to the monotonic tests, all cyclic tests were performed under constant-volume conditions in order to replicate undrained loading. Cyclic shear loading values were specified in the form of cyclic stress ratios (CSR), defined as the ratio of applied shear stress to the effective vertical stress after consolidation in the equation below:

(Eq. 5-1) $$CSR = \frac{\tau}{\sigma'_{vc}}$$

Like many other researchers (e.g., Vaid and Sivathayalan 1996; Wijewickreme et al. 2005; Rutherford 2012), cyclic shear loading was applied at a frequency of 0.1 Hz, as it provided consistent and stable cyclic stress paths. Stability issues would arise at higher frequencies when a specimen is close to failure and at large shear strains. This occurs as the shearing actuator would need to travel farther while maintaining a specified value of shear stress, yet a cycle must be completed by the end of the specified period (i.e. 1/0.1 Hz = 10 seconds). Adopting a higher

frequency, limits the ability of the shearing actuator to reach a specified shear load before a new cycle is set to start.

MICP treated specimens at consolidation relative densities (D_{rc}) of 52% and 65% were subjected to an additional cyclic shearing stage after the first liquefaction event, by zeroing the shear load, reconsolidating the specimen to the same initial σ'_{vc} = 100 kPa, and subsequently re-applying the same CSR as in the first cyclic shearing stage. This was done in order to compare the specimens' cyclic behaviour and re-liquefaction resistance with that exhibited in its first liquefaction event.

As previously described, two series of bender element and direct simple shear tests were conducted, namely those performed on untreated FRS specimens and those done on MICP treated specimens. In summary, the testing program comprised a total of 15 monotonic DSS tests, 25 cyclic DSS tests, and 25 bender element tests.

5.3. Test Results

5.3.1. Bender Element Tests

Shear wave velocity (V_S) was measured to monitor and determine the effectiveness MICP treatment on FRS samples. Values of maximum V_S in treated samples were recorded approximately 48 hours after treatment application, when the magnitudes of V_S stabilized and reached a constant value. As shown in Figure 5-10, the value of V_S recorded for a sample with e = 0.871 and consolidated to σ'_{vc} = 100 kPa immediately after saturation with the treatment was ~50 m/s higher than that of the original untreated sand, and the values were observed to asymptotically reach a maximum limit of 275 m/s after 48 hours of treatment application.

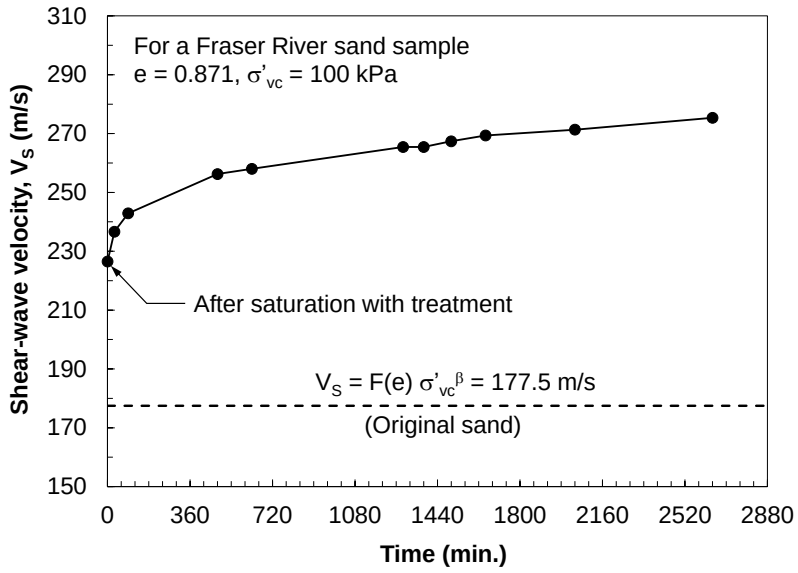

Figure 5-10: Increase in V_S immediately after application of MICP treatment and a subsequent 48-hour period for a Fraser River sand sample with e = 0.871 and σ'_{vc} = 100 kPa.

From the series of bender element tests, V_S was found to be higher in the MICP treated specimens compared to those measured in untreated samples of FRS. As shown by the V_S profiles in Figure 5-11, V_S measured in the untreated samples (with D_{rc} = 16 – 36 %) increase from about 149 m/s to a maximum of 300 m/s with the increasing of σ'_{vc} from 50 to 900 kPa. V_S values reported by Jones (2017) for the same FRS tested here with D_{rc} = 26 – 84% show the same general trend obtained in this study, for which the value of β was found to equal 0.26, irrespective of sample density. This value concurs with that typically used for silica sands. As also shown in Figure 5-11, in spite of their lower densities in some cases, MICP treated samples with D_{rc} = 7 – 38 % registered higher maximum shear-wave velocities than the V_S of untreated samples. V_S values of the treated specimens increase from a minimum of 219 m/s to a maximum of 395 m/s with increasing σ'_{vc} from 100 to 900 kPa. Accordingly, the stress normalization exponent fitted for the MICP-treated samples reduces to β = 0.21.

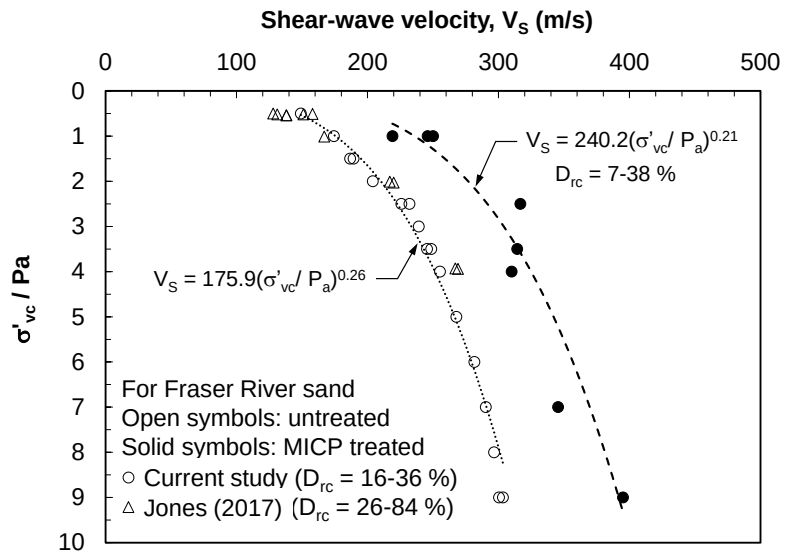

Figure 5-11: V_S profiles with normalized σ'_{vc} showing an increase in shear-wave velocity after 48 hours of a single application of MICP treatment.

5.3.2. SEM Images

The distribution of precipitated $CaCO_3$ has been reported to initiate mostly at particles points of contact, binding particles together, and increasing particle-to-particle stiffness (DeJong et al. 2010). Figure 5-12 shows several SEM images of the treated samples. Particle-to-particle bonds are clearly visible in Figures 5-12 (a) and (b), and calcite crystals were seen to have formed on particle surfaces as shown in the higher magnification images in Figures 5-12 (c) and (d).

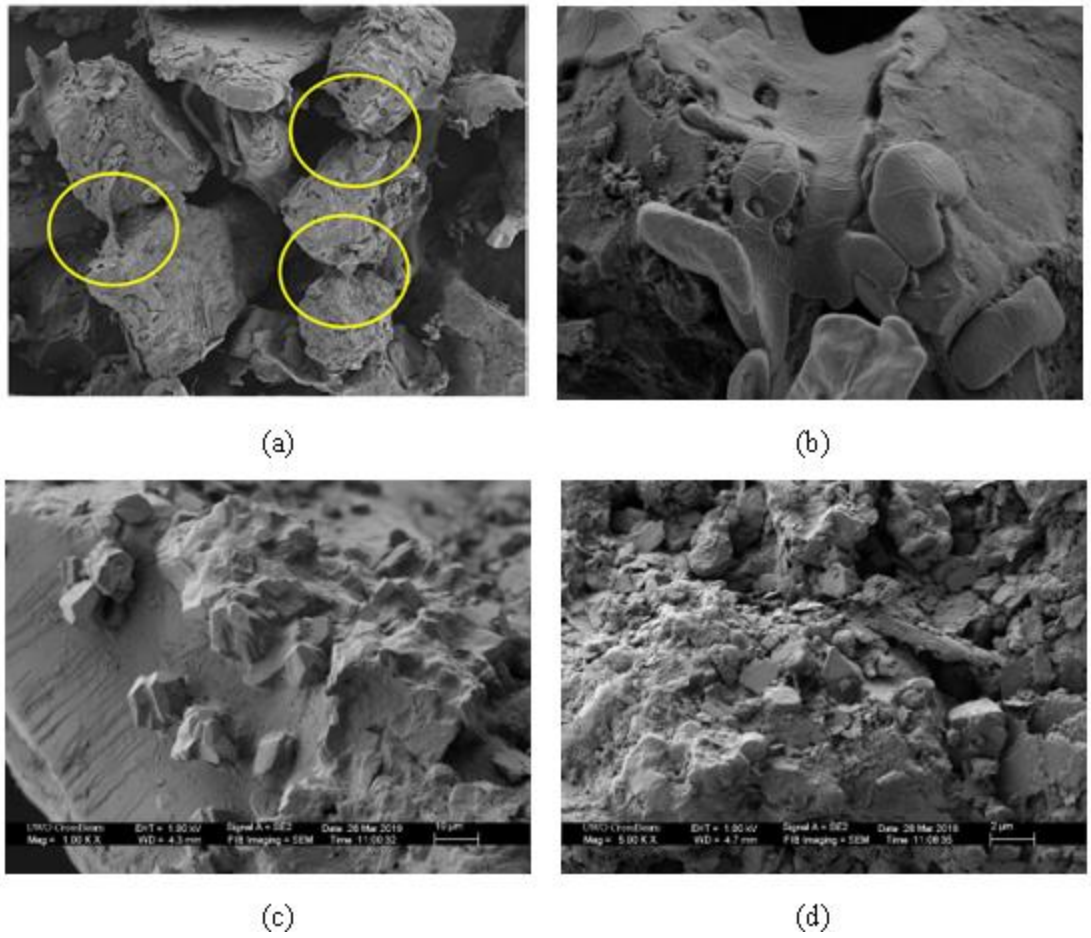

Figure 5-12: SEM images of MICP treated Fraser River sand highlighting (a and b) particle cementation at particle-particle contacts and (c and d) increased particle angularity and surface roughness produced by $CaCO_3$ crystals on particle surfaces.

5.3.3. Monotonic DSS Tests

Figure 5-13 compares the undrained monotonic shearing behaviours of the original and MICP-treated FRS samples. Both untreated and treated samples in the figure were tested at relatively loose densities (D_{rc} = 7 – 38%) to induce static liquefaction upon shearing. As shown, all specimens display progressive mobilization of undrained strength up to a peak value at s_u(yield), after which strain-softening and strength loss occur until an undrained post-liquefaction strength, s_u(liq), is attained. This ultimate strength values correspond to those at which a critical state is reached. However, MICP treated samples exhibit steeper strength mobilization (or higher stiffness) and slower reductions in effective stress up to s_u(yield). Treated samples also reached higher

s_u(yield) and s_u(liq) than their untreated counterparts at nearly similar initial conditions (σ'_{vc}, e_c). These can be attributed to calcite cementation and particle bonding in the treated samples.

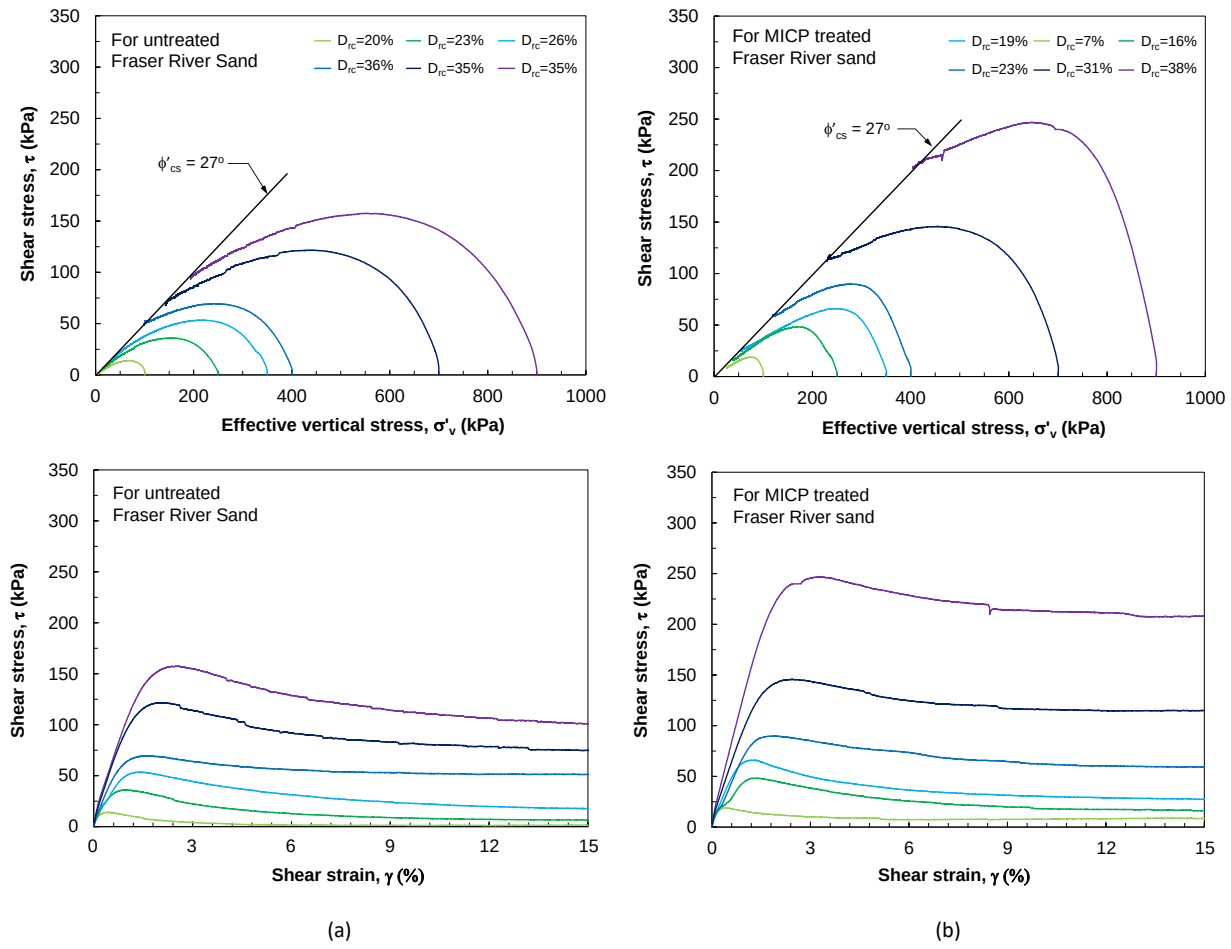

Figure 5-13: Comparison of undrained monotonic shear behaviour between (a) untreated and (b) MICP treated Fraser River sand samples.

5.3.4. Cyclic DSS Tests

The undrained cyclic shearing behaviour of the original untreated Fraser River sand used in this study has been extensively investigated by Jones (2017). Therefore, only MICP treated specimens consolidated to σ'_{vc} = 100 kPa were subjected to cyclic shearing in this study, and the results

obtained are compared with those reported by Jones (2017). Additionally, all medium dense and dense samples (D_{rc} = 45% and 65 %) were subjected to a repeated cyclic shearing stage in order to study the effect of a prior cyclic loading on the re-liquefaction resistance of the treated sand.

As an example, Figure 5-14 shows the cyclic stress paths and stress-strain responses obtained from the first and second cyclic loading stages of a treated specimen at D_{rc} = 62%. The steady decrease in σ'_{vc} shown by the cyclic stress path in Figure 5-14(a) demonstrates the gradual build-up of pore water pressure (also shown in Figure 5-15) as the MICP treated specimen approaches failure. Liquefaction failure criterion is defined here as the number of cycles (N_L) required to cause a single-amplitude shear strain (γ_{SA}) of 3.75% (Vaid and Sivathayalan 1996; Wijewickreme et al. 2005; Porcino et al. 2008). This strain level is equivalent to reaching a 2.5% single-amplitude axial strain in a triaxial samples, which is the definition of liquefaction adopted by the National Research Council (NRC 1985). As indicated by the stress-strain curve for this specimen (Figure 5-14a), a total of 11 load cycles were required to reach liquefaction (at γ_{SA} = 3.75%), with the majority of cycles restrained at small strains. As shown in the figure, these shear strains were observed to progressively increase after about γ = 0.5% in the 7th cycle until failure was reached. Following the first cyclic loading, the same specimen was re-consolidated to σ'_{vc} = 100 kPa and sheared at the same CSR = 0.17. Despite a higher D_{rc} (= 69%), the stress path in Figure 5-14(b) shows a more rapid decrease in σ'_{vc} during the repeated cyclic loading stage and a more consistent increase in shear strain with each load cycle, requiring only 5 cycles for the specimen to liquefy. This contrast in cyclic behaviour is further demonstrated in Figure 5-15, which shows the contrast between the gradual generation of excess pore water pressure ratio (expressed as $r_u = \Delta u_e/\sigma'_{vc}$) during the first cyclic loading and the sharp increase in pore water pressure produced when the cyclic loading was repeated.

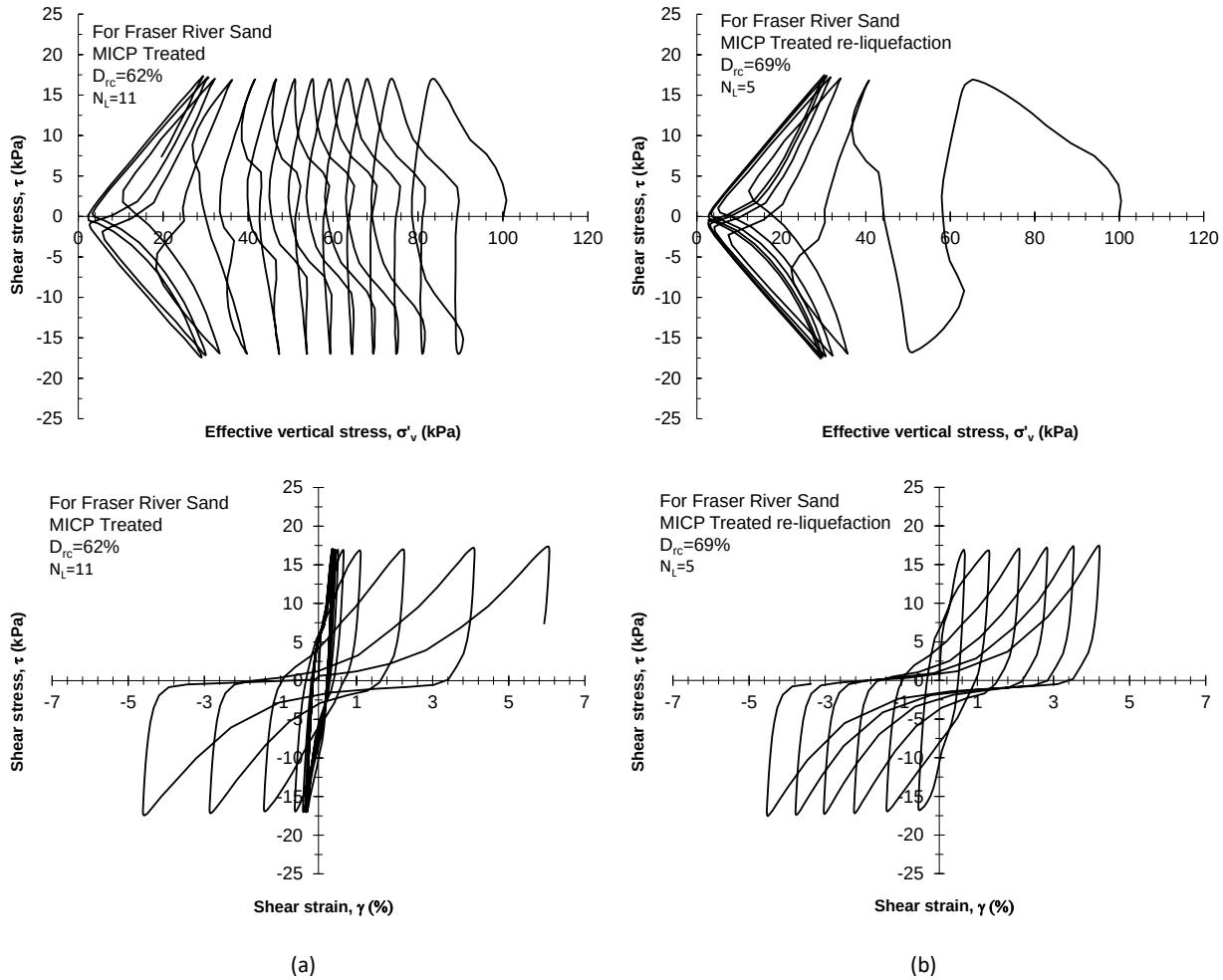

Figure 5-14: Comparison of cyclic shear behaviour between MICP treated samples of Fraser River sand in (a) first event of liquefaction and (b) re-liquefaction.

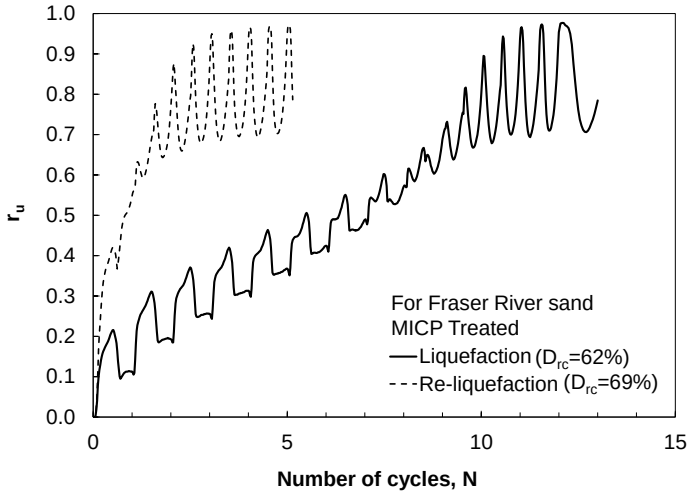

Figure 5-15: Comparisons in the development of excess pore water pressure with increasing cycles of shear loading between the first event of liquefaction and re-liquefaction in MICP treated Fraser River sand.

5.4. Discussion of Results

5.4.1. Static Liquefaction Behaviour

Useful comparisons of the undrained shearing behaviour of untreated and treated Fraser River sand samples can be readily established within a critical state framework. Because the CSL plays an important role in understanding the undrained shear behaviour of the Fraser River sand tested, its parameters were obtained from the final stages of the constant-volume DSS tests. Despite the slight scatter, evident trends can be distinguished for CSL of each sand (i.e. original and treated) in Figure 5-16. Likewise, the normal compression line (NCL) of the original sand was established from the one-dimensional consolidation stages of the DSS tests and is shown to lie above the CSLs in the figure. The relatively wide separation between the NCL and CSL of the untreated sand indicates highly positive ψ, which concurs with the strain-softening and static liquefaction behaviour observed in Figure 5-13.

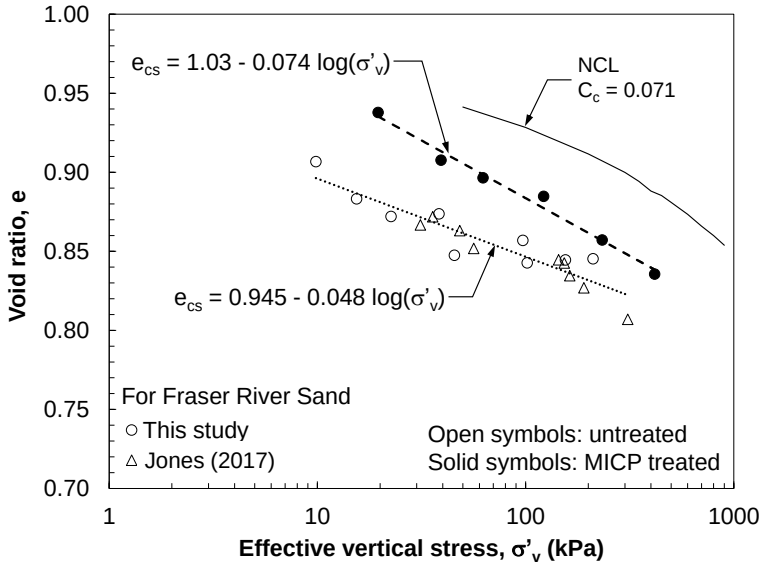

Figure 5-16: Void ratio and σ'_v relationships for Fraser River sand showing the changes in CSL due to MICP treatment and its distance relative to the NCL.

As shown in Figure 5-16, the treated sand exhibited an entirely different CSL (Γ = 1.03; λ_{10} = 0.074), which is looser (higher Γ) and steeper (higher λ_{10}) than that of the original sand (Γ = 0.945; λ_{10} = 0.048). Several studies have shown that the CSL becomes steeper with increasing particle angularity (Poulos et al. 1985; Sladen et al. 1985; Been and Jefferies 1985; Hird and Hassona 1986), as sands with angular particles will tend to form larger void ratios. The SEM images previously shown in Figure 5-11 show that $CaCO_3$ precipitation occurred on the surfaces of individual sand particles as a result of the treatment. Hence, not only were the particles bonded by $CaCO_3$ precipitated at particle-to-particle contacts, but also their surface roughness and angularity increased. Accordingly, the changes in CSL observed for the treated sand are most likely due to the increase in surface roughness and particle angularity caused by $CaCO_3$ precipitation at particle surfaces. Similar changes to CSL have also been reported by DeJong et al. (2006) and Feng and Montoya (2016) in triaxial compression tests on MICP treated sand samples. In contrary, irrespective of the treatment, the same critical state friction angle (ϕ'_{cs}) of 27^o was mobilized in both sands as shown in the stress paths of Figure 5-13. This suggests that most of the particle-to-particle bonds produced by a single application of the treatment were broken, and the calcite crystals cemented on particle surfaces were plausibly abraded at the large strains (> 15%)

associated with critical states. In other words, while sand particle alterations (bonding and texture) by single application of MICP treatment somewhat persisted during shearing (implied by changes in CSL), these were ultimate abolished at large strains.

As discussed earlier, undrained yield, S_u(yield), and post-liquefaction, S_u(liq), strengths were measured from the stress paths of the DSS tests. These strength values are often normalized by the initial stress (σ'_{vc}) to capture the effect of overburden pressure and soil depth in undrained triggering and post-liquefaction stability analyses. According to Figure 5-17, while $S_u(liq)/\sigma'_{vc}$ and $S_u(yield)/\sigma'_{vc}$ decrease with increasing e_c for both the original and the treated sand (as described by the relationships in Eq. 10 - 13), the treated samples consistently exhibit larger undrained strength ratios.

For the original Fraser River sand:

(Eq. 5-2) $$\frac{S_u(liq)}{\sigma'_{vc}} = \frac{0.8\ {e_c}^{-28.9}}{1000}$$

(Eq. 5-3) $$\frac{S_u(yield)}{\sigma'_{vc}} = 0.108\ {e_c}^{-2.72}$$

For the MICP treated Fraser River sand:

(Eq. 5-4) $$\frac{S_u(liq)}{\sigma'_{vc}} = \frac{32.1\ {e_c}^{-10.6}}{1000}$$

(Eq. 5-5) $$\frac{S_u(yield)}{\sigma'_{vc}} = 0.150\ {e_c}^{-2.92}$$

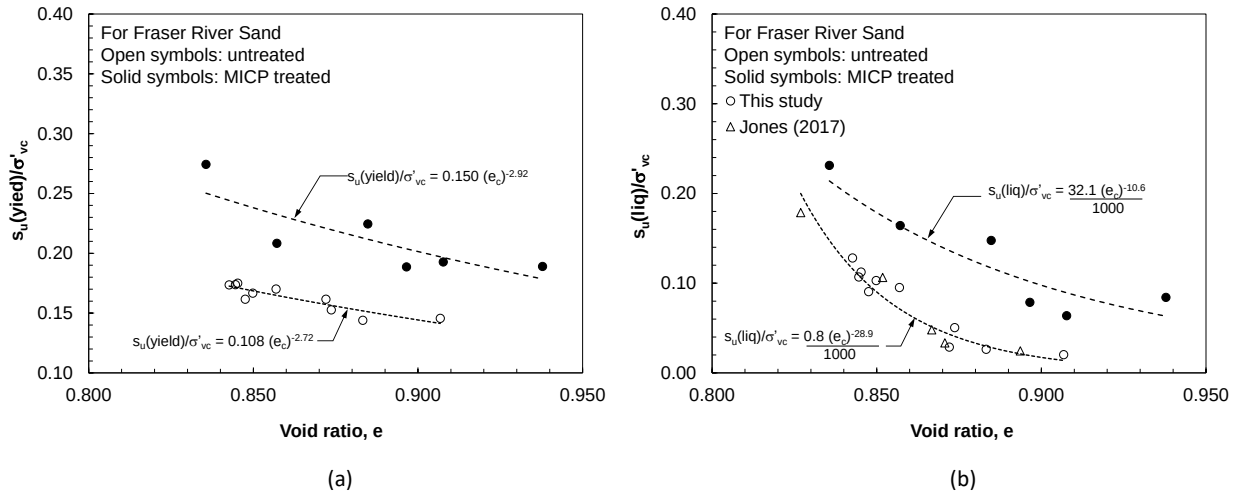

Figure 5-17: Relationships between (a) $S_u(yield)/\sigma'_{vc}$ and (b) $S_u(liq)/\sigma'_{vc}$ with e_c for Fraser River sand displaying the changes produced by MICP treatment.

In order to better visualize improvements in undrained strength produced by the MICP treatment, Figure 5-18 shows increases of $S_u(yield)/\sigma'_{vc}$ and $S_u(liq)/\sigma'_{vc}$ with relative density (D_{rc}) calculated from the fitted correlations in Equations 10-13 for the range of void ratios tested. According to this figure, the increments of both strength ratios increase with increasing values of D_{rc} (as the sand becomes denser). This is plausibly due to the larger number of particle-to-particle contacts in a denser soil matrix, which allows a higher degree of particle binding and cementation to occur. Additionally, the figure further shows that MICP treatment in the sand results in a relatively larger improvement of $S_u(liq)$ compared to the increase in $S_u(yield)$ at any given D_{rc}, reaching a maximum value at ~Drc = 30%, while $S_u(yield)$ continues to steadily increase.

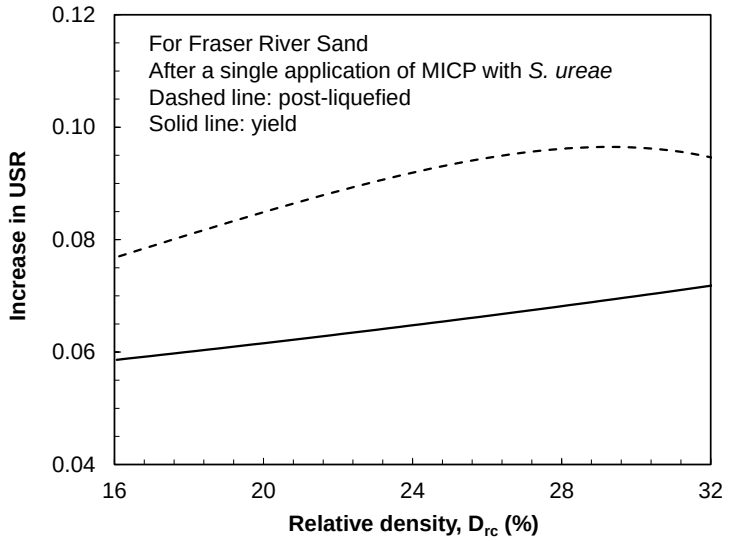

Figure 5-18: Observed increase in undrained strength ratios (USR) for the range of relative density of samples tested.

Given that the state of a soil element is better represented by the state parameter, Figure 5-19 presents the trends of $S_u(yield)/\sigma'_{vc}$ and $S_u(liq)/\sigma'_{vc}$ with changes in ψ for the untreated and treated sands. As shown in Figure 5-19 (a), $S_u(yield)/\sigma'_{vc}$ for both materials show a gentle exponential decrease with increasing ψ. In contrast, Figure 5-19 (b) shows $S_u(liq)/\sigma'_{vc}$ has a tendency to exponentially decay more sharply as ψ increases. Nevertheless, similar to Figure 5-17, the treatment caused a significant increase of these strength ratios, particularly for $S_u(liq)/\sigma'_{vc}$ at any given ψ. These relationships are expressed by the following equations:

For the original Fraser River sand:

(Eq. 5-6) $$\frac{S_u(yield)}{\sigma'_{vc}} = 0.190\exp(-3.33\psi)$$

(Eq. 5-7) $$\frac{S_u(liq)}{\sigma'_{vc}} = 0.308\exp(-38.3\psi)$$

For MICP treated Fraser River sand:

(Eq. 5-8) $$\frac{S_u(yield)}{\sigma'_{vc}} = 0.320\exp(-6.19\psi)$$

(Eq. 5-9) $$\frac{S_u(liq)}{\sigma'_{vc}} = 0.490\exp(-22.2\psi)$$

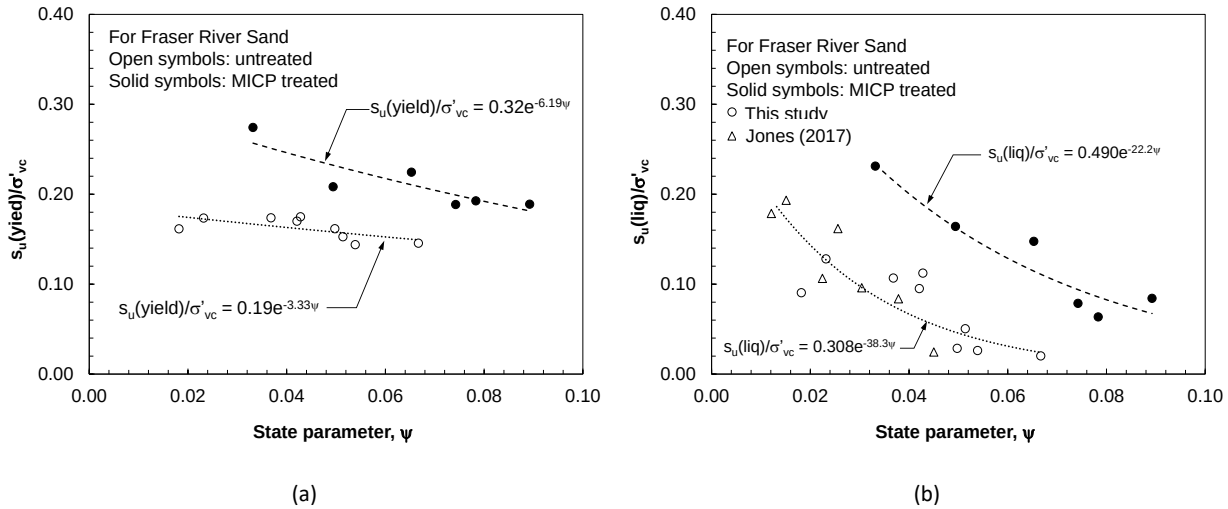

Figure 5-19: Relationships between (a) $S_u(yield)/\sigma'_{vc}$ and (b) $S_u(liq)/\sigma'_{vc}$ with ψ for Fraser River sand showing increases in magnitude produced by MICP treatment.

It is evident from the preceding discussion that a soil element must be saturated and loose (i.e. $\psi > 0$) for it to experience static liquefaction to a greater or lesser extent. Nevertheless, the severity of liquefaction as well as the travel distance of an ensuing flow slide would depend on the magnitude of undrained strength reduction from $S_u(yield)$ to $S_u(liq)$. This strength loss can be quantified by the brittleness index (I_B) as defined below (Bishop 1967):

(Eq. 5-10) $$I_B(\%) = \frac{S_u(yield) - S_u(liq)}{S_u(yield)} \times 100$$

The severity of static liquefaction would increase by increasing I_B, with I_B = 0 and 1 indicating non-liquefied (or dilative), and liquefaction behaviours, respectively. Based on the results of the constant-volume monotonic DSS tests, a comparison is made in Figure 5-20 between I_B exhibited by the original and the treated specimens at any particular ψ. The trends obtained for both materials

show that I_B increases exponentially with increasing ψ. However, and despite the higher values of S_u(yield) for the treated samples shown in Figure 5-13, the exponential trend in brittleness for the treated samples is considerably lower than that for the untreated sand. This is explained by the greater gain in S_u(liq) than S_u(yield) in the treated specimens as shown in Figure 5-18. Therefore, a single application of MICP treatment not only increases S_u(yield) and S_u(liq), but also reduces the propensity for a severe flow failure to occur.

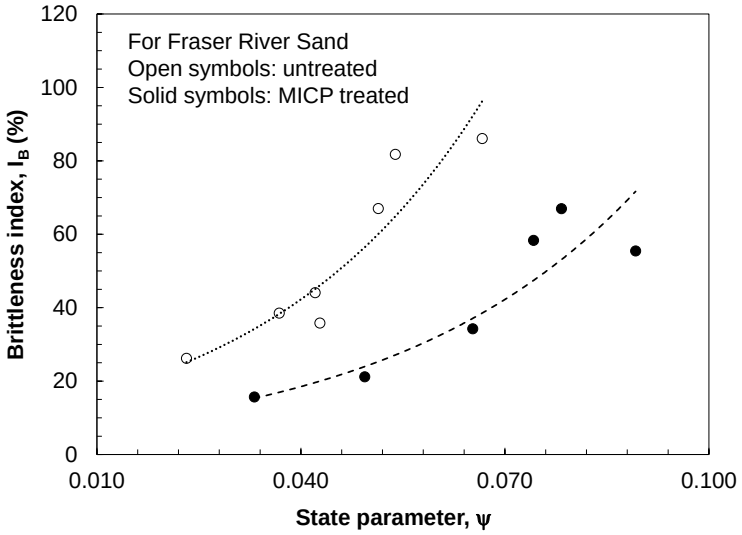

Figure 5-20: Changes in brittleness due to single application of MICP treatment on Fraser River sand for the range of state parameters tested.

As shown by the undrained (i.e. constant-volume, CV) loading stress paths in Figure 5-13, strain softening and strength loss occur when the applied shear stress exceeds the undrained yield strength, S_u(yield). The locus of yield points projecting linearly down to the origin of the stress path is commonly referred to as the instability line (IL) (Lade 1992; Chu et al. 2003). More generally, however, it has been observed that static liquefaction can be triggered when a stress path crosses IL, irrespective of drainage conditions (Morgenstern et al. 2016). This general situation corresponds to a mobilized friction angle (ϕ'_{mob}) equal to or greater than the IL slope – the yield friction angle, ϕ'_{yield}. Accordingly, Figure 5-21 presents the observed changes in ϕ'_{yield} with increasing e_c and ψ . As shown in Figure 5-21, the values of ϕ'_{yield} for both sands decrease

as (a) e_c and (b)ψ increase. However, ϕ'_{yield} of the treatment specimens are approximately 4° to 6° higher than those of the untreated samples, thus reflecting a general increase in ϕ'_{yield} due to the particle cementation produced by the single application of MICP treatment. The resulting relationships between ϕ'_{yield}, and e_c and ψ are fittingly described by following equations:

For the original Fraser River sand:

(Eq. 5-11) $$\phi'_{yield} = 530\exp(-4.16e_c)$$

(Eq. 5-12) $$\phi'_{yield} = 17.8\exp(-4.70\psi)$$

For MICP-treated Fraser River sand:

(Eq. 5-13) $$\phi'_{yield} = 476\exp(-3.77e_c)$$

(Eq. 5-14) $$\phi'_{yield} = 26\exp(-6.71\psi)$$

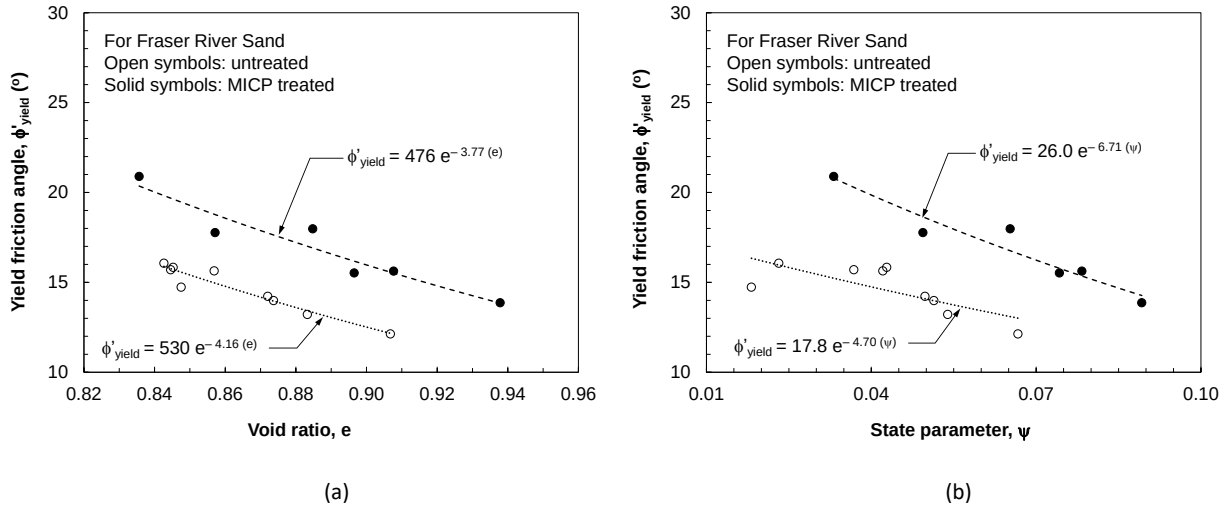

Figure 5-21: Relationships between ϕ'_{yield} with (a) e_c and (b) ψ for Fraser River sand displaying the changes produced by MICP treatment.

The observed increase in the yield strength of treated samples is mostly attributed to the calcite cementation produced at particle-to-particle contacts by the single application of MICP as shown

in Figure 5-12(a), which increases the sand's stiffness. This assertion is confirmed in Figure 5-22 by the higher trend in the tangent shear modulus (G) at $\gamma = 0.1\%$ with e_c for the treated samples relative to that for the untreated specimens. Although both trends indicate exponential gains in stiffness as the sands become denser (as e_c decreases), treated specimens exhibit and consistently maintain G values at least 3 MPa higher than the untreated samples, seemingly reaching a minimum value of approximately 10 MPa at a very loose state with $e_c = 0.938$ or $D_{rc} = 7\%$.

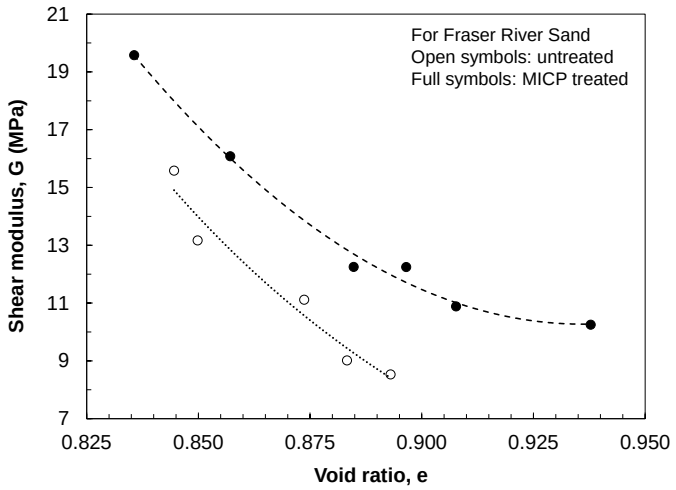

Figure 5-22: G and e_c relationships for untreated and treated Fraser River sand displaying an increase in shear stiffness of the sand due to a single application of MICP treatment.

5.4.2. Cyclic Liquefaction Behaviour

Figures 5-23 to 5-25 compare the cyclic strength curves obtained for the MICP treated samples tested in this study with those reported by Jones (2017) for the same Fraser River sand without treatment. These curves describe the number of shear-loading cycles required to produce liquefaction (N_L) at specific CSR values.

In general, the CSR curves in Figures 5-23 to 5-25 show that larger magnitudes of CSR are required to reach any particular N_L in the treated samples than in the untreated sand. This increased resistance comes primarily as a result of $CaCO_3$ cementation at particle-to-particle contacts, which helps maintain the majority of loading cycles at small shear strains (see Figure 5-14) and reduces the rate of excess pore pressure generation (see Figure 5-15) that eventually leads to failure.

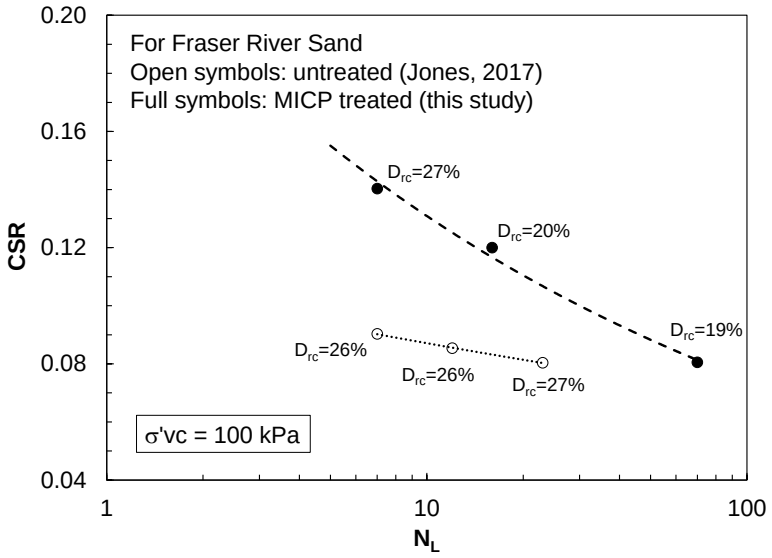

Figure 5-23: Contrast in cyclic strength curves between untreated (D_{rc} = 26-27%) and MICP treated (D_{rc} = 19-27%) samples of Fraser River sand.

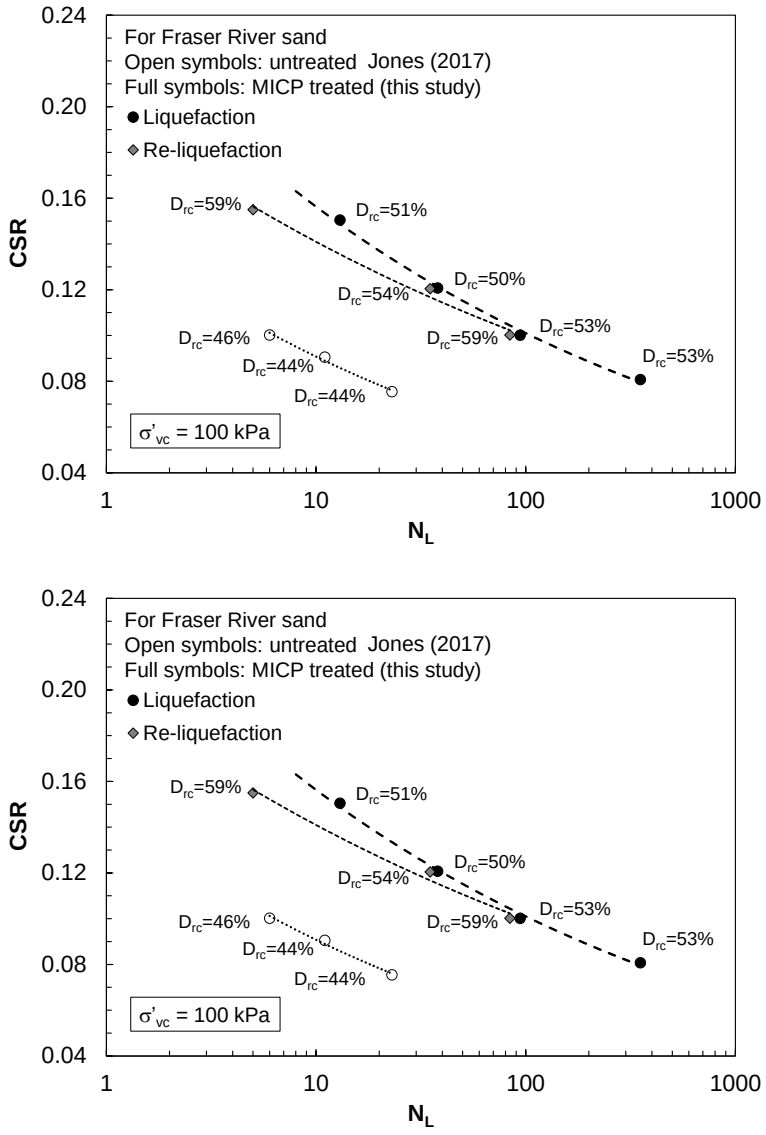

Figure 5-24: Contrast in cyclic strength curves between untreated (D_{rc} = 44-46%) and MICP treated (D_{rc} = 50-53%) samples of Fraser River sand in liquefaction and re-liquefaction.

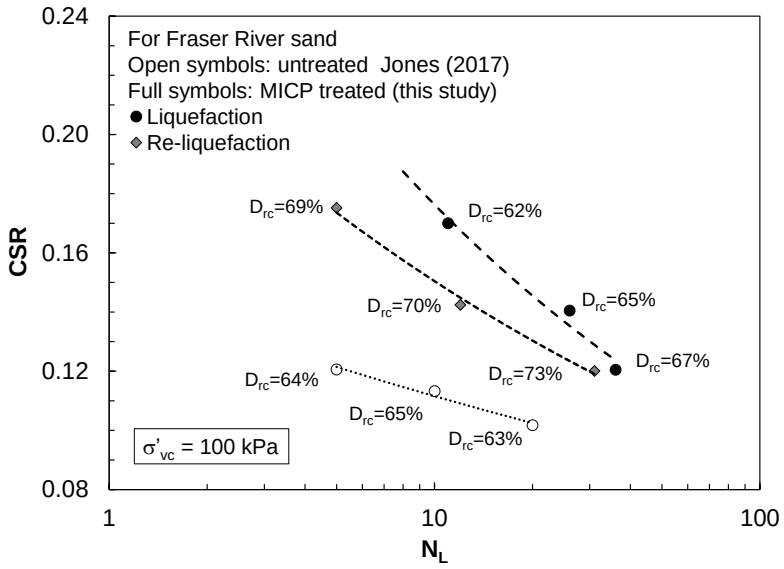

Figure 5-25: Contrast in cyclic strength curves between untreated (D_{rc} = 63-65%) and MICP treated (D_{rc} = 62-67%) samples of Fraser River sand in liquefaction and re-liquefaction.

Because of densification during post-consolidation flushing of samples with the MICP treatment reagent, precise control of D_{rc} was quite difficult in preparing the treated specimens. The resulting D_{rc} of the treated specimens are thus somewhat different from those of the untreated sand, particularly for the loose and the medium-dense tests (Figures 5-23 and 5-24). This may have produced some bias in examining the effect of MICP treatment on the cyclic strength curves of Figures 5-23 to 5-25. To mitigate this bias, comparisons are made based the cyclic resistance ratio (CRR_{15}), defined here as the CSR required to produce liquefaction in N_L = 15 cycles. This corresponds to the equivalent number of cycles produced by an earthquake magnitude of 7.5. Figure 5-26 shows variations of CRR_{15} with D_{rc} and the state parameter (ψ). Although the values of CRR_{15} for both the treated and the untreated sand increase with increasing D_{rc} or decreasing ψ at roughly the same rate, the trends established for the treated sand indicate 50 to 60% increase in CRR_{15} than those for the untreated sand due to MICP treatment. In order to quantify this relative increase in cyclic resistance, the following empirical relationships are established between CRR_{15}, D_{rc}, and ψ.

For the original Fraser River sand:

(Eq. 5-15) $$CRR_{15} = 0.068\exp(0.623D_{rc})$$

(Eq. 5-16) $$CRR_{15} = 0.084\exp(-1.897\psi)$$

For MICP-treated Fraser River sand:

(Eq. 5-17) $$CRR_{15} = 0.111\exp(0.514D_{rc})$$

(Eq. 5-18) $$CRR_{15} = 0.133\exp(-1.583\psi)$$

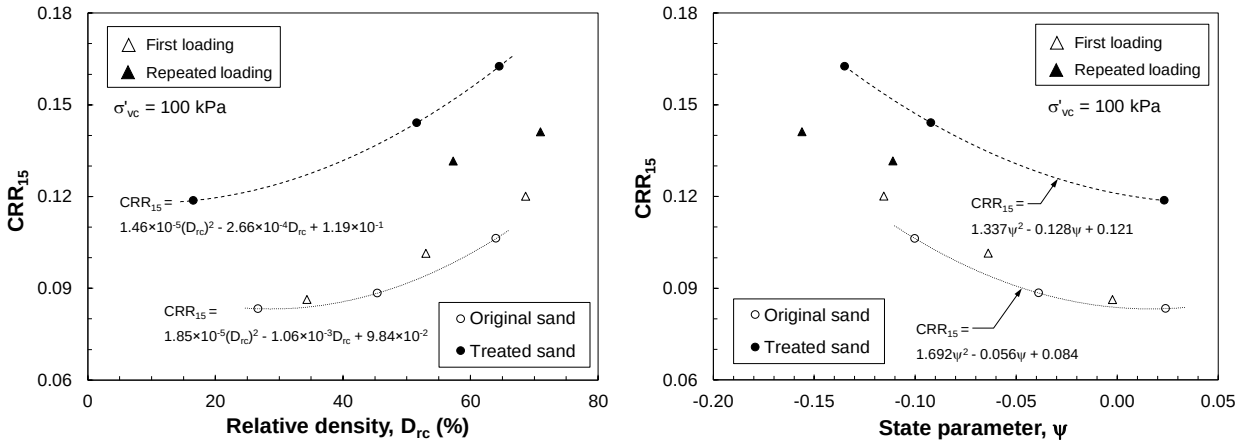

(a) (b)

Figure 5-26: Variations of CRR_{15} in treated vs. untreated FRS with (a) D_{rc} and (b) ψ

The above discussion showed that MICP treatment can significantly reduce the liquefaction potential of Fraser River sand. However, an in-situ sand deposit could experience repeated cyclic loads due to an aftershock or future seismic events. Therefore, a major concern is if the strengthening effect of MICP would remain following cyclic liquefaction, or diminish, requiring additional treatment. To address this question, MICP treated specimens of medium-dense and dense FRS were to a repeated cyclic loading. Following the first cyclic shearing in these tests, the shear stress was removed, the specimens were reconsolidated to σ'_{vc}, and the same CSR was subsequently re-applied. For the untreated FRS, Jones (2017) shows that the densification of the

sand structure due to reconsolidation would increase the re-liquefaction resistance (i.e. requiring a higher N_L for a given CSR). In contrast, Figures 5-24 and 5-25 show a relatively small reduction of re-liquefaction resistance in the MICP treated samples, requiring fewer N_L to liquefy despite a higher D_{rc} during the second cyclic loading application. This reduction probably occurs due to the breakage of the cementation bonds between sand particles. Nevertheless, treated samples show higher resistance to cyclic loading than the untreated original sand, perhaps due to the combined effects of densification due to $CaCO_3$ formation, increased particle angularity and surface-roughness through MICP, as well as some residual $CaCO_3$ particle bonds. Accordingly, the reinforcing effect of MICP treatment may remain to a large extent – not principally through $CaCO_3$ bonds – and still reduce the liquefaction potential of treated sand deposits in future seismic events.

In general, the combined effects of cementation, increased particle angularity, and densification due to $CaCO_3$ precipitation produced a remarkable increase in the sand's resistance to cyclic loading. Finally, we note that the results and discussions present here are applicable to a freshly deposited young sand subject to a level-ground cyclic loading. Further research is required to determine the effect of MICP treatment on aging or in a sloping ground.

5.4.3. Post-Liquefaction Volumetric Strain

An important feature of post-liquefaction behaviour is the accumulation of settlement as excess pore pressure dissipates. Liquefaction-induced ground settlement has often caused significant damages to critical lifelines and structures supported on shallow foundations in past earthquakes. Post-earthquake settlement can be particularly detrimental if it occurs unevenly, resulting in differential settlement of buildings, foundations, bridge abutment, and underground structures. Settlements in the order of 10 to 20 cm have been documented in many sand deposits following previous earthquakes (Grantz et al. 1964; Waller 1966; Seed and Silver 1972). Differential settlement from the compression of loose sand pockets caused severe damage to major structures following the 1963 Skopke earthquake in Macedonia (Seed and Silver 1972). Extensive building settlement was observed in response to the subsoil liquefaction following the 1990 Luzon earthquake at the city of Dagupan (Ishihara et al. 1993).

Post-liquefaction reconsolidation vertical strain (ε'_v) was measured in the medium-dense and dense specimens by unloading shear stresses applied on the specimen, and then reconsolidating them to the original σ'_{vc} = 100 kPa. Because of the lateral constraint provided by the stack of annular rings around the sample, ε'_v is ultimately equal to the reconsolidation volumetric strain (ε'_{vol}). This would represent reconsolidation volumetric strain for a nearly level-ground sand deposit (far away from any free face with little or no lateral displacement), beneath a wide building, or in a deep sublayer, following an earthquake. Irrespective of D_{rc}, CSR, or MICP treatment, Figure 5-27 indicates a direct relationship between ε'_{vol} and the maximum shear strain (γ_{max}) attained in the first cyclic loading stage in DSS tests on FRS samples. γ_{max} can be regarded as a measure of the amount of disturbance sustained by a soil deposit following an earthquake. Although these data are obtained from uniformly loaded specimens, the type of cyclic loading (whether uniform or irregular), loading frequency, and saturation are generally found to have a small effect on the $\varepsilon'_{vol} - \gamma_{max}$ relationship (Youd 1971; Tsukamoto et al. 2004). The strong effect of γ_{max} on post-liquefaction volumetric strain has been also reported by several other investigators (Silver and Seed 1971; Tatsuoka et al. 1984; Matsuda et al. 2004; Ishihara et al. 2016) in cyclic DSS tests. Furthermore, the range of ε'_{vol} (= 0.8 - 3.3%) shown in Figure 5-27 is consistent with those reported by several other investigators in laboratory element tests (Silver and Seed 1971; Yoshimi 1967; Nagase and Ishihara 1988; Ishihara 1993), shaking table experiments (Seed and Silver 1972; Whitman 1970), or field observations (Grantz et al. 1964; Silver and Seed 1971; Nagase and Ishihara 1988). For example, Nagase and Ishihara (1988) measured ε'_{vol} of as much as 4%, 2.5%, and 1.2% following cyclic DSS tests on specimens of Fuji River sand prepared at D_{rc} = 47%, 73%, and 93%, respectively. Likewise, re-consolidation of a 12.1 m deep sand fill resulted in level-ground surface settlements of 0.10 to 0.15 m following the 1971 San Francisco earthquake (Seed and Silver 1972), which correspond to ε'_{vol} = 0.8 - 1.2%.

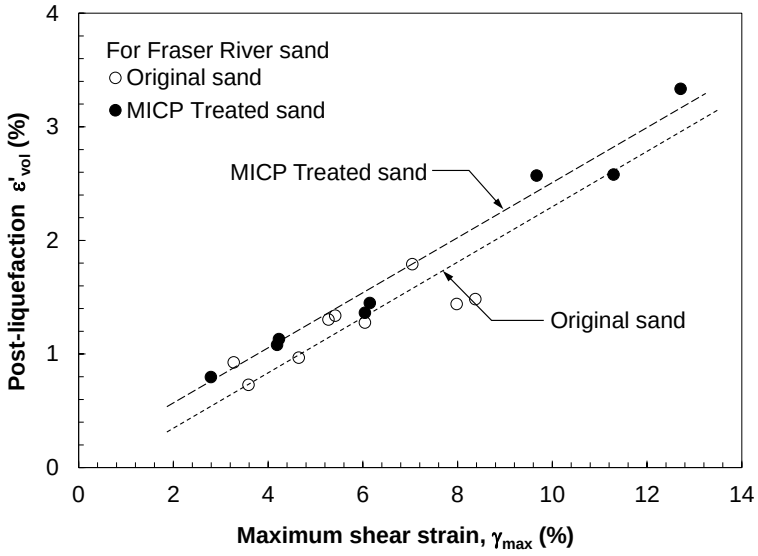

Figure 5-27: Relationship between ε'_{vol} and γ_{max} measured in the cyclic DSS tests of this study.

5.4.4. V_S and G_{max}

Shear-wave velocity (V_S) measurements provide a good indication of the cementation effect produced by MICP treatment in sands (DeJong et al. 2010; Montoya and DeJong 2015; Feng and Montoya 2017; Mortensen et al. 2011; Montoya et al. 2013; Zamani et al. 2018; Zamani and Montoya 2018). The results shown in Figure 5-13 for the tests performed in this study concur with this assertion. The relative gain in V_S and its effect on sand's stiffness after a single application of MICP treatment are quantified and discussed in the following paragraphs.

The effect of σ'_{vc} on both untreated and treated samples was described in Figure 5-11 by power functions with respective values of β = 0.26 and 0.21, demonstrating an increase in V_S due to a single application of the MICP treatment in the sand. Similarly, DeJong et al. (2006) report an increase in V_S of approximately 60 m/s after the first application of MICP treatment in a silica sand sample consolidated to a confining stress of 50 kPa. When estimating the increase in V_S for FRS that would result from treatment application in a sample at σ'_{vc} = 50 kPa using the relationships in Figure 5-11, the ensuing increase of 60.8 m/s is comparable with that obtained by DeJong et al. (2010).

V_S is often normalized by the overburden stress in order to account for the effect of σ'_{vc} using the relationship below (Robertson et al. 1995):

(Eq. 5-19) $$V_{S1} = V_S \left(\frac{P_a}{\sigma'_{vc}}\right)^{\beta}$$

Where, V_{S1} is the overburden stress-normalized shear wave velocity, β is the stress normalization exponent, and P_a is a reference pressure (= 100 kPa). Figure 5-28 presents the observed increase in V_S due to a single application of MICP treatment by comparing the larger constant V_{S1} = 240 m/s obtained from the treated specimens with the constant V_{S1} = 180 m/s of the original sand. Despite some scatter in the data, the general trends for the treated and untreated materials describe the small effect of e_c (Figure 5-14a) and ψ (Figure 5-14b) in V_S for FRS and a general increase of ~60 m/s (as shown earlier for a low σ'_{vc} = 50 kPa) in shear-wave velocity produced by the MICP treatment.

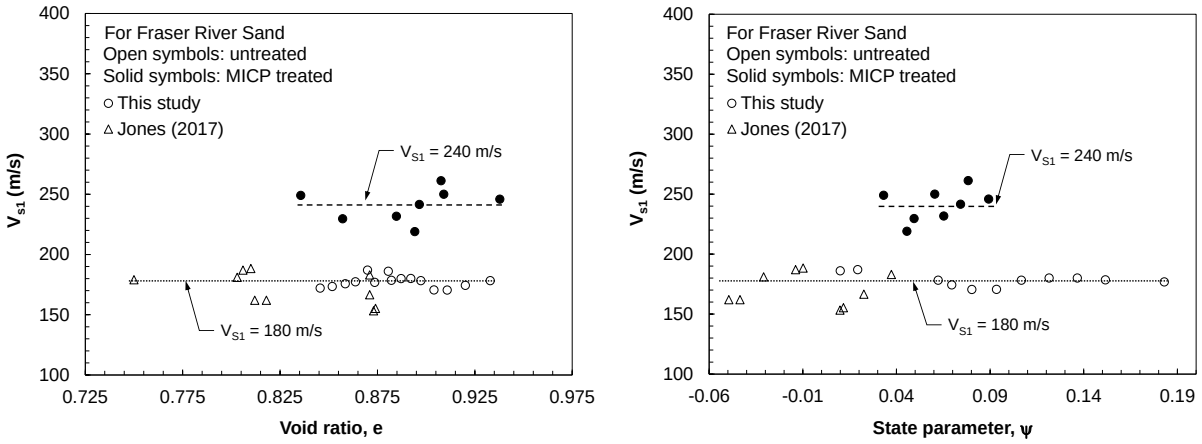

Figure 5-28: Variation of V_{S1} with (a) e_c and (b) ψ for untreated and MICP treated Fraser River sand.

The increased V_S values of MICP treated samples are also indicative of their higher stiffness relative to the untreated sand. Given the small shear-strains induced by shear-waves, the maximum shear modulus (G_{max}) can be estimated from V_S as follows:

(Eq. 5-20) $$G_{max}(MPa) = \rho V_S^2$$

Where, ρ is the total density in kg/m^3. Figure 5-29 compares the computed G_{max} values of the untreated sand with those of the treated specimens. As similarly observed with G at larger shear strains (Figure 5-22), treated samples in Figure 5-29 show significantly higher G_{max} values than the original sand as a result of calcite cementation and stiffer particle contacts, with the trend consistently maintaining a gain in G_{max} of about 70-100 MPa.

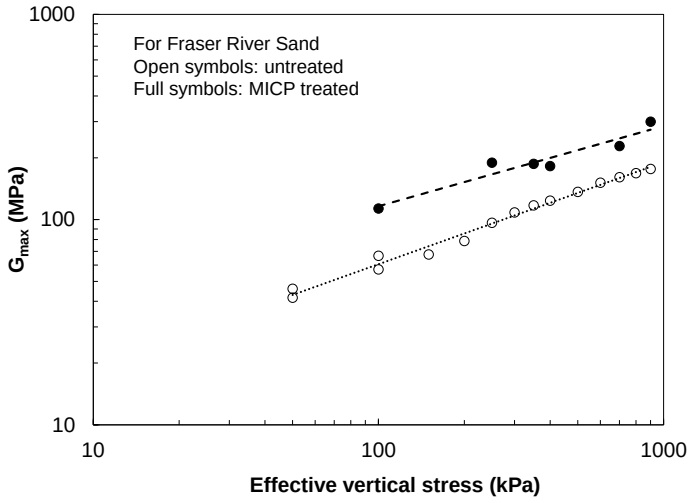

Figure 5-29: G_{max} and σ'_{vc} log-log relationships for Fraser River sand displaying an increase in small-strain stiffness due to a single application of MICP treatment.

5.5. Conclusions

Improvement of soil properties through the precipitation of inorganic calcium carbonate ($CaCO_3$) is currently an area of active research. Many microbial metabolic processes play a role in the

natural deposition of carbonate minerals on the Earth's surface, and harnessing them for the improvement of stiffness and strength is a promising substitute of synthetic soil improvement techniques.

Microbially Induced Calcite Precipitation (MICP) is a bio-mediated process that makes use of microbial enzymatic activities, typically urea hydrolysis, and results in the formation of calcium carbonate. By employing *S. ureae* as the ureolytic microorganism, the shear behaviour of Fraser River sand samples was improved in this study with a single application of an MICP-based treatment.

Microscopic images of treated samples confirm that application of the treatment by dry-mixing and saturation with precipitation reagents produced particle bonding and an increase in particle angularity. Principally as a result of the higher stiffness caused by particle cementation, shear-wave velocities (V_S) of the sand at various stress-state conditions were increased by 60 – 70 m/s with a single application of the treatment. $CaCO_3$ bonds at particle-particle contacts in the sand were not only shown to increase the sand's rigidity at small strains with gains in maximum shear modulus (G_{max}) of 70 – 100 MPa at small strains, but also at larger strains ($\gamma = 0.1\%$) with gains in tangent shear modulus (G) of 3 – 4 MPa.

The MICP treatment used also improved the undrained monotonic shear behaviour of the sand. While ϕ'_{cs} was essentially unchanged, the sand's yield and post-liquefied strengths were noticeably increased by the combined effect of particle bonding, densification of pore-space, and changes in particle angularity and surface roughness produced by $CaCO_3$ precipitation. Gains in the post-liquefied strength of the sand were consistently higher than those in its yield strength for the range of densities tested, owing to changes in the sand's critical state caused by the treatment, which produced an upward shift in the location of the CSL relative to that of the natural sand, thus getting closer to the sand's NCL and reducing the magnitude of the state parameter. This shift also caused a decrease in the sand's brittleness, as the difference between the yield and post-liquefied strength at any given stress-state was reduced compared to that of the natural sand.

The sand's resistance to cyclic liquefaction was also enhanced by the treatment, as indicated by the larger number of cycles required to induce failure at any specific CSR. While the trends in CRR_{15} with relative density and state parameter for both the treated and untreated sand were shown to parallel each other, the treatment caused a vertical offset of the trend, producing higher CRR_{15}

values for the range of densities tested. Furthermore, re-liquefaction of treated medium dense specimens showed a small decrease in the cyclic resistance from that exhibited in a first liquefaction event, perhaps due to the breakage of some of the $CaCO_3$ bonds after the first event. Nonetheless, the strengthening effect of MICP treatment was shown to partially remain plausibly due to the combined effect of residual unbroken bonds and densification, thus continuing to reduce the liquefaction potential of treated sand deposit in future seismic events. Lastly, post-liquefaction settlements, measured as the volumetric strains produced after a first liquefaction event, were shown to be unaffected by the treatment, as they were seen to follow the same direct relationship with the maximum shear strain applied as the original sand.

In summary, *S. ureae* was proven to be suitable for applications of MICP treatments in Fraser River sand. By producing $CaCO_3$ bonds at particle contact points and densifying available pore-space within the soil matrix, as well as by increasing particle angularity and surface roughness, a single application of the treatment appreciably improved the shear strength and stiffness of Fraser River sand. Although clear trends with high correlation coefficients were established for the correlations presented, there remains a small level of uncertainty in the repeatability of the results. Additionally, the present study was restricted to assessing the treatment's effectiveness in a laboratory setting, and a more comprehensive study may be required to assess possible effects on the treatment caused by its application in-situ.

5.6. References

Airey, D., and Wood, D. (1987). An evaluation of direct simple shear tests on clay. *Geotechnique*, Vol 37, No. 1, pp. 25-35.

Airey, D., Budhu, M., and Wood, D. (1985). Some aspects of the behaviour of soils in simple shear. In E. P. Butterfield, *Development in Soil Mechanics and Foundation* (pp. Vol. 2, pp. 185-). Elsevier.

Alarcon-Guzman, A., Leonards, G., and Chameau, J. L. (1988). Undrained monotonic and cyclic strength of sands. *Journal of Geotechnical Engineering*, 114(10), 1089-1109.

Allen, T. (2015). *Microscopy: A Very Short Introduction.* Oxford, UK: Oxford University Press.

Anbu, P., Kang, C. H., Shin, Y. J., and So, J. S. (2016). Formations of calcium carbonate minerals by bacteria and its multiple applications. *SpringerPlus*. doi:DOI 10.1186/s40064-016-1869-2

ASTM D6528-17, A. (2017). Standard Test Method for Consolidated Undrained Direct Simple Shear Testing of Fine Grain Soils. *ASTM International*.

ASTMD422-63. (2007). *Standard Test Method for Particle-Size Analysis of Soils.* ASTM. doi:10.1520/D0422-63R07E02

ASTMD4253—16. (2016). Standard Test Methods for Maximum Index Density and Unit Weight of Soils Using a Vibratory Table1. *ASTM*. Retrieved from https://doi-org.proxy1.lib.uwo.ca/10.1520/D4253-16

ASTMD4254—16. (2016). Standard Test Methods for Minimum Index Density and Unit Weight of Soils and Calculation of Relative Density1. *ASTM*. Retrieved from https://doi-org.proxy1.lib.uwo.ca/10.1520/D4254-16

ASTMD6528-17. (2017). Standard Test Method for Consolidated Undrained Direct Simple Shear Testing of Fine Grain Soils. *ASTM*. Retrieved from https://doi-org.proxy1.lib.uwo.ca/10.1520/D6528-17

ASTMD854—14. (2014). Standard test methods for specific gravity of soil solids by water pycnometer. *ASTM*. Retrieved from https://doi-org.proxy1.lib.uwo.ca/10.1520/D0854-14

Bavendamm, W. (1932). Die mikrobiologische Kalkfällung in der tropischen. *Arch Microbiol*, 3:205–276.

Been, K., and Jeffries, M. G. (1985). A state parameter for sands. *Geotechnique*, 35(2), 99-112.

Been, K., Jeffries, M. G., and Hachey, J. E. (1991). The critical state of sands. *Geotechnique*, 41(3), 365-381.

Bjerrum, L., and Landva, A. (1966). Direct simple shear test of Norwegian quick clay. *Geotechnique*, 16(1): 1-20.

Bosak, T., and Newman, D. K. (2003). Microbial nucleation of calcium carbonate in the Precambrian. *Geology*, 31:577–580.

Bosak, T., and Newman, D. K. (2005). Microbial kinetic controls on calcite morphology in supersaturated solutions. *J Sed Res*, 75:190–199.

Bosak, T., Stolarski, J., and Meiborn, A. (2015). Microbial Formation and Degradation of Carbonates. In H. L. Ehrlich, D. K. Newman, and A. Kappler, *Ehrlich's Geomicrobiology* (6th ed., pp. 209-236). Chapman and Hall/CRC.

Brignoli, E., Gotti, M., and Stokoe, K. (1996). Measurement of Shear Waves in Laboratory Specimens by Means of Piezoelectric Transducers. *Geotechnical Testing Journal, Vol. 19, No. 4*, 384-397. Retrieved from https://doi-org.proxy1.lib.uwo.ca/10.1520/GTJ10716J.

Buikema, N. D. (2015). *Stabilization of iron mine tailings through microbially induced calcite precipitation.* Michigan Technological University. Retrieved from http://digitalcommons.mtu.edu/etds/981

Burbank, M., Weaver, ,. T., Lewis, R., Williams, T., Williams, B., and Crawford, R. (2013). Geotechnical Tests of Sands Following Bioinduced Calcite Precipitation Catalyzed by Indigenous Bacteria. *J. Geotech. Geoenviron. Eng.*, 139(6): 928-936. doi:10.1061/(ASCE)GT.1943-5606.0000781

Camacho-Tauta, J. F., CASCANTE, G., VIANA DA FONSECA, A., and A, S. J. (2015). ime and frequency domain evaluation of bender element systems. *Geotechnique*, 65:548-562.

Casagrande, A. (1936). Characteristics of cohesionless soils affecting the stabilityof earth fills. *Journal of Boston Society of Civil Engineers*, 23, 257-276.

Chafetz, H. S., and Buczynski, C. (1992). Bacterially induced lithification of microbial mats. *Palaios*, 7:277–293.

Cheng, L., Shahin, M. A., and Cord-Ruwisch, R. (2014). Bio-cementation of sandy soil using microbially induced carbonate precipitation for marine environments. *Geotechnique*, 64, No. 12, 1010–1013. Retrieved from http://dx.doi.org/10.1680/geot.14.T.025

Chillarige, V. A. (1995). *Liquefaction and seabed instability in the fraser river delta.* Ph.D. Dissertation, University of Alberta. Retrieved from https://www-lib-uwo-ca.proxy1.lib.uwo.ca/cgi-bin/ezpauthn.cgi?url=http://search.proquest.com.proxy1.lib.uwo.ca/docview/230795815?accountid=15115

Chou, C. W., Seagren, E. A., Aydilek, A. H., and Lai, M. (2011). Biocalcification of Sand through Ureolysis. *Journal of Geotechnical and Geoenvironmental Engineering*, 1179–1189. doi:10.1061/(ASCE)GT.1943-5606.0000532

Christian, H. A., Woeller, D. J., Robertson, P. K., and Courtney, R. C. (1997). Site investigations to evaluate flow liquefaction slides at Sand Heads, Fraser River delta. *Can. Geotech. J.*, 34: 384–397.

De Yoreo, J. J., and Vekilov, P. G. (2003). Principles of crystal nucleation and growth. *Rev Mineral Geochem*, 54:57–93.

DeJong, J. T., Fritzges, M. B., and Nüsslein, K. (2006). Microbially Induced Cementation to Control Sand Response to Undrained Shear. *Journal of Geotechnical and Geoenvironmental Engineering*, 1381–1392.

DeJong, J. T., Mortensen, B. M., Martinez, B. C., and Nelson, D. C. (2010). Bio-mediated soil improvement. *Ecological Engineering*, 36: 197–210.

Dobry, R., Vasquez-Herrera, A., and Ramly, M. (1985). Liquefaction flow failure of silty sand by torsional cyclic tests. *Advances in the art of testing soils under cyclic conditions* (pp. 29-50). Detroit, MI: ASCE.

Dyvik, R., Berre, T., Lacasse, S., and Raadim, B. (1987). Comparison of truly undrained and constant volume direct simple shear tests. *Geotechnique*, 37(1): 3-10.

East, D., Ransone, J., and Cincilla, W. (1988). Testing of the Homestake mine tailings deposit. *Proceedings 2nd International Conference on Case Histories in Geotechnical Engineering*, (pp. pp. 495-502).

Favre, N., Christ, M. L., and Pierre, A. C. (2009). Biocatalytic capture of CO2 with carbonic anhydrase and its transformation to solid carbonate. *J Mol Catal B Enzym*, 60:163–170.

Feng, K., and Montoya, B. M. (2016). Influence of Confinement and Cementation Level on the Behavior of Microbial-Induced Calcite Precipitated Sands under Monotonic Drained Loading. *J. Geotech. Geoenviron. Eng.*, 142(1): 04015057. doi:10.1061/(ASCE)GT.1943-5606.0001379.

Feng, K., and Montoya, B. M. (2017). Quantifying Level of Microbial-Induced Cementation for Cyclically Loaded Sand. *Journal of Geotechnical and Geoenvironmental Engineering*, 143(6):. doi:10.1061/(ASCE)GT.1943-5606.0001682

Ferrer, M. R., Quevedo-Sarmiento, J., Bejar, V., Delgado, R., Ramos-Cormenzana, A., and Rivadeneyra, M. A. (1988). Calcium carbonate formation by Deleya halophila: Effect of salt concentration and incubation temperature. *Geomicrobiol J*, 6:49–57.

Ferris, F. G., Fratton, C. M., Gerits, J. P., Schultze-Lam, S., and Lollar, B. S. (1995). Microbial precipitation of a strontium calcite phase at a groundwater discharge zone near Rock Creek, British Columbia, Canada. *Geomicrobiol J* , 13:57–67.

Ferris, F. G., Phoenix, V., Fujita, Y., and Smith, R. W. (2003). Kinetics of calcite precipitation induced by ureolytic bacteria at 10 to 20 °C in artificial groundwater. *Geochim Cosmochim Acta*, 67:1701–1710.

Finn, W. D., and Vaid, Y. P. (n.d.). Liquefaction potential from drained constant constant volume cyclic simple shear tests. *the 6th World Conference on Earthquake Engineering*, (pp. 6: 7-12). New Delhi.

Fujita, Y., Taylor, J. L., Gresham, T., Delwiche, M., Colwell, F., McLing, T., . . . Smith, R. (2008). Stimulation of microbial urea hydrolysis in groundwater to enhance calcite precipitation. *Environ Sci Technol*, 42:3025–3032.

Galindon da Fonseca, P., and Galindo da Fonseca, I. (2016). Brazil's Greatest Environmental Catastrophe – Samarco's Fundão Tailings Dam –. *Environmental Policy and Law*, 46/5: 334-337.

Gat, D., Tsesarsky, M., Shamir, D., and Ronen, Z. (2014). Accelerated microbial-induced CaCO3 precipitation in a defined coculture of ureolytic and non-ureolytic bacteria. *Biogeosciences*, 11, 2561–2569.

Goldman, M., and Wilson, D. (1977). Growth of Sporosarcina ureae in defined media. *FEMS Microbiology Letters*, 113-115.

Gonzalez-Munoz, M. T., Rodriguez-Navarro, C., Martinez-Ruiz, F., Arias, J. M., Merroun, M. L., and Rodriguez-Gallego, M. (2010). Bacterial biomineralization: new insights from Myxococcus – induced mineral precipitation. *Geol Soc Lond Sp Pub*, 336:31–50.

Gorospe, C., Han, S., Kim, S., Park, J., Kang, C., Jeong, J., and So, J. (2013). Effects of different calcium salts on calcium carbonate crystal formation by Sporosarcina pasteurii KCTC 3558. *Biotechnology and Bioprocess Engineering*, 903-908. doi:10.1007/s12257-013-0030-0

Hamel, J., and Gunderson, J. (1973). Shear Strength of Homestake Slimes Tailings. *J. of Soil Mech. and Fdn. Div., ASCE*, Vol. 99, No. SM5, pp. 247-234.

Hanazawa, H., itoh, Y., and suzuki, K. (1980). Shear characteristics of a quick sand in the arabian gulf. *International Journal of Rock Mechanics and Mining Sciences and Geomechanics Abstracts, 17(5)*, 81-81. doi:10.1016/0148-9062(80)90840-2.

Hardin, B. O., and Richart Jr., F. E. (1963). Elastic wave velocities in granular soils. *Journal of Soil Mechanics and Foundation Division, ASCE*, 89(1), 33 - 65.

Hicks, M. A., and Boughrarou, R. (1988). Finite element analysis of the Nerlerk underwater berm failures. *Géotechnique*, 48:2, 169-185 .

Jeffries, M. G., and Been, K. (1987). Use of critical state representations of sand in the method of stress characteristics. *Canadian Geotechnical Journal*, 24: 441-446.

Jeffries, M., and Been, K. (1987). Use of Critical State Representations of Sand in the Method of Stress Characteristics. *Canadian Geotechnical Journal*, 24, pp. 441-446.

Jeffries, M., and Been, K. (2016). *Soil Liquefaction -- A Critical State Approach, 2nd Ed.* Boca Raton: Taylor and Francis Group.

Jones, S. (2017). *Liquefaction Susceptibility Analysis of Fraser River Sand in Miniature Cone Penetration Tests and Cyclic Direct Simple Shear Tests.* Electronic Thesis and Dissertation Repository. Retrieved from https://ir.lib.uwo.ca/etd/4782

Jones, S. (2018). *Miniature Cone Penetration Tests on Fraser River Sand.*

Jovičić, V., and Coop, M. (1998). The Measurement of Stiffness Anisotropy in Clays with Bender Element Tests in the Triaxial Apparatus. *Geotechnical Testing Journal Vol. 21, No. 1*, 3-10. Retrieved from https://doi-org.proxy1.lib.uwo.ca/10.1520/GTJ10419J

Kammerer, A. M. (2002). *Undrained Response of Monterey 0 /30 Sand Under Multidirectional Cyclic Simple Shear Loading Conditions.* ProQuest Dissertations Publishing.

Krumbein, W. E. (1974). On the precipitation of aragonite on the surface of marine bacteria. *Naturwissenschaften*, 61:167.

Kuerbis, R., Negussey, D., and Vaid, Y. (1988). Effects of gradation and fines content on the undrained response of sands. In E. b. Vick, *Hydraulic fill structures* (pp. 330-345). ASCE.

Lee, M., Soon, N. W., Khun, T. C., and Ling, H. S. (2012). Bio-mediated soil improvement under various concentrationsof cementation reagents. *Appl. Mech. Mater.*, 326—329.

Martinez, B. C. (2012). *Up-Scaling of Microbial Induced Calcite Precipitation in Sands for Geotechnical Ground Improvement.* UC Davis, Civil and Environmental Engineering. Ann Arbor, MI: UMI.

Martinez, B. C. (2013). *Up-scaling of microbial induced calcite precipitation in sands for geotechnical ground improvement.* Ann Arbor, MI: ProQuest LLC.

McCoy, D., Cetin, A., and Hausinger, R. (1992). Characterization of urease from Sporosarcina ureae. *Archives of Microbioloy*, 157:411-416.

Mitchell, J. K., and Santamarina, J. C. (2005). Biological Considerations in Geotechnical Engineering. *J. Geotech. Geoenviron. Eng.*, 131(10): 1222-1233.

Mitchell, J., and Soga, K. (2013). *Fundamntals of Soil Behavior, 3rd ed.* Hoboken, NJ: John Wiley and Sons.

Montoya, B. M. (2012). *Bio-mediated soil improvement and the effect of cementation on the behavior, improvement, and performance of sand.* Ann Arbor, MI: ProQuest LLC.

Montoya, B. M., and DeJong, J. T. (2015). Precipitation, Stress-Strain Behavior of Sands Cemented by Microbially Induced Calcite. *J. Geotech. Geoenviron. Eng.*, 141(6): 04015019. doi:10.1061/(ASCE)GT.1943-5606.0001302.

Montoya, B. M., Dejong, J. T., and Boulanger, R. W. (2013). Dynamic response of liquefiable sand improved by microbial-induced calcite precipitation. *Geotechnique 63*, No. 4, 302–312. Retrieved from http://dx.doi.org/10.1680/geot.SIP13.P.019

Monty, C. L. (1972). Recent algal stromatolitic deposits, Andros Island, Bahamas. Preliminary report. *Geol Rundschau*, 61:742–783.

Mortensen, B. M., Haber, M. J., DeJong, J. T., Caslak, L. F., and Nelson, D. C. (2011). Effects of environmental factors on microbial induced calcium carbonate precipitation. *Journal of Applied Microbiology*, 111, 338–349. doi:doi:10.1111/j.1365-2672.2011.05065.x

Murtala, U., Khairul, A. K., and Kenny, T. P. (2016). Biological process of soil improvement in civil engineering: A review. *Journal of Rock Mechanics and Geotechnical Engineering*, 767-774. Retrieved from http://dx.doi.org/10.1016/j.jrmge.2016.02.004

Okwadha, G. D., and Li, J. (2010). Optimum conditions for microbial carbonate precipitation. *Chemosphere*, 81:1143–1148.

Park-Talaro, K. (2008). *Foundation in microbiology, 6th ed.* New York, NY: McGraw HIll.

Pitman, T. D., Robertson, P. K., and Sego, D. C. (1994). Influence of fines on the collapse of loose sands. *Canadian Geotechnical Journal*, 31(5): 728-739. Retrieved from https://doi-org.proxy1.lib.uwo.ca/10.1139/t94-084

Putz, H. (2019). *Match! Phase Identification from Powder Diffraction: Manual.* CRYSTAL IMPACT .

Robertson, P. K., Sego, D. C., and Cunning, J. C. (1995). Shear Wave Velocity to Evaluate in Situ State of Cohesionless Soils. *Canadian Geotechnical Journal 32*, no. 5: 848-858.

Rodriguez-Navarro, C., Jimenez-Lopez, C., Rodriguez-Navarro, A., Gonzalez-Munoz, M. T., and Rodriguez-Gallego, M. (2007). Bacterially mediated mineralization of vaterite. *Geochim Cosmochim Acta*, 71:1197–1213.

Roscoe, K., Schofield, A. N., and Wroth, C. P. (1958). On the yielding of soils. *Geotechnique*, 8(1), 22-53.

Rowe, P., and Craig, W. (1976). Studies of offshore caissons founded on Oostershelde sand. In e. J. Monroe, *Design and Construction of Offshore Structures* (pp. 49-55). London, U.K.: Institution of Civil Engineers.

Rutherford, C. (2012). *Development of a Multi-Directional Direct Simple Shear Testing Device for Characterization of the Cyclic Shear Response of Marine Clays.* ProQuest Dissertations Publishing.

Sadrekarimi, A. (2016). Static Liquefaction Analysis Considering Principal Stress Directions and Anisotropy. *Geotech Geol Eng*, 34:1135–1154. doi:10.1007/s10706-016-0033-7

Sadrekarimi, A., and Olson, S. M. (2012). Effect of Sample-Preparation Method on Critical-State Behavior of Sands. *Geotechnical Testing Journal,*, ol. 35, No. 4, 2012, pp. 548-562. Retrieved from https://doi-org.proxy1.lib.uwo.ca/10.1520/GTJ104317

Schofield, A., and Wroth, C. P. (1968). *Critical state soil mechanics.* London, UK: McGraw Hill.

Sharmaa, A., and Ramkrishnan, R. (2016). Study on effect of microbial induced calciteprecipitates on strength of fine grainedsoils. *Perspectives in Science*, 8, 198—202.

Shozen, T. (1991). *Deformation under the constant stress state and its effect on stress-strain behaviour of Fraser River Sand.* MASc Thesis, University of British Columbia, Civil Engineering, Vancouver, BC.

Sladen, J. A., D'hollander, R. D., and Krahn, J. (1985). The liquefaction of sands, a collapse surface approach. *Canadian Geotechnical Journal No. 4*, 564-578.

Soderberg, R., and Busch, R. (1977). *Design Guide for Metal and Nonmetal Tailings Disposal.* U.S. Bureau of Mines.

Spanos, N., and Koutsoukos, P. G. (1998). The transformation of vaterite to calcite: effect of the conditions of the solution in contact with the mineral phase. *Crystal Growth*, 191:783–790.

Stocks-Fischer, S., Galinat, J. K., and Bang, S. S. (1999). Microbiological precipitation of CaCO3. *Soil Biology and Biochemistry*, 31: 1563-1571.

Terzaghi, K., Peck, R., and Mesri, G. (1996). *Soil Mechanics in Engineering Practice, 3rd Ed.* John Wiley and Sons.

Thompson, J. B., and Ferris, F. G. (1990). Cyanobacterial precipitation of gypsum, calcite and magnesite from natural alkaline lake waters. *Geology*, 18:995–998.

U.S. Geological Survey. (1857). *Introduction to Geology and Resources of Gold, and Geochemistry of Gold.* Denver: U.S. Department of the Interior.

Vaid, Y. P., and Sivathalayan, S. (1996). Static and cyclic liquefaction potential of FRaser Delta sand in simple shear and triaxial tests. *Canadian Geotechnical Journal*, 33(2), 281-289.

Vaid, Y. P., and Sivathalayan, S. (1998). Fundamental factors affecting liquefaction susceptibility of sand. In P. V. Lade, and J. A. Yamamuro (Ed.), *International Workshop on the Physics and Mechanics of Soil Liquefaction*, (pp. 105-120). Baltimore, MD.

Vaid, Y. P., Stedman, J. D., and Sivathalayan, S. (2001). Confining stress and static shear effects in cyclic liquefaction. *Canadian Geotechnical Journal*, 38, 580-591.

Vaid, Y., and Chern, J. (1985). Cyclic and monotonic undrained response of sands. In V. K. ed., *Advances in the Art of Testing Soils under Cyclic Conditions* (pp. 120-147). New York: ASCE.

Viggiani, G., and Atkinson, J. H. (1995). Interpretation of bender element tests. *International Journal of Rock Mechanics and Mining Sciences and Geomechanics Abstracts*, 32(8), A373-A373. doi:10.1016/0148-9062(95)99498-M

Watts, B. D., Seyers, W. C., and Stewart, R. A. (1992). Liquefaction susceptibility of Greater Vancouver area soils. *Geotechnique and natural hazards Symposium* (pp. 145–157). Vancouver Geotechnical Society and the Canadian Geotechnical Society.

Weast, R. C., and Astle, M. J. (Eds.). (1982). *CRC Handbook of Chemistry* (63rd ed.). Boca Raton, FL: CRC Press.

Webb, E. C. (1992). *Enzyme nomenclature 1992: recommendations of the Nomenclature Committee of the International Union of Biochemistry and Molecular Biology on the nomenclature and classification of enzymes.* Academic Press.

Whitman, W. (2009). *BERGEY'S Manual of Systematic Bacteriology, 2nd Ed.* Athens, GA: Springer Dordrecht Heidelberg London New York.

Wijewickreme, D., Sriskandakumar, S., and Byrne, P. (2005). Cyclic loading response of loose air-pluviated fraser river sand for validation of numerical models simulating centrifuge tests. *Canadian Geotechnical Journal*, 42(2), 550-561. doi:10.1139/t04-119

Zamani, A., and Montoya, B. M. (2018). Undrained Monotonic Shear Response of MICP-Treated Silty Sands. *J. Geotech. Geoenviron. Eng.*, 144(6): 04018029. doi:10.1061/(ASCE)GT.1943-5606.0001861

Zamani, A., Feng, K., and Montoya, B. M. (2018). Improved Liquefaction Resistance from Microbial Induced Carbonate Cementation. *Geotechnical Earthquake Engineering and Soil Dynamics*, 296-303.

Chapter 6

6. Conclusions

In this series of studies, liquefaction was shown to be the weakening behaviour of particulate cohesionless materials that can be induced cyclically or statically in both undrained and drained conditions (i.e. constant shear stress). It is indeed this unexpected reduction of strength that has led to the misestimation of strength in geotechnical design, resulting in many failures such as those discussed in Chapter 1.

For example, by evaluating the stability of the failing section of the Fundão dam in a static liquefaction iterative analysis, the dam's slope was found to be reasonably unstable and quite susceptible to flow failure with a safety factor of 0.56. Comparison of the results obtained with those reported by the official investigation panel indicate that the effects of stress anisotropy, mode of shear, and stress path included in the analysis conducted here play a crucial role in the accurate estimation of shear strength from in-situ test data. As discussed, the mobilized shear strength is dependent on the soil's stress state and mode of shear; hence, adopting a constant value of strength (i.e. USR and ϕ'_{yield}) as generally done by the panel, liquefiable areas of high anisotropy in extension shear in the breakout section were overlooked.

The liquefication behaviour of gold mine tailings was analyzed through an experimental program comprised of direct simple shear and bender element tests, and the results were compared with those of other similar tailings (some from real case studies such as the Merriespruit dam collapse). Accordingly, it was established that the effects of fabric produced by diverse deposition methods (e.g. hydraulically and compaction) in sand tailings were practically negligible, as all the tested samples exhibited similar strength loss. Subsequently, based on a critical state framework, empirical methods correlating the shear-wave velocity of gold sand tailings with their susceptibility to static liquefaction and their undrained strength were developed, and their accuracy confirmed by comparing liquefaction susceptibility assessments and undrained shear strengths reported by other researchers on fairly similar tailings. These correlations serve as powerful tools in the analysis and design of tailings dams in order to prevent other failures such as those in Fundão and Merriespruit.

Lastly, as a potential technique to mitigate strength loss in soils susceptible to liquefaction, the effectiveness of Microbially Induced Calcite Precipitation (MICP) – a bio-mediated process that makes use of microbial enzymatic activities to form calcium carbonate – in improving a soil's shear strength was evaluated. By employing *S. ureae* as the ureolytic microorganism, the shear behaviour of liquefiable Fraser River sand samples was shown to improve considerably with a single application of the treatment. Microscopic images of treated samples confirmed that application of the treatment produced particle bonding and an increase in particle angularity, which in turn produced increases in stiffness, undrained strength, and cyclic shear resistance.

Concisely, this series of investigations provides insights into the nature of soil liquefaction, explains the various triggering mechanisms possible, applies an innovative static liquefaction triggering analysis method in evaluating dam stability, presents empirical correlations to determine liquefaction susceptibility and undrained strength in gold sand tailings, and proposes a mitigating soil improvement technique for liquefiable natural sands; all in an effort to present a state of the art summary and plan to prevent any future catastrophes caused by liquefaction.

Limitations in the methods of adopted in the different studies include: the simplification of the static liquefaction analysis of the Fundão dam to a series of limit equilibrium analyses, not accounting for other phenomena such as 3D effects, partial saturation, void redistribution, the kinematics of failure, and the possible effects of microstructure that may have also taken part in the actual failure; the application of a static liquefaction analysis, for which shear behaviour and strength were derived from laboratory testing in sands and silty sands, in order to characterize the behaviour of the liquefying tailings in Fundão; and the assessment of the effectiveness of MICP in a laboratory setting by only evaluating the produced gains in strength, not accounting for detrimental effects that unfavourable in-situ conditions may present.

Consequently, future research opportunities based on these studies include: the addition of laboratory tests on cohesionless tailings of different kinds to the database used to develop the static liquefaction analytical method and evaluating any possible changes to the method; and assessing the effectiveness of MICP treatment application in-situ, perhaps characterized by shear-wave velocity measurements by means of seismic cone penetration tests.

Chapter 7

7. Appendices

7.1. Appendix I: Direct Simple Shear Tests on Gold Tailings

7.1.1.1. Moist-tamped Whole Tailings Specimens

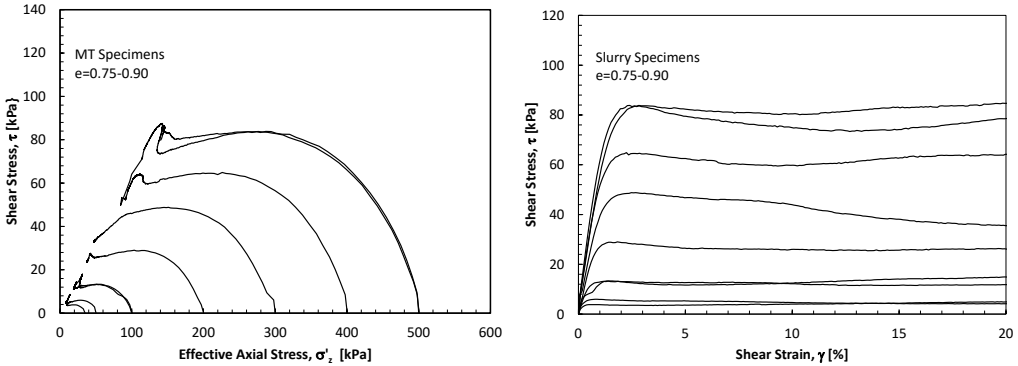

7.1.1.2. Slurry Whole Tailings Specimens

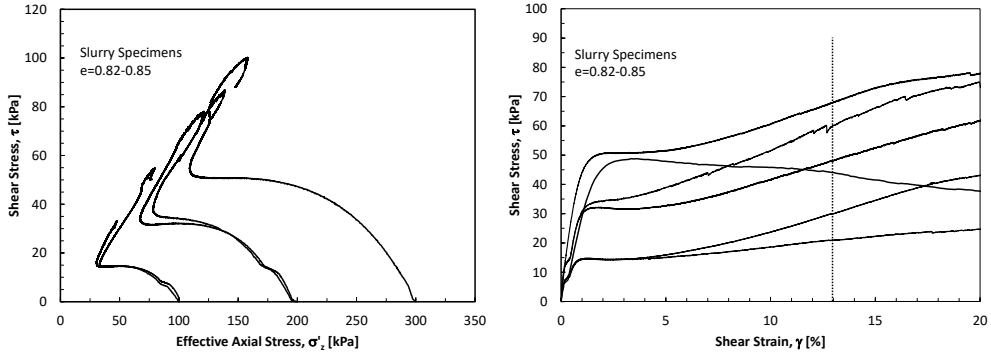

7.1.1.3. Moist-tamped Sand Tailings Specimens

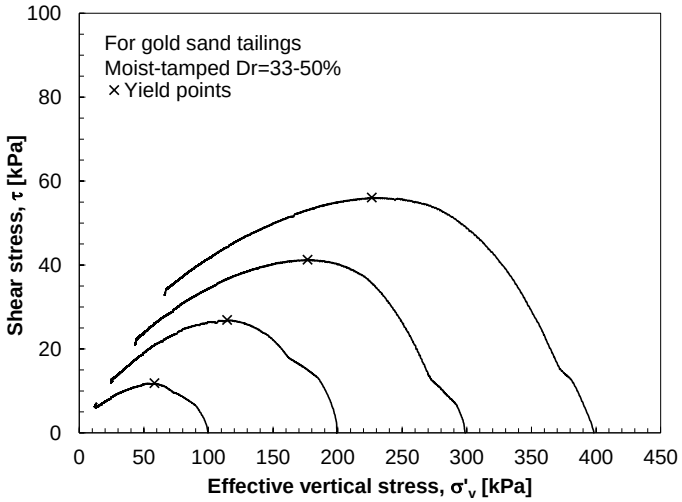

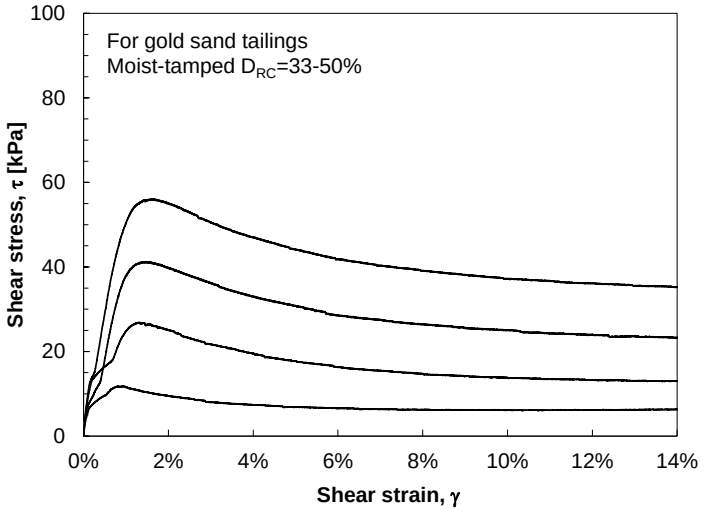

7.1.1.4. Slurry Sand Tailings Specimens

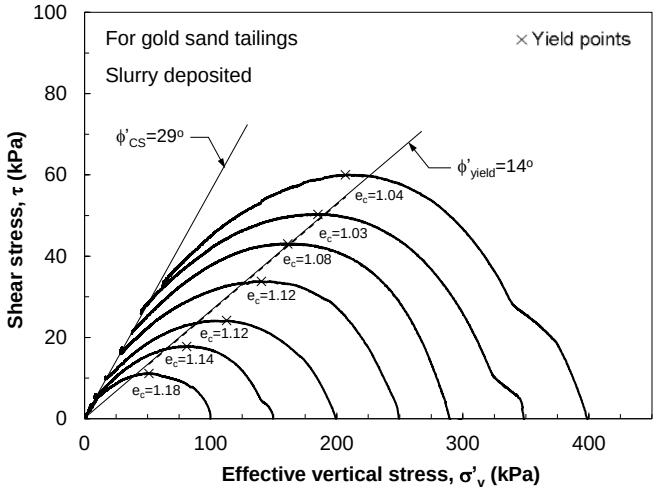

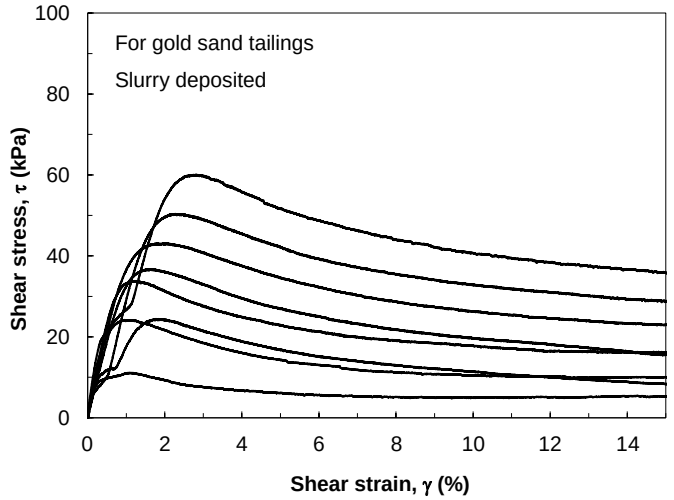

7.2. Appendix II: Direct Simple Shear Tests on Fraser River Sand

7.2.1.1. Monotonic Tests

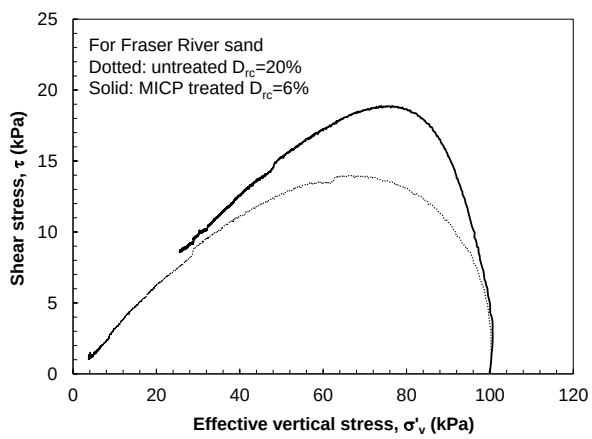

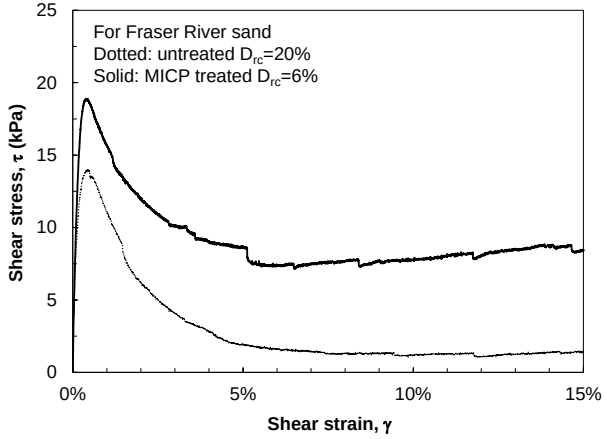

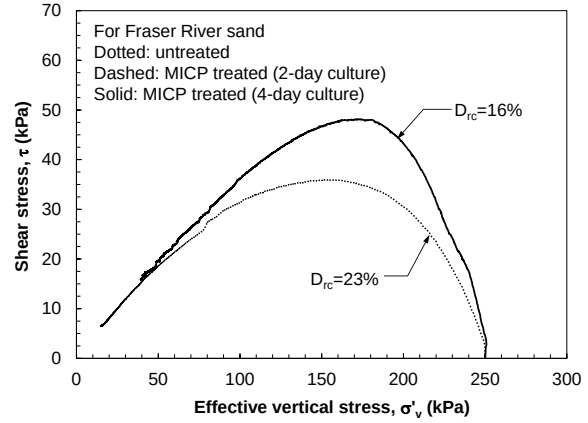

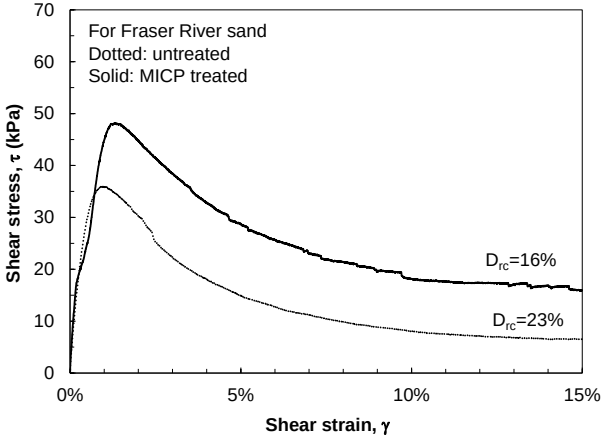

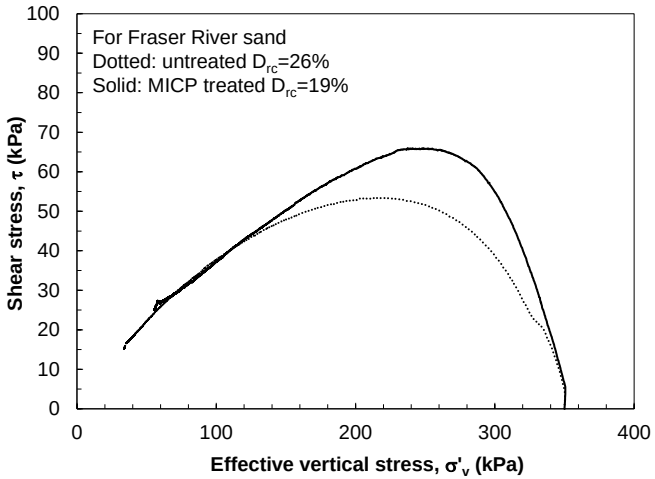
For Fraser River sand
Dotted: untreated D_{rc}=26%
Solid: MICP treated D_{rc}=19%
Shear stress, τ (kPa)
Effective vertical stress, σ'v (kPa)

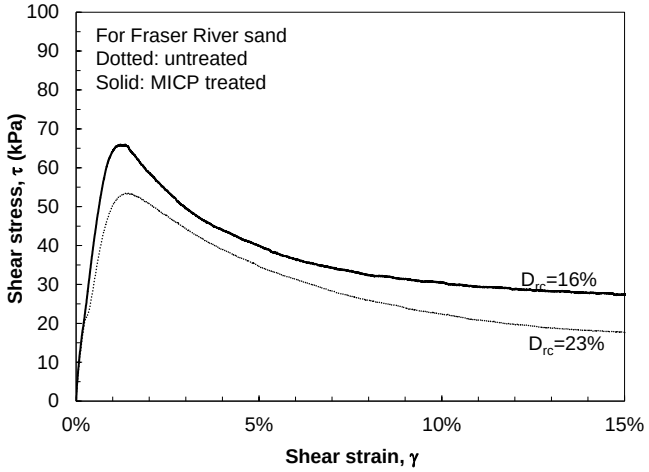
For Fraser River sand
Dotted: untreated
Solid: MICP treated
D_{rc}=16%
D_{rc}=23%
Shear stress, τ (kPa)
Shear strain, γ

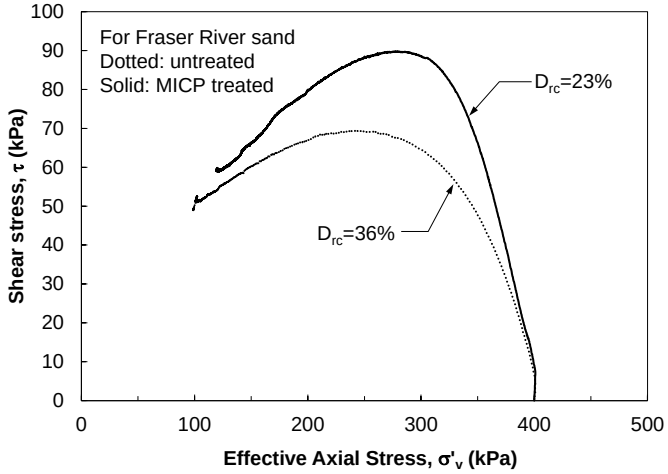
For Fraser River sand
Dotted: untreated
Solid: MICP treated
D_{rc}=23%
D_{rc}=36%
Shear stress, τ (kPa)
Effective Axial Stress, σ'v (kPa)

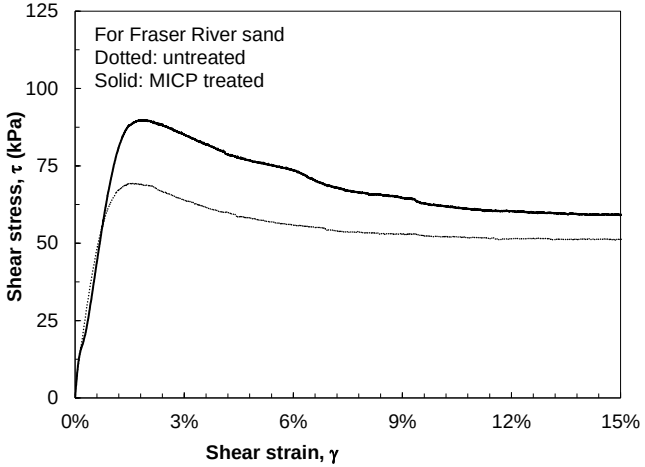
For Fraser River sand
Dotted: untreated
Solid: MICP treated
Shear stress, τ (kPa)
Shear strain, γ

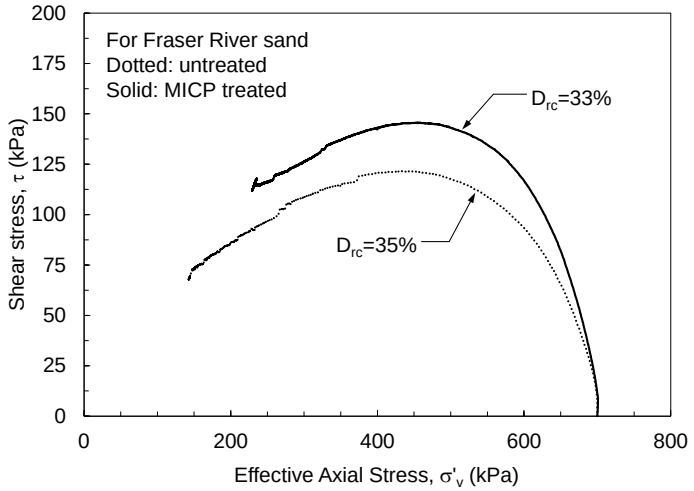
For Fraser River sand
Dotted: untreated
Solid: MICP treated
D_{rc}=33%
D_{rc}=35%
Shear stress, τ (kPa)
Effective Axial Stress, σ'v (kPa)
0
25
50
75
100
125
150
175
200
0
200
400
600
800

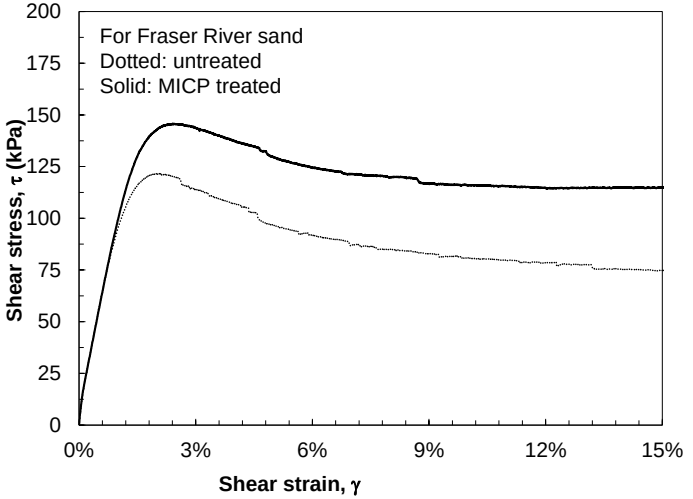
For Fraser River sand
Dotted: untreated
Solid: MICP treated
Shear stress, τ (kPa)
Shear strain, γ
0
25
50
75
100
125
150
175
200
0%
3%
6%
9%
12%
15%

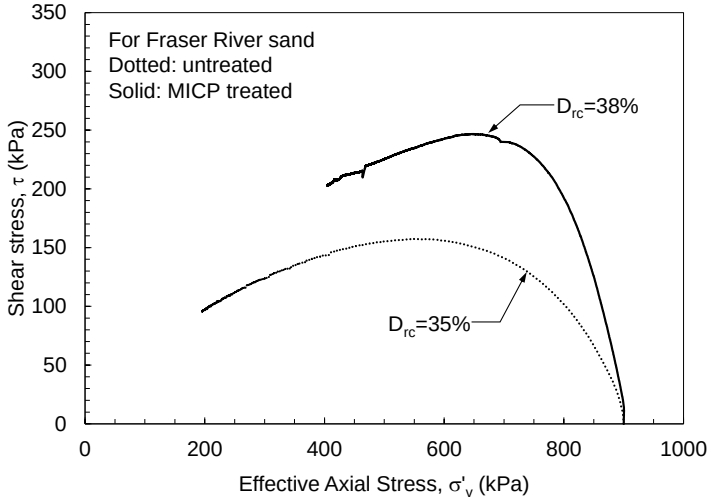
For Fraser River sand
Dotted: untreated
Solid: MICP treated
D_{rc}=38%
D_{rc}=35%
Shear stress, τ (kPa)
Effective Axial Stress, σ'v (kPa)
0
50
100
150
200
250
300
350
0
200
400
600
800
1000

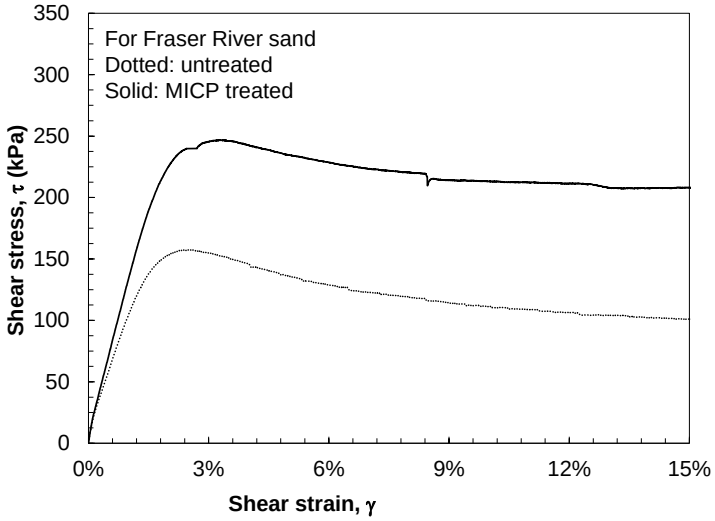
For Fraser River sand
Dotted: untreated
Solid: MICP treated
Shear stress, τ (kPa)
Shear strain, γ
0
50
100
150
200
250
300
350
0%
3%
6%
9%
12%
15%

7.2.1.2. Cyclic Tests (MICP Treated)

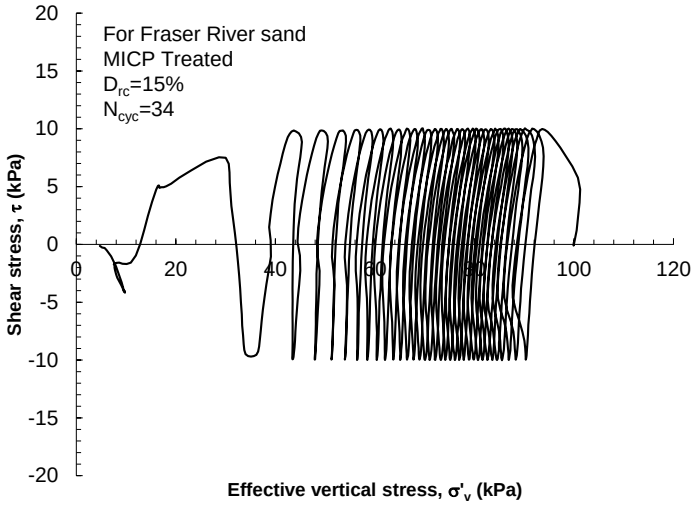

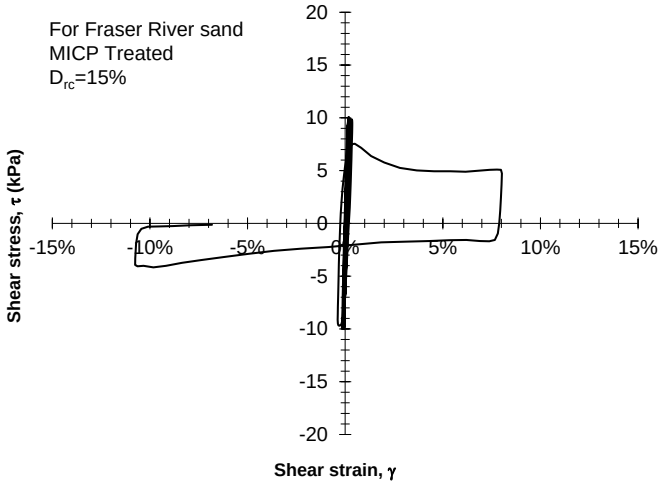

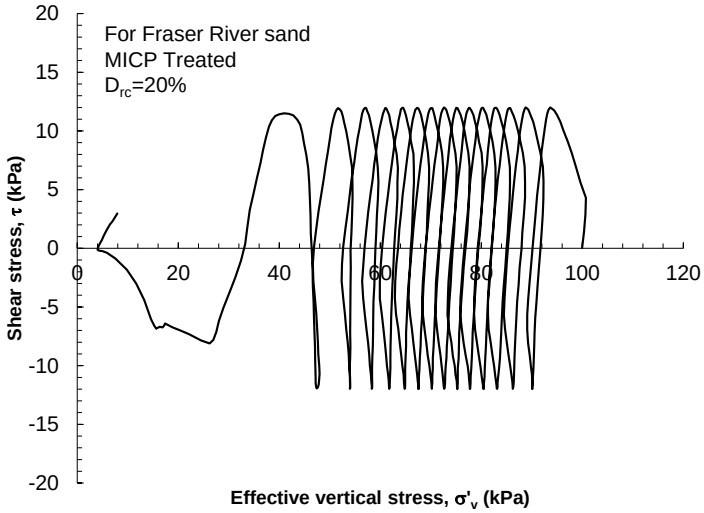

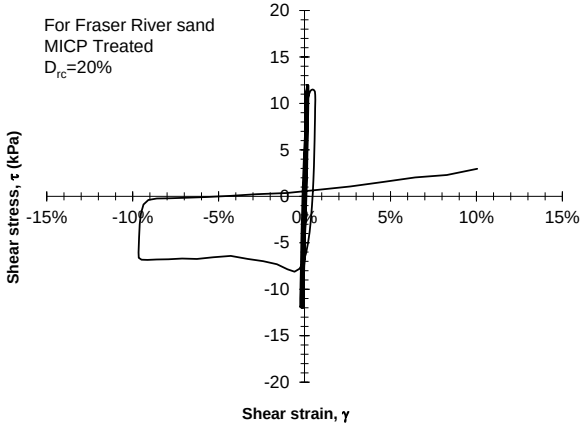

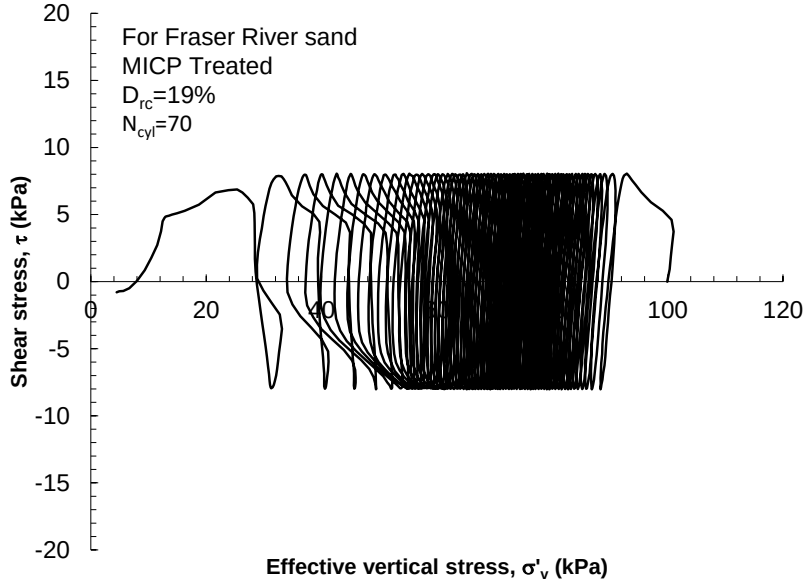
For Fraser River sand
MICP Treated
D_{rc}=19%
N_{cyl}=70
Shear stress, τ (kPa)
Effective vertical stress, σ'v (kPa)

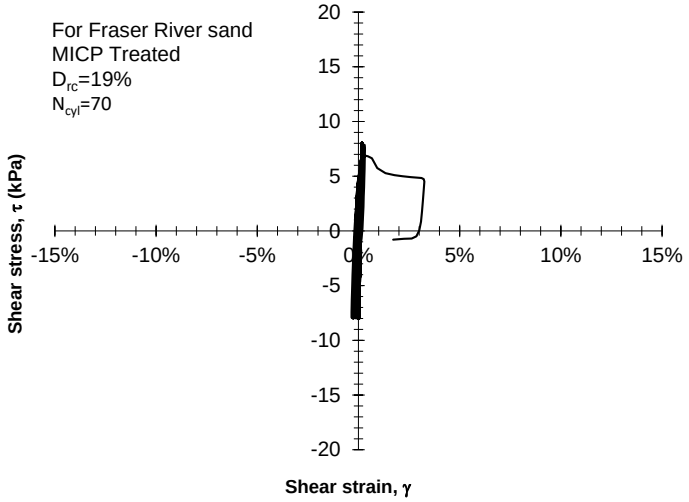
For Fraser River sand
MICP Treated
D_{rc}=19%
N_{cyl}=70
Shear stress, τ (kPa)
Shear strain, γ

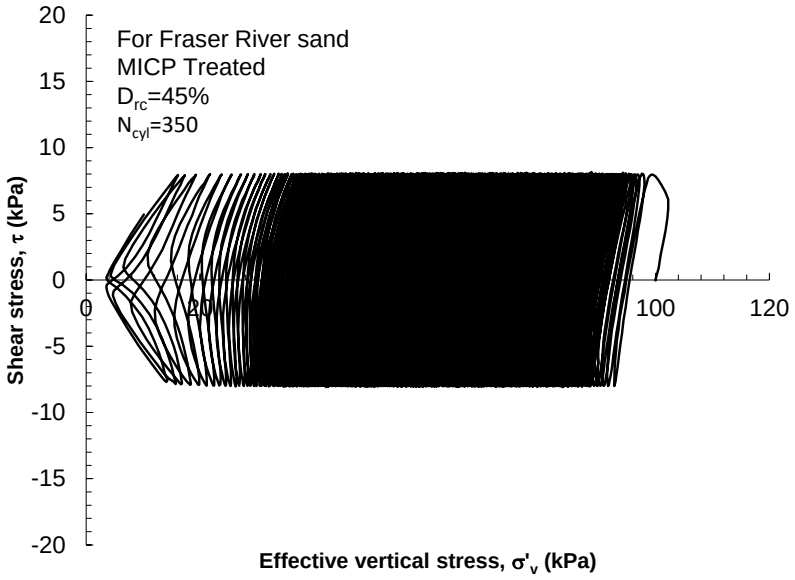
For Fraser River sand
MICP Treated
D_{rc}=45%
N_{cyl}=350
Shear stress, τ (kPa)
Effective vertical stress, σ'v (kPa)

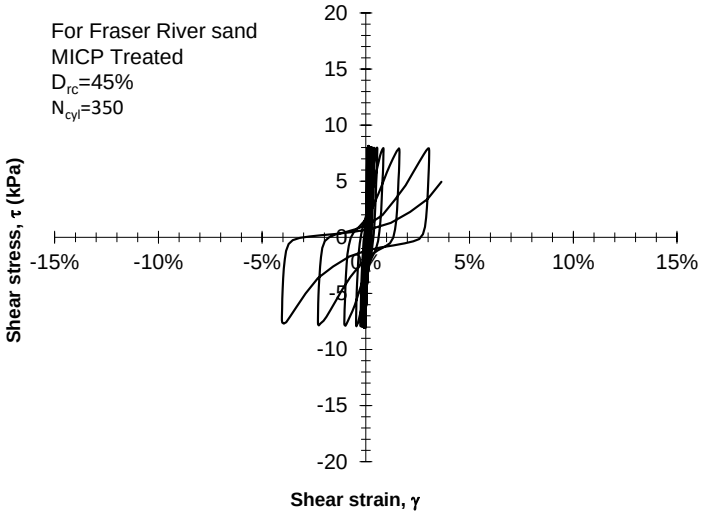
For Fraser River sand
MICP Treated
D_{rc}=45%
N_{cyl}=350
Shear stress, τ (kPa)
Shear strain, γ

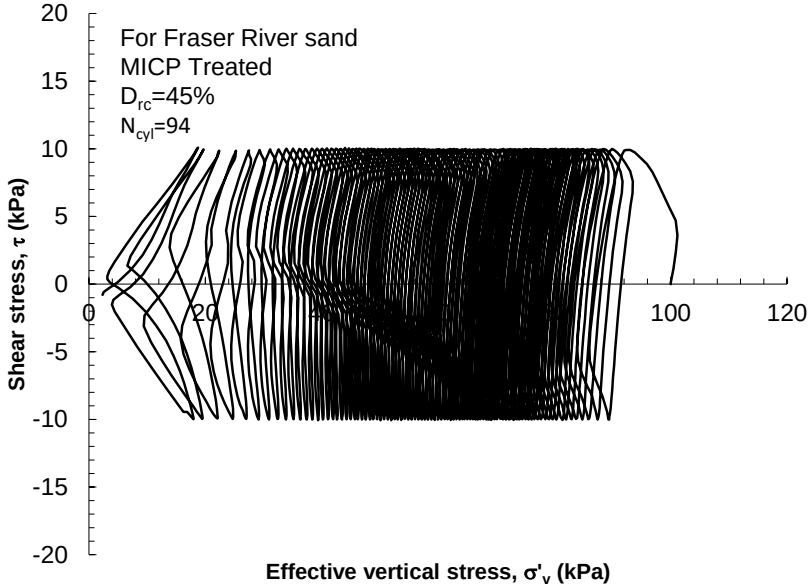
For Fraser River sand
MICP Treated
D_{rc}=45%
N_{cyl}=94
Shear stress, τ (kPa)
Effective vertical stress, σ'v (kPa)

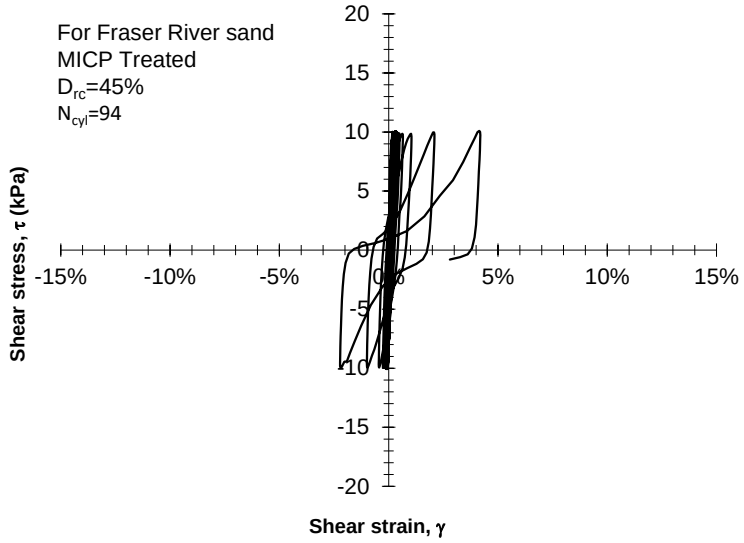
For Fraser River sand
MICP Treated
D_{rc}=45%
N_{cyl}=94
Shear stress, τ (kPa)
Shear strain, γ

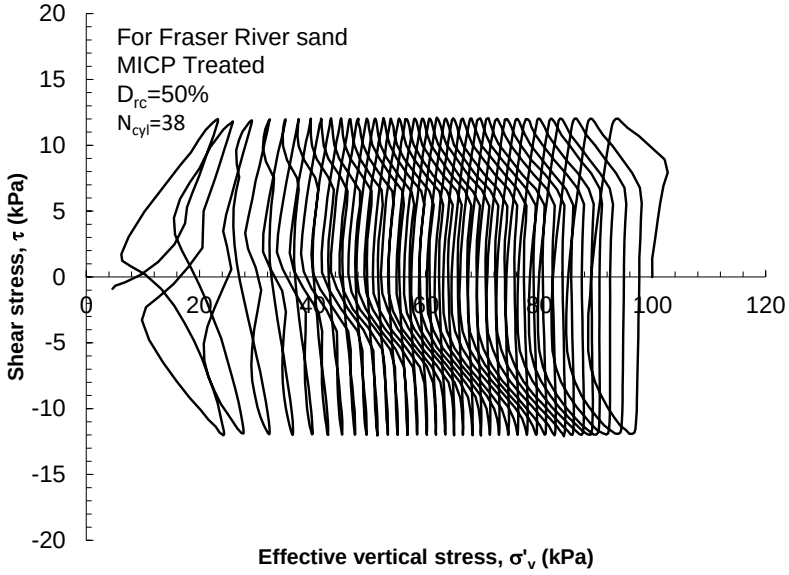
For Fraser River sand
MICP Treated
D_{rc}=50%
N_{cyl}=38
Shear stress, τ (kPa)
Effective vertical stress, σ'v (kPa)

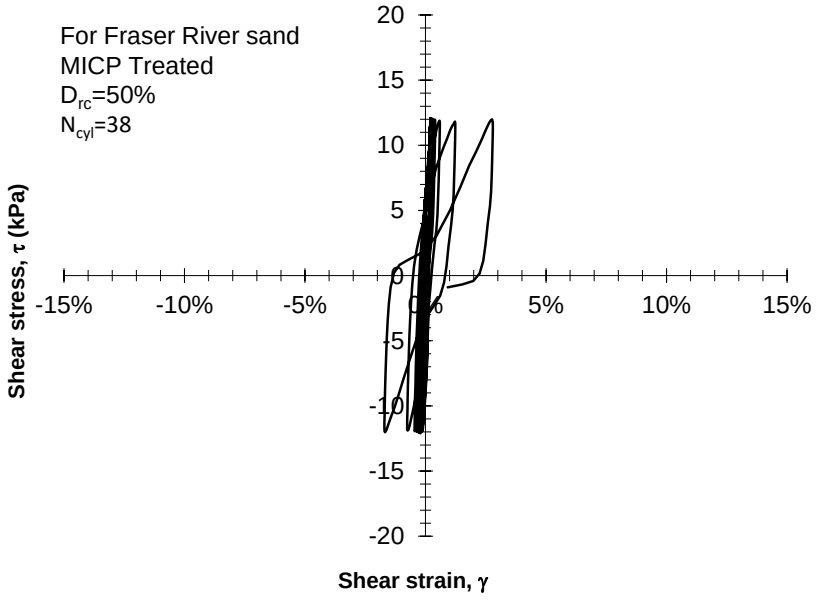
For Fraser River sand
MICP Treated
D_{rc}=50%
N_{cyl}=38
Shear stress, τ (kPa)
Shear strain, γ

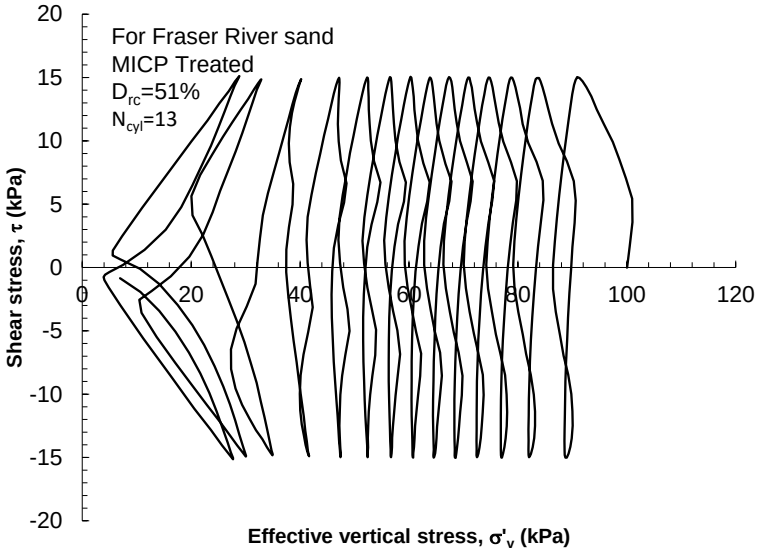
For Fraser River sand
MICP Treated
D_{rc}=51%
N_{cyl}=13
Shear stress, τ (kPa)
Effective vertical stress, σ'v (kPa)

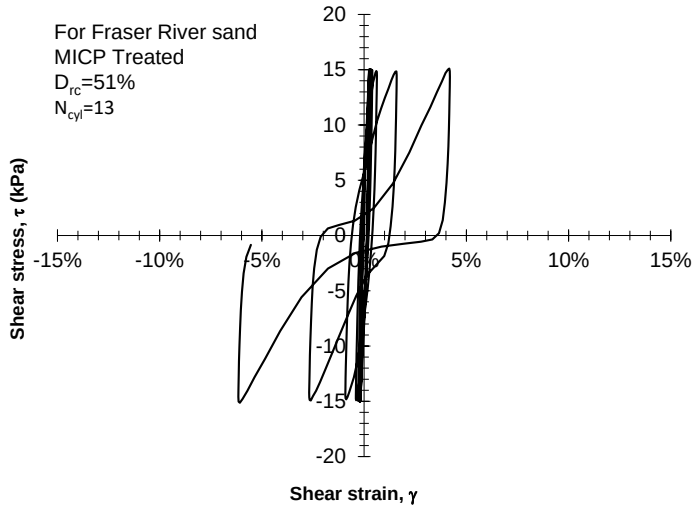
For Fraser River sand
MICP Treated
D_{rc}=51%
N_{cyl}=13
Shear stress, τ (kPa)
Shear strain, γ

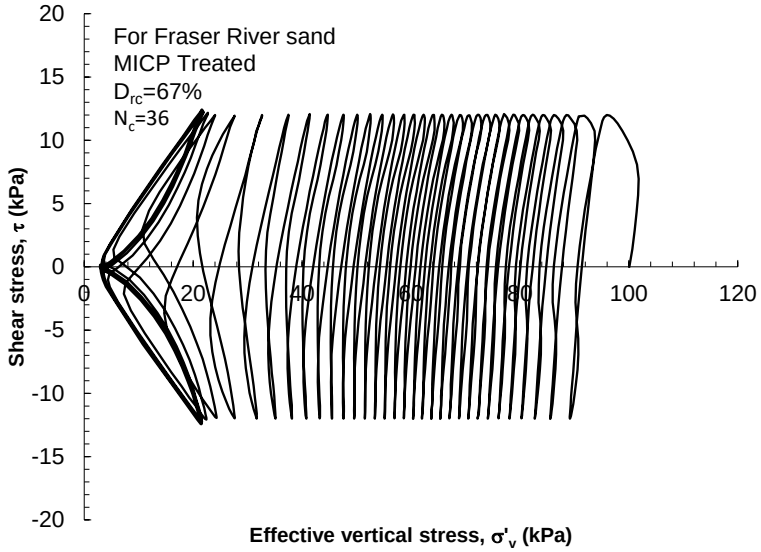
For Fraser River sand
MICP Treated
D_{rc}=67%
N_c=36
Shear stress, τ (kPa)
Effective vertical stress, σ'v (kPa)

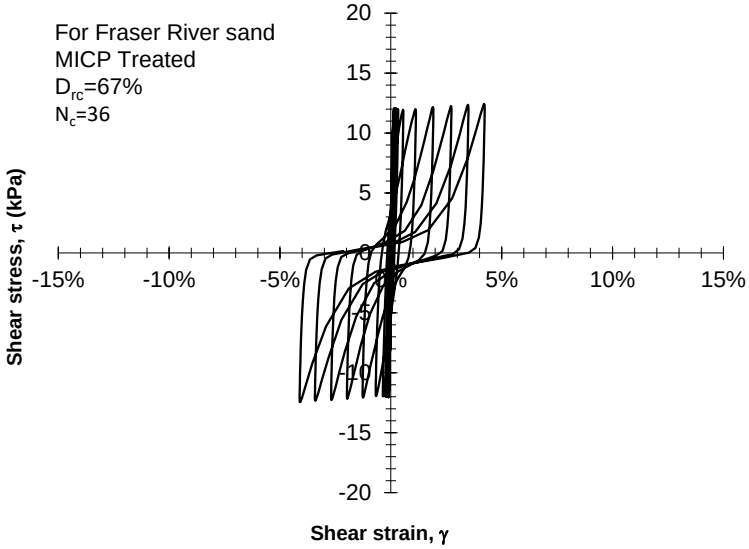
For Fraser River sand
MICP Treated
D_{rc}=67%
N_c=36
Shear stress, τ (kPa)
Shear strain, γ

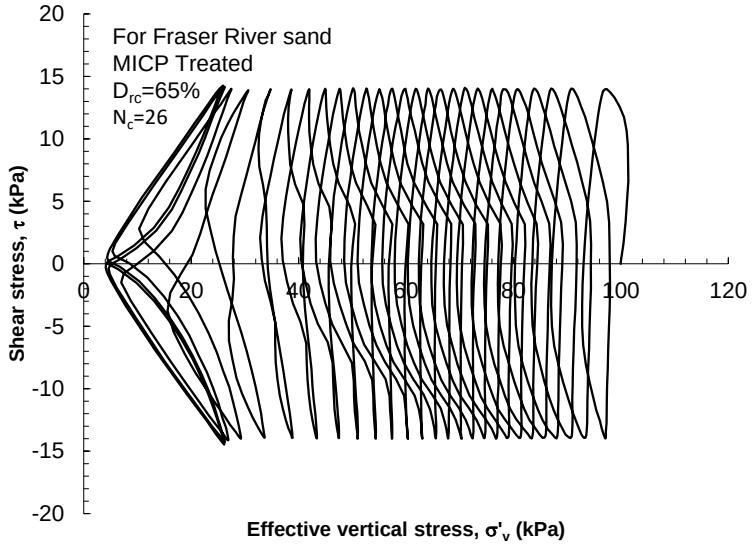
For Fraser River sand
MICP Treated
D_{rc}=65%
N_c=26
Shear stress, τ (kPa)
Effective vertical stress, σ'v (kPa)

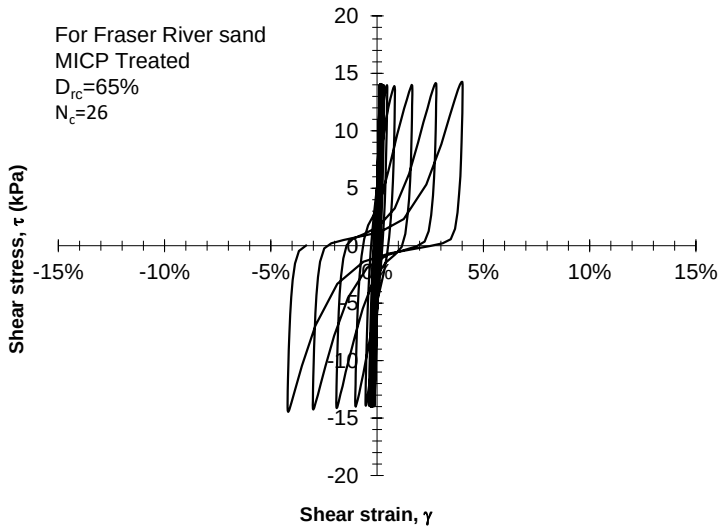
For Fraser River sand
MICP Treated
D_{rc}=65%
N_c=26
Shear stress, τ (kPa)
Shear strain, γ

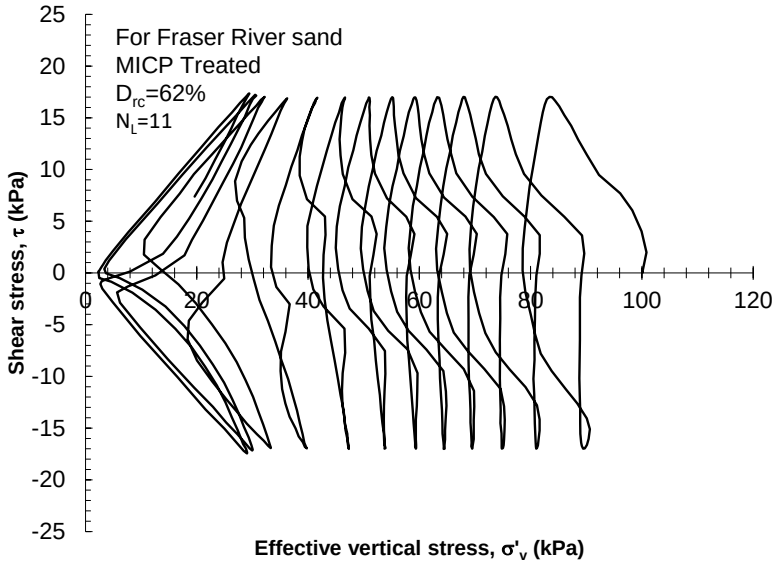
For Fraser River sand
MICP Treated
D_{rc}=62%
N_L=11
Shear stress, τ (kPa)
Effective vertical stress, σ'v (kPa)

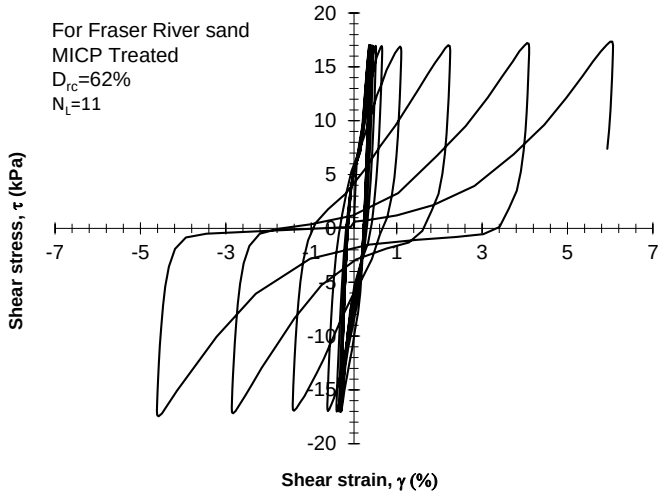
For Fraser River sand
MICP Treated
D_{rc}=62%
N_L=11
Shear stress, τ (kPa)
Shear strain, γ (%)

Curriculum Vitae

Name:	Guillermo Alexander Riveros
Post-secondary Education and Degrees:	Penn Foster College Scottsdale, AZ, USA 2008-2010 AET (Mechanical Engineering Technology) The University of Western Ontario London, Ontario, Canada 2013-2017 B.ASc (Civil and Environmental Engineering) The University of Western Ontario London, Ontario, Canada 2017-2019 M. ESc.(Geotechnical Engineering)
Honours and Awards:	NSERC – USRA Undergraduate Student Research Assistantship (2016) CGS Scholarship for Excellence in Geotechnical Engineering (2016) CGS Undergraduate Report Award – 2nd place (2017)
Related Work Experience	Teaching Assistant The University of Western Ontario 2017-2019 Junior Geotechnical Specialist Golder Associates May 2019 – Present